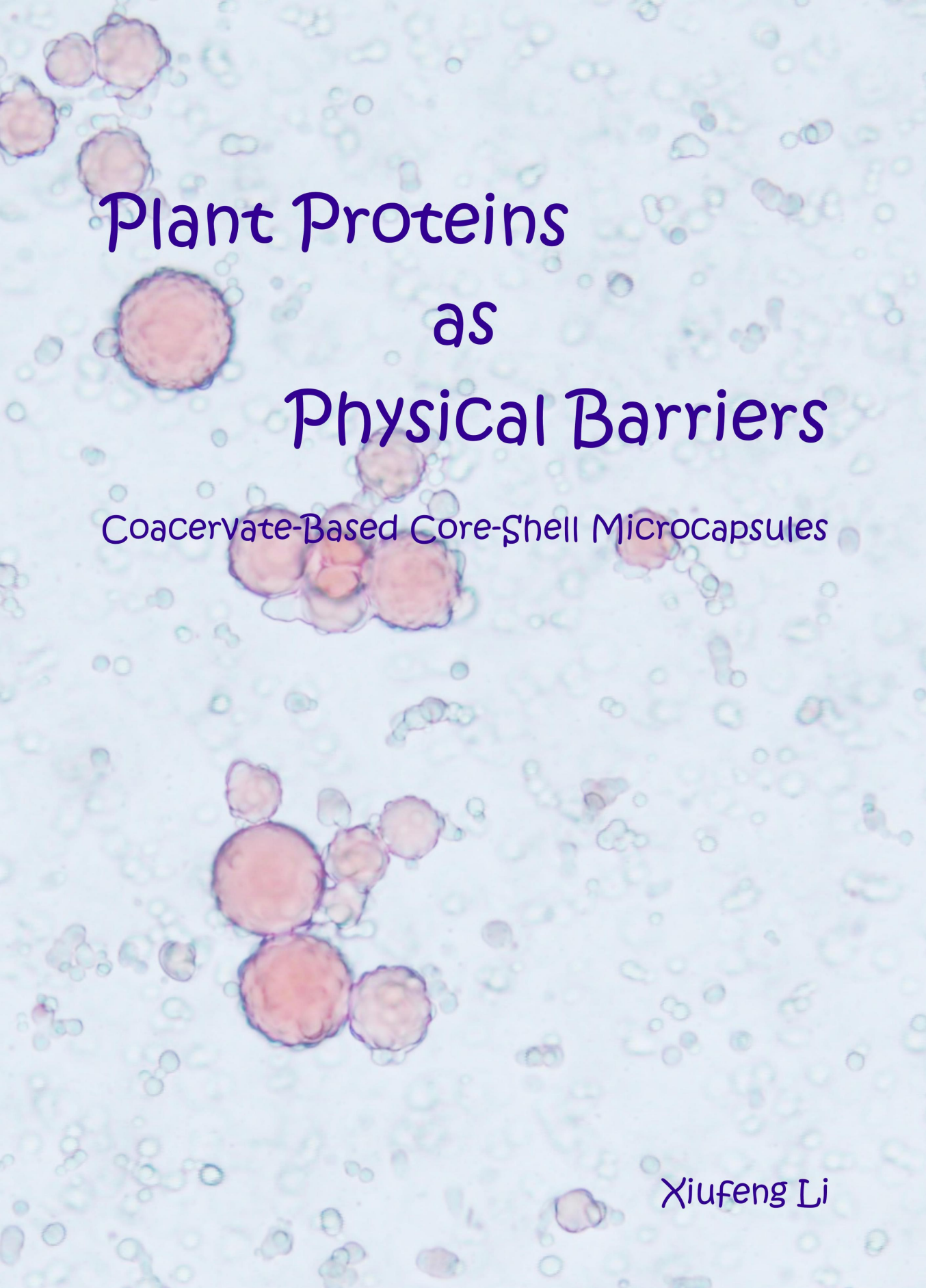

Plant Proteins as Physical Barriers

Coacervate-Based Core-Shell Microcapsules

Xiufeng Li

Propositions

1. Producing microstructures with raw ingredients from plants yields better results than using the purified ones.
(this thesis)

2. Active microrheology is a powerful tool to simultaneously probe the viscoelastic and interfacial properties of coacervates.
(this thesis)

3. Abandoning impact factors in employment and promotion decisions helps researchers focus on the real challenges of our society.

4. Finding a good research question is as important as addressing it.

5. In the transition to a fossil-free society, equal attention should be placed on reducing the production cost of biodegradable polymers as achieving desired properties.

6. Getting married has a positive impact on finishing a PhD project.

Propositions belonging to the thesis, entitled:
Plant Proteins as Physical Barriers
Coacervate-Based Core-Shell Microcapsules

Xiufeng Li
Wageningen, 27 October 2021

Plant Proteins as Physical Barriers

Coacervate-Based Core-Shell Microcapsules

Xiufeng Li

Thesis committee

Promotors

Dr R.J. de Vries
Associate professor, Physical Chemistry and Sof Matter
Wageningen University & Research

Prof. Dr J. van der Gucht
Professor of Physical Chemistry and Sof Matter
Wageningen University & Research

Co-Promotor

Dr P. Erni
Laboratory Head, Research & Development Division
Firmenich SA, Switzerland

Other members

Prof. Dr R. Mezzenga, ETH Zürich, Switzerland
Prof. Dr A.J. van der Goot, Wageningen University & Research
Dr M. Habibi, Wageningen University & Research
Prof. Dr M.M.G. Kamperman, University of Groningen

This research was conducted under the auspices of Graduate School VLAG (Advanced studies in Food Technology, Agrobiotechnology, Nutrition and Health Sciences).

Plant Proteins as Physical Barriers

Coacervate-Based Core-Shell Microcapsules

Xiufeng Li

Thesis

submitted in fulfillment of the requirements for the degree of doctor
at Wageningen University
by the authority of the Rector Magnificus,
Prof. Dr A.P. J. Mol,
in the presence of the
Thesis Committee appointed by the Academic Board
to be defended in public
on Wednesday 27 October 2021
at 4 p.m. in the Aula.

Xiufeng Li
Plant Proteins as Physical Barriers: Coacervate-Based Core-Shell Microcapsules
136 pages

PhD thesis, Wageningen University, Wageningen, the Netherlands (2021)
With references, with summary in English

ISBN 978-94-6395-944-5
DOI https://doi.org/10.18174/551838

Contents

Chapter 1

Introduction

This thesis is the result of collaboration between industry and academia: flavor & fragrance industry and soft matter science. This thesis aims to explore sustainable encapsulation techniques for industry, reducing carbon footprint and meeting the growing consumer preference for products with green labeling. We achieve this goal by replacing polymers from animal and petrochemical routes with green and biodegradable plant-based polymers in the encapsulation process. In this thesis, we focus on a specific type of encapsulation technique: coacervate-based core-shell microcapsule. We look for suitable plant-based polymers and processing methods to formulate coacervates, reveal the structure to property relations in complex systems, linking science to industrial solutions. Moreover, we provide new fundamental insights in the underlying physics governing the core-shell microcapsule formation via microrheology. In the following, we provide the context of this study and conclude with an outline of the thesis.

1.1 Flavor Molecules & Encapsulation Techniques

Flavors greatly impact on consumers' preference for many products, including food, cosmetics, and personal care products.[1, 2, 3] In general, flavors can be categorized into two groups. The first group of flavor molecules interact with the gustatory receptors in the mouth and cause taste.[4] These taste flavor molecules are usually not volatile. The second category is the aroma. In contrast to taste flavor molecules, aroma molecules are mostly volatile. They can stimulate the olfactory receptors in the nose.[5] In this thesis, we focus on the latter, and the use of 'flavor' refers to 'aroma' unless otherwise specified.

Most of the flavor molecules have low molecular weights, typically ranging from 100 to 250 g/mol.[6] These molecules are often present in gas or liquid states. Their level of hydrophilicity and lipophilicity is usually described by the logarithm of the partition coefficient between octanol and water (log P). A higher log P means the molecule is more lipophilic. Flavor molecules usually stay in the range log P=-1...7, and the majority of these is lipophilic.[6] In this thesis, as a model flavor compound, we use a volatile and lipophilic oil: limonene (log P=4.45).

Controlling the release of flavor molecules is a central challenge in flavor delivery.[7, 8] Due to their volatility, the flavor molecules easily escape from the products into the air. Thus, encapsulation techniques are often applied to enhance the stability and functionality of flavors. Some major benefits of flavors being encapsulated were discussed by Zuidam and Heinrich:[6]

- Easier transportation and better safety. Converting volatile flavor molecules from a liquid state to a powder form reduces their flammability.
- Controlled release, improved stability and shelf life.
- Adjustable flavor properties, such as changing the particle size and concentration in the end-use products.

Despite the variety of encapsulation techniques that have been developed for delivering flavor molecules, it seems like there is always one strategy in common, which is creating a physical barrier between flavor molecules and their surrounding medium. In most cases, these physical barriers present either as a core-shell

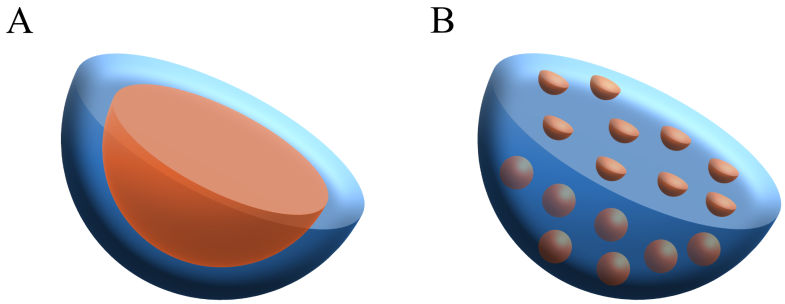

Figure 1.1: Graphical illustration of the core-shell capsule (A) and matrix particle (B).

Matrix	**Core-shell**	**others**
Spray-drying,[11, 12]	Coacervates,[13]	Yeast cells,[14]
Agglomeration/ Granulation,[15]	Co-extrusion[16]	Cyclodextrin (molecule inclusion)[17]
Fluid bed coating,[18]		
Spray-chilling/ cooling,[19]		
Melt extrusion,[20]		
Silica particles[21]		

Table 1.1: Flavor encapsulation techniques.

capsule or a matrix around flavor oil droplets (Figure 1.1). Some commonly used encapsulation techniques were summarized by several articles.[9, 10] Here, we provide a brief overview of these techniques and categorize them by their morphology (Table 1.1).

The selection criteria of encapsulation techniques are varied, including the physicochemical properties of flavors, production cost, and consumer acceptance. Moreover, these techniques sometimes are combined. In this thesis, we focus on coacervate-based core-shell microcapsules, which are being used for encapsulating lipophilic molecules or solid particles. This technique can create a thick polymer shell (μm scale) around the volatile flavor droplets/particles with

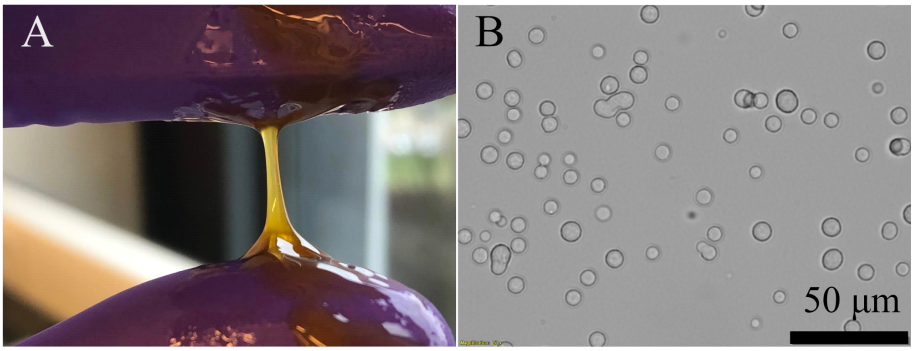

Figure 1.2: (A) Photograph of the continuous zein simple coacervate phase between fingers. This simple coacervate was obtained in a water/propylene glycol binary solvent. Reprinted from[23] with permission from The American Chemical Society. (B) Micrograph of pea protein extract/Gum Arabic complex coacervate droplets in the polymer-dilute phase.

encapsulation effeciency up to 90%.[6, 10]

1.2 Coacervates & Biopolymers

Coacervation is a liquid-liquid phase separation phenomenon that leads to a polymer-dilute phase and a polymer-rich (coacervate) phase still containing a large amount of the surrounding solvent.[22] Coacervates exist as viscoelastic fluids after bulk separation (Figure 1.2A).[23] Before bulk separation, microscopic droplets are suspended in the polymer-dilute phase (Figure 1.2B). The polymers undergoing coacervation must have a strong affinity to the solvent and be completely soluble so that they can still hold up the solvent molecules after phase separation. Otherwise, another type of phase separation, solid precipitation, will occur.[24, 25]

Depending on the number of polymers involved in coacervates, there are simple coacervates and complex coacervates. A simple coacervate only contains one type of polymer, whereas a complex coacervate contains two or more polymers. Simple coacervates are usually induced by changing the solvent conditions, such as solvent ratio and salt concentration. For instance, some pro-

teins from natural sources, such as gelatin and prolamins, can form simple coacervates in water-ethanol binary solvents.[26, 27] Moreover, it was reported that a cationic recombinant mussel foot protein can form a simple coacervate after adding salts.[28] Complex coacervates are formed by associative phase separation and are usually caused by electrostatic interactions among the oppositely charged polymers. Complex coacervates have been more extensively studied than simple coacervates, possibly because many oppositely charged polymers can be mixed to form complex coacervates, such as proteins, colloids, and polysaccharides.[25]

Despite the different building blocks, two general features are shared among most coacervates. First, the coacervate phase has a high polymer content (typically between 10 and 40%) while still remaining liquid. Second, the interfacial tension between the two phases is low (of order 100 μN/m).[29] Many applications of using coacervates take advantage of these two features. For instance, their ultra-low interfacial tension enables coacervates to spread on many surfaces, which is essential for designing adhesives,[30] coatings and capsules.[31] The high polymer content in coacervates provides more robust adhesion strength for adhesives and better barrier properties for coatings and capsules.

Biopolymers are widely used in coacervate formulations for food and personal care applications due to their biocompatibility. As cationic biopolymers, one often chooses animal proteins, such as whey protein and gelatin, because they carry positive net charges at pH lower than their isoelectric points and show excellent solubility in water. As anionic polymers, one often chooses soluble polysaccharides, including Gum Arabic and pectin,[25] since they carry negative net charges in a wide range of pH. This thesis aims to substitute animal-derived biopolymers with plant biopolymers. However, compared with the traditionally used animal proteins, plant proteins are generally less soluble in water and require much harsher processing in protein isolation and purification steps. Plant protein isolates available on the market are usually highly denatured and aggregated, hindering their use in simple or complex coacervate formulations. This thesis deals with such issues by selecting suitable plant protein materials and processing conditions. In this thesis, we find that instead of starting from commercial plant protein isolates of low functionality, we can start from less purified

ingredients, such as flours, and still use coacervation to achieve microencapsulation. In this way, we both circumvent the low functionality of commercial plant protein isolates and improve the sustainability of the process.

1.3 Core-Shell Microcapsule Formation

A core-shell microcapsule is a compound droplet that has payloads being engulfed by a continuous coacervate layer. Whether such core-shell capsules can form or not is determined by a number of factors: interfacial tensions among three phases, coacervate viscoelasticity, and the surrounding flow environment.[31] Of these factors, interfacial tensions play the most critical role as they determine whether the wetting of coacervate droplets on the surface of oil droplets takes place, which is the first step of capsule formation. If we think of the capsule formation purely from a thermodynamical perspective, without considering the other two factors, the compound droplet in an equilibrium state has three possibilities, as shown in Figure 1.3: non-wetting, partial wetting, and complete wetting. The contact angle between a coacervate droplet and an oil droplet in an immiscible liquid (polymer-dilute phase) is completely determined by three interfacial tensions, according to classical theoretical work from Torza & Mason.[32] Complete wetting or partial wetting should be a precondition for forming core-shell capsules. Generally, the interfacial tension between the coacervate phase and the polymer-dilute phase is very low, which favors the deposition and spreading of coacervate droplets on a third phase, leading to complete or partial wetting.

After coacervate droplets wet the interface, the other two factors will influence the kinetics of core-shell capsule formation. The elasticity and viscosity of coacervates will resist and slow down the spreading. The flow environment around the compound droplets usually promotes the spreading of coacervates or break-up of the compound droplets.[33, 34] In addition, if the coacervate is a yield stress fluid, then the yield strength must be overcome before spreading.

Therefore, depending on the relative spreading rate and deposition rate of coacervates, the coacervate layer around a core oil droplet could be formed by the spreading of coacervate droplets at the interface or continuous deposition and coalescence of them. In this thesis, we will discuss the above factors affecting

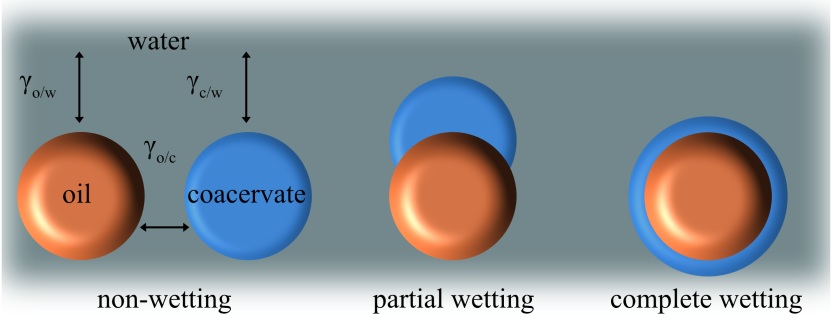

Figure 1.3: Graphical illustration of the wetting phenomenon in a three-phase system. This figure is reproduced by following the work from Torza & Mason[32] and Dardelle & Erni.[31]

capsule formation in greater detail.

1.4 Experimental Techniques for Studying the Interfacial Tension of Coacervates

While the rheological properties of coacervates, including viscoelasticity and flow behavior, can be conveniently studied by standard rheometry,[35, 36] accurate measurement of the interfacial tension between the coacervate phase and its coexisting polymer-dilute phase is not straightforward. This is because the combination of ultra-low interfacial tension, viscoelasticity, and sometimes lack of optical contrast pose problems for techniques such as pendant drop and spinning drop. Ideally, one would like to assess the viscoelastic and interfacial properties of coacervates in a single experiment, and this is even harder to do.

Until now, several techniques have been developed to study the interfacial properties with or without considering the rheology of coacervates. Some of the techniques are shown in Figure 1.4 and listed below:

- A capillary thinning method was developed to determine the interfacial tension by measuring the thinning dynamics of a coacervate filament suspended in the polymer-dilute phase.[31, 23] This method uses independently obtained rheological data to calculate the interfacial tension. (Figure

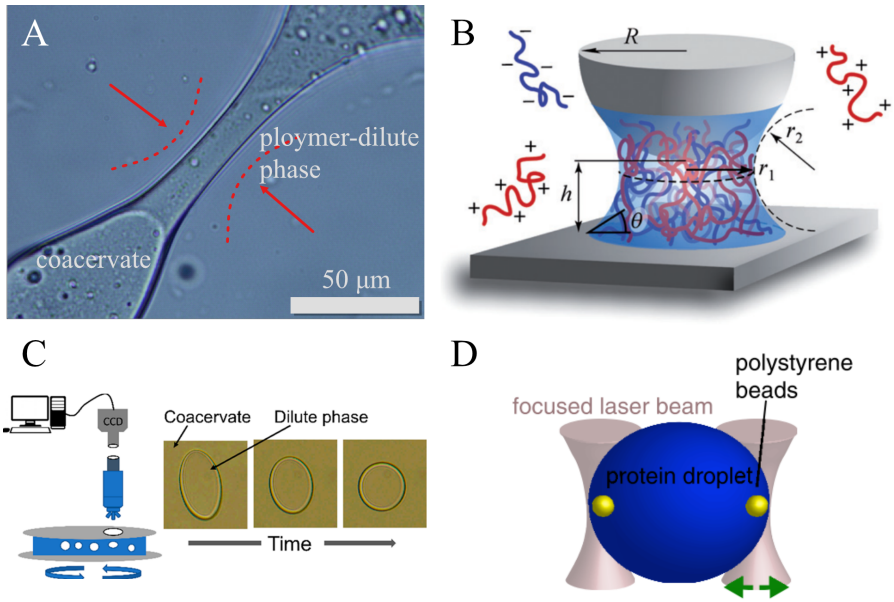

Figure 1.4: (A) Illustration of the capillary thinning method. A coacervate filament is suspended in its polymer-dilute phase. The neck width is monitored to measure the thinning dynamics, which is driven by the interfacial tension. Reproduced from[23] with permission from The American Chemical Society. (B) Illustration of the nanomechanical method. The capillary bridge is formed between the probe and substrate. Reprinted from[29] with permission from The Royal Society of Chemistry. (3) Illustration of determining the interfacial tension by following the recovery of the polymer-dilute phase droplet in the coacervate phase. Reprinted from[37] with permission from The American Chemical Society. (D) A schematic graph of the dual optical trap setup for performing microrheology on a coacervate droplet. Reprinted from[38] with permission from The American Physical Society.

1.4A)

- Nanomechanical techniques (Atomic Force Microscopy[39, 29, 40] and Surface Force Apparatus[41]) have been applied to measure the interfacial tension by linking it to the pull-off force. This method is usually sensitive to retraction rates and surface contamination, and it requires the delicate design of the experiment. The interfacial tensions in most of the studies were obtained without considering the coacervate rheology. (Figure 1.4B)

- The interfacial tension can also be obtained by monitoring the recovery

of a deformed droplet of the polymer-dilute phase within the coacervate phase.[37] To analyze the recovery data, the coacervate rheology must be known. (Figure 1.4C)

- An optical trap-based microrheology method has been developed to study the rheological and interfacial properties of coacervates.[38] In this method, the shape of coacervate droplets can be modulated at different frequencies where the mechanical properties at different time scales can be studied. (Figure 1.4D)

With interfacial properties being such a crucial property for using coacervates for encapsulation, we have invested significantly in extending existing interfacial characterization techniques and developing new ones. In this thesis, we have applied the capillary thinning method to study the interfacial tensions of a coacervate in its polymer-dilute phase and a third oil phase, understanding the three-phase transportation phenomena (Chapter 3). Moreover, we have optimized the analytical method for nanomechanical techniques, which can more accurately measure the interfacial tensions via pull-off forces (Chapter 4). Finally, we have developed a Colloidal Probe Atomic Force Microscopy (CP-AFM) based microrheology method to study the interplay between the interfacial tension and viscoelasticity (Chapter 5).

1.5 Outline

This thesis aims to identify suitable plant biopolymers and biopolymer mixtures, plus associated processing methods for the delivery of flavor molecules. We design core-shell delivery systems using coacervates and study the capsule formation process from a soft matter physics perspective. Here we give a summary of each chapter and describe its contribution to the central aim of this thesis.

In **Chapter 2**, we review recent developments on using complexes of plant proteins and polysaccharides for interfacial stabilization, thus looking for available options and challenges of formulating coacervates by using polymer from plant sources. We find that most research focuses on Pickering emulsions, the emulsions that are stabilized by solid particles. Plant proteins for coacervate formulations are much less reported due to their generally poor solubility in water.

Therefore, searching for more soluble plant proteins or suitable processing conditions may open the window for using them in formulating coacervate-based core-shell microcapsules.

In **Chapter 3**, we investigate using simple coacervates to design core-shell microcapsules. We use zein, a prolamin, as an example to study its phase behavior in binary solvents. Moreover, we study the wetting phenomenon of the zein simple coacervate at the interface of the polymer-dilute phase and oil phase by experimentally measuring interfacial tensions. Our results indicate that wetting is thermodynamically favorable due to ultra-low interfacial tensions of the coacervate in both the polymer-dilute phase and oil phase.

In **Chapter 4**, we study complex coacervates for making core-shell microcapsules by using legume proteins. We find that legume flours can be directly used as raw starting materials for formulating complex coacervates in an acidic environment. The resulting coacervate droplets show an excellent affinity for the oil droplet surface and form a continuous layer. Hence we show that less purification can in fact be beneficial when using plant proteins for encapsulation. This work provides a new thought that delicate protein purification is not always necessary for using plant proteins to design well-defined microstructures. Moreover, we optimize the analytical method of using CP-AFM to determine the ultra-low interfacial tensions.

In **Chapter 5**, we develop a CP-AFM based microrheology technique to measure the interfacial tension and viscoelasticity of coacervates at different time scales. We build a mechanical model that well describes the capillary bridge's stress response between the probe and substrate under sinusoidal modulation. Both our experimental data and mechanical model indicate that the interfacial tension dominates the force response at low frequencies, and the viscoelasticity of coacervates takes over the stress response at high frequencies.

Finally, in **General Discussion**, we discuss our findings in a broader context, expound what scientific gaps this thesis fills, and give an outlook for further research and applications.

References

[1] Thais Estevão dos Santos, Amanda Menescal, and Lauro Melo. Do consumers perceive the flavors announced on food packages? *European Food Research and Technology*, 246(11):2309–2322, 2020.

[2] FD White, Anna VA Resurreccion, and DA Lillard. Effect of warmed-over flavor on consumer acceptance and purchase of precooked top round steaks. *Journal of Food Science*, 53(5):1251–1252, 1988.

[3] Gabriella Baki and Kenneth S Alexander. *Introduction to cosmetic formulation and technology*. John Wiley & Sons, 2015.

[4] Craig Montell. Gustatory receptors: not just for good taste. *Current Biology*, 23(20):R929–R932, 2013.

[5] G Reineccius. Flavor and aroma chemistry. In *Quality attributes and their measurement in meat, poultry and fish products*, pages 184–201. Springer, 1994.

[6] Nicolaas Jan Zuidam and Emmanuel Heinrich. Encapsulation of aroma. In *Encapsulation technologies for active food ingredients and food processing*, pages 127–160. Springer, 2010.

[7] Usha R Pothakamury and Gustavo V Barbosa-Cánovas. Fundamental aspects of controlled release in foods. *Trends in food science & technology*, 6(12):397–406, 1995.

[8] Lisa Brannon-Peppas. Controlled release in the food and cosmetics industries. 1993.

[9] Md Saifullah, Mohammad Rezaul Islam Shishir, Rayhana Ferdowsi, Md Ramim Tanver Rahman, and Quan Van Vuong. Micro and nano encapsulation, retention and controlled release of flavor and aroma compounds: A critical review. *Trends in Food Science & Technology*, 86:230–251, 2019.

[10] Nicolaas Jan Zuidam and Krassimir P Velikov. Choosing the right delivery systems for functional ingredients in foods: an industrial perspective. *Current Opinion in Food Science*, 21:15–25, 2018.

[11] Gary A Reineccius. The spray drying of food flavors. *Drying technology*, 22(6):1289–1324, 2004.

[12] Gary A Reineccius. Spray-drying of food flavors. ACS Publications, 1988.

[13] Ronald J Versic. Coacervation for flavor encapsulation. ACS Publications, 1988.

[14] Valery Normand, Gregory Dardelle, Pierre-Etienne Bouquerand, Laetitia Nicolas, and David J Johnston. Flavor encapsulation in yeasts: limonene used as a model system for characterization of the release mechanism. *Journal of agricultural and food chemistry*, 53(19):7532–7543, 2005.

[15] BJ Wright, SE Zevchak, Jonathan M Wright, and MA Drake. The impact of agglomeration and storage on flavor and flavor stability of whey protein concentrate 80% and whey protein isolate. *Journal of food science*, 74(1):S17–S29, 2009.

[16] Thomas Mangos, Norbert Fischer, Pierre Chauchadis, Wolfgang Fexer, and Christian Schütte. Mononuclearly filled microcapsules, September 8 2009. US Patent 7,585,538.

[17] L Szente and J Szejtli. Molecular encapsulation of natural and synthetic coffee flavor with β-cyclodextrin. *Journal of Food Science*, 51(4):1024–1027, 1986.

[18] Turchiuli Christelle and Dumoulin Elisabeth. Aroma encapsulation in powder by spray dry-

ing, and fluid bed agglomeration and coating. In *Advances in Food Process Engineering Research and Applications*, pages 255–265. Springer, 2013.

[19] JD Oxley. Spray cooling and spray chilling for food ingredient and nutraceutical encapsulation. In *Encapsulation technologies and delivery systems for food ingredients and nutraceuticals*, pages 110–130. Elsevier, 2012.

[20] Natalia Castro, Vanessa Durrieu, Christine Raynaud, Antoine Rouilly, Luc Rigal, and Christian Quellet. Melt extrusion encapsulation of flavors: A review. *Polymer Reviews*, 56(1):137–186, 2016.

[21] Muhammad Aqeel Ashraf, Ayesha Masood Khan, Maliha Sarfraz, and Mushtaq Ahmad. Effectiveness of silica based sol-gel microencapsulation method for odorants and flavors leading to sustainable environment. *Frontiers in chemistry*, 3:42, 2015.

[22] Jasper Van der Gucht, Evan Spruijt, Marc Lemmers, and Martien A Cohen Stuart. Polyelectrolyte complexes: Bulk phases and colloidal systems. *Journal of colloid and interface science*, 361(2):407–422, 2011.

[23] Xiufeng Li, Philipp Erni, Jasper Van Der Gucht, and Renko De Vries. Encapsulation using plant proteins: Thermodynamics and kinetics of wetting for simple zein coacervates. *ACS applied materials & interfaces*, 12(13):15802–15809, 2020.

[24] Fatih Comert, Alexander J Malanowski, Fatemeh Azarikia, and Paul L Dubin. Coacervation and precipitation in polysaccharide–protein systems. *Soft Matter*, 12(18):4154–4161, 2016.

[25] Cornelus G De Kruif, Fanny Weinbreck, and Renko de Vries. Complex coacervation of proteins and anionic polysaccharides. *Current opinion in colloid & interface science*, 9(5):340–349, 2004.

[26] B Mohanty and HB Bohidar. Systematic of alcohol-induced simple coacervation in aqueous gelatin solutions. *Biomacromolecules*, 4(4):1080–1086, 2003.

[27] Rishi Shukla and Munir Cheryan. Zein: the industrial protein from corn. *Industrial crops and products*, 13(3):171–192, 2001.

[28] Sangsik Kim, Hee Young Yoo, Jun Huang, Yongjin Lee, Sohee Park, Yeonju Park, Sila Jin, Young Mee Jung, Hongbo Zeng, Dong Soo Hwang, et al. Salt triggers the simple coacervation of an underwater adhesive when cations meet aromatic π electrons in seawater. *ACS nano*, 11(7):6764–6772, 2017.

[29] Evan Spruijt, Joris Sprakel, Martien A Cohen Stuart, and Jasper van der Gucht. Interfacial tension between a complex coacervate phase and its coexisting aqueous phase. *Soft Matter*, 6(1):172–178, 2010.

[30] Marco Dompé, Francisco J Cedano-Serrano, Olaf Heckert, Nicoline van den Heuvel, Jasper van der Gucht, Yvette Tran, Dominique Hourdet, Costantino Creton, and Marleen Kamperman. Thermoresponsive complex coacervate-based underwater adhesive. *Advanced Materials*, 31(21):1808179, 2019.

[31] Gregory Dardelle and Philipp Erni. Three-phase interactions and interfacial transport phenomena in coacervate/oil/water systems. *Advances in colloid and interface science*, 206:79–91, 2014.

[32] S Torza and SG Mason. Three-phase interactions in shear and electrical fields. *Journal of*

colloid and interface science, 33(1):67–83, 1970.

[33] Robert E Johnson and SS Sadhal. Fluid mechanics of compound multiphase drops and bubbles. *Annual review of fluid mechanics*, 17(1):289–320, 1985.

[34] KA Smith, JM Ottino, and M Olvera De La Cruz. Encapsulated drop breakup in shear flow. *Physical review letters*, 93(20):204501, 2004.

[35] Evan Spruijt, Joris Sprakel, Marc Lemmers, Martien A Cohen Stuart, and Jasper Van Der Gucht. Relaxation dynamics at different time scales in electrostatic complexes: time-salt superposition. *Physical review letters*, 105(20):208301, 2010.

[36] Evan Spruijt, Martien A Cohen Stuart, and Jasper van der Gucht. Linear viscoelasticity of polyelectrolyte complex coacervates. *Macromolecules*, 46(4):1633–1641, 2013.

[37] Samim Ali and Vivek M Prabhu. Characterization of the ultralow interfacial tension in liquid–liquid phase separated polyelectrolyte complex coacervates by the deformed drop retraction method. *Macromolecules*, 52(19):7495–7502, 2019.

[38] Louise M Jawerth, Mahdiye Ijavi, Martine Ruer, Shambaditya Saha, Marcus Jahnel, Anthony A Hyman, Frank Jülicher, and Elisabeth Fischer-Friedrich. Salt-dependent rheology and surface tension of protein condensates using optical traps. *Physical review letters*, 121(25):258101, 2018.

[39] J Sprakel, NAM Besseling, FAM Leermakers, and MA Cohen Stuart. Equilibrium capillary forces with atomic force microscopy. *Physical review letters*, 99(10):104504, 2007.

[40] Seonghye Lim, Dustin Moon, Hyo Jeong Kim, Jeong Hyun Seo, In Seok Kang, and Hyung Joon Cha. Interfacial tension of complex coacervated mussel adhesive protein according to the hofmeister series. *Langmuir*, 30(4):1108–1115, 2014.

[41] Dimitrios Priftis, Robert Farina, and Matthew Tirrell. Interfacial energy of polypeptide complex coacervates measured via capillary adhesion. *Langmuir*, 28(23):8721–8729, 2012.

Chapter 2

Interfacial Stabilization Using Complexes of Plant Proteins and Polysaccharides

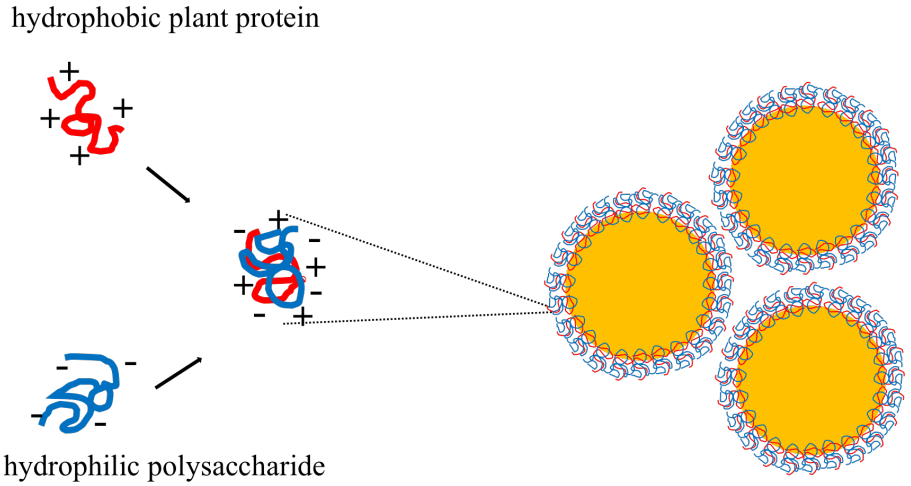

This chapter was published as:
Li, X., & De Vries, R. (2018). Interfacial stabilization using complexes of plant proteins and polysaccharides. *Current Opinion in Food Science*, 21, 51-56.

In view of their favourable sustainability profile, plant proteins are gaining interest as replacement ingredients for applications that are traditionally dominated by animal proteins such as the stabilization of emulsions and foams. For animal proteins it has been extensively demonstrated how the complexation of proteins with polysaccharides can be exploited to modulate interfacial stabilization. Many plant proteins are much less hydrophilic and often cannot be easily extracted from the raw plant material in their native state. This gives rise to a new set of challenges and opportunities when considering the use of protein–polysaccharide complexes for interfacial stabilization. Here we review the recent literature on the use of complexes of plant proteins with polysaccharides for interfacial stabilization. This includes the use of composite plant protein/polysaccharide nanoparticles and microparticles, plant protein–polysaccharide complex coacervates and plant protein–polysaccharide multilayer emulsions. While on the one hand the lower solubility of the plant proteins presents a challenge, by association with very hydrophylic polysaccharide, very strong amphiphilicity is obtained that can lead good stabilization of oil–water and air–water interfaces.

2.1 Introduction

Protein–polysaccharide interactions are well-known to be a crucially important determinant of food structure. Both physical interactions[1, 2] and chemical bonding, especially through Maillard reactions,[3] have been exploited to create novel food structures: composite nanoparticles and microparticles,[4, 5] interfacial layers,[6, 7] films[8] and hydrogels.[9] In view of the trend towards the use of more sustainable protein sources, much recent work in this area deals with the specific case of plant proteins. Plant proteins and polysaccharides are being combined not only for food structuring, but also for non-food applications such as packaging films[10] and fibers for fabrics.[11, 12] As compared to widely studied soluble globular animal proteins such as proteins from milk and eggs, many plant proteins are much less hydrophilic and often cannot be easily extracted from the raw plant material in their native state.[13, 14] This gives rise to a new set of challenges and opportunities when considering protein–polysaccharide interactions.

Here we aim at identifying this set of challenges and opportunities by reviewing recent literature on composite nanoparticles and microparticles, and interfacial layers coassembled from plant proteins and polysaccharides. While protein–polysaccharide segregation can also be used as a means of bulk structuring (for example via gelation-induced or aggregation-induced phase separation),[15]

we here focus on protein–polysaccharide association, either through physical interactions, or through Maillard-types or other types of chemical reactions.

A number of related reviews have appeared recently. Lin et al.[16] review the broader area of interactions of plant proteins with other biopolymers and note that most work concerns proteins from legumes rather than proteins from cereals or oils seeds. Braudo et al.[17] review the more narrow area of associative interactions between legumous proteins and polysaccharides, focusing on opportunities to modulate the interfacial activity of legumous proteins via interactions with polysaccharides. Finally, Wan et al.[18] focus on a specific opportunity for the more lipophilic plant proteins: that of using them as carriers for various bioactives. Some of the examples discussed in this last review also involve polysaccharides.

We focus mainly on emulsions and foams. A first section deals with mixed colloidal particles of polysaccharides and plant proteins that can be used for interfacial stabilization, but also for many other applications. A second section describes the various ways in which combinations of plant proteins and polysaccharides have been used to stabilize foams and emulsions: Pickering stabilization using plant protein/polysaccharide composite colloidal particles, and direct coating of interfaces with plant protein polysaccharide complexes (either as complex coacervates, or by constructing multilayer interfaces). An overview of the papers reviewed here is provided in Table 2.1.

The common theme is that by themselves plant proteins often do not provide optimal amphiphilicity for interfacial stabilization since they are often too hydrophobic. By complexation/conjugation with polysaccharides, a hybrid stabilization is obtained that does have the right amphiphilicity (balance between hydrophobicity and hydrophilicity). For the case of oil-in-water emulsions (the most common type of interfacial stabilization for which plant proteins are being sought to be used) consider in somewhat more detail the mechanisms by which polysaccharides contribute to better stability.

First, optimal Pickering stabilization requires careful tuning of the hydrophilicity/hydrophobicity of the particles that are used: ideally they should sit right at the middle of the oil–water interface, but for particles based on (hydrophobic) plant proteins alone, the particles will have a tendency to be located on

the oil-side which leads to poor emulsion stability. Complexation with polysaccharides provides a handle to tune the hydrophilicity and hence the location of the particles at the oil–water interface and therefore finally also their emulsifying ability.

Next, for direct coating of interfaces with plant protein polysaccharide complexes (either as complex coacervates, or by constructing multilayer interfaces), a hydrophobicity that is too large leads to flocculation of the droplets, which in turn may promote coalescence. Therefore the key role for the polysaccharides in this case is to provide colloidal stability to the coated oil droplets by keeping them away from each other.

2.2 Composite Microparticles and Nanoparticles

Protein microparticles and nanoparticles have a wide range of applications as functional food ingredients,[38] ranging from applications in high protein foods, encapsulation and delivery of bioactives, to Pickering stabilizers of interfaces.[39] Given their more hydrophobic nature, plant protein particles are promising candidates for encapsulating hydrophobic bioactives, as well as Pickering stabilizers. In many cases however, nanoparticles and microparticles composed of only plant proteinhave very poor colloidal stability. Also, in some cases their hydrophobicity may be too high to be used as efficient Pickering stabilizers. Stabilizing hydrophobic plant proteins can be achieved via coating with more hydrophilic (macro)molecules. For instance, zein colloids can be stabilized by caseinate.[40] In this review, we are more concerned with polysaccharide stabilizers. Complexation with more hydrophilic polysaccharides is an attractive handle to tune both the overall hydrophobicity as well as the colloidal stability of plant protein microparticles and nanoparticles. Here we give some recent examples of work along these lines.

A first approach is to use polysaccharides as classical colloidal stabilizers, by adsorbing them on plant protein nanoparticles and microparticles.[16, 18] As shown in Table 2.1, various combinations plant proteins and polysaccharides have been explored. In a study of zein/ alginate complex particles, compared with pure zein particles, core-shell particles formed by zein and alginate

Structure	Protein	Polysac-charide	Reaction type	Particle size	Stability	Ref
Complex particle	Zein	Alginate	Physical	80 nm zein core + 40 nm alginate shell	Stable from pH 2 to 8, up to 100 mM NaCl at pH 7, up to 2 M NaCl at pH 4	[19]
Complex particle	Zein and case-inate	Pectin	Physical	<200 nm	Pectin coating improves particle stability under stimulated gastrointest-inal conditions	[20]
Complex particle	Rice glutelin	Alginate	Physical		Complexes aggregate between pH 2 and 7	[21]
Complex particle	Zein	i-Carrageenan	Physical	Radius 200–400 nm (between pH 5–7)	Carrageenan improves pH stability of particles	[22]
Complex particle	Zein	Pectin	Physical	Around 250 nm	Pectin coating allows for drying and re-dispersion of particles	[23]
Complex particle	Zein	Shellac	Physical		In Curcumin loaded zein shellac compos-ite particles, shellac improves curcumin stability while still allowing sustained release under simulated gastrointestinal condi-tions	[24]
Complex particle	Zein	Propylene Glycol Alginate	Physical			[25]
Complex particle	Soy protein	Soy polysacchar-ide	Physical			[26]
Emulsion (com-plex particles)	Zein	Gum Arabic	Physical	220 nm	Emulsion gel, long-term storage stability (30 days)	[27]
Emulsion (com-plex particles)	Gliadin	Chitosan	Physical	Around 600 nm	Emulsion gel, long-term storage stability	[28]
Emulsion (com-plex particles)	Hydrolyzed rice glutelin	Xanthan gum/Pectin/Alginate/Gum Arabic	Physical			[29]
Emulsion (con-jugate)	Soy protein isolate	Soy soluble poly-saccharide	Chemical			[30]
Emulsion (con-jugate)	Pea protein isolate	Pectin	Chemical			[31]
Emulsion (con-jugate)	Oat protein isolate	Dextran	Chemical			[32]
Emulsion (con-jugate)	Canola pro-tein isolate	Gum Arabic	Chemical			[33]
Foam (complex coacervate or aggregate)	Lentil legumin-like protein	Guar gum/Xanthan gum/Pectin	Physical		Foam stability was greatly enhanced at pH 3.0 and 5.0	[34]
Emulsion (com-plex coacervate)	Alpha gli-adin/Pea protein	Gum Arabic	Physical			[35]
Emulsion (com-plex coacervate)	Soy protein	Chitosan	Physical			[36]
Emulsion (com-plex coacervate)	Flaxseed pro-tein	Flaxseed gum	Physical			[37]

Table 2.1: Complex structures formed by plant proteins and polysaccharides.

were found to be stable over a broader pH range and also up to higher ionic strengths.[19] McClements and coworkers investigated emulsions stabilized by hydrolyzed rice glutelin additionally coated with various anionic polysaccharides. Generally speaking, the polysaccha-ride-coated emulsions were stable over a broader range of solution conditions as a result of the enhancement of steric

and electrostatic repulsion between the droplets.[29] Mixed particles of zein/caseinate coated with pectin have been studied for oral delivery applications. It was shown that not only electrostatic interactions, but also hydrogen bonding and hydrophobic interactions contributed to the complex formation with pectin, as deduced from FTIR and fluorescence spectroscopy. In simulated gastrointestinal conditions, the pectin coated complex particles exhibit better stability as compared to the bare zein/caseinate particles.[20] Core–shell particles of soy protein (SPI) and soy polysaccharide (SSPS) have been investigated as carriers for curcumin. At pH 7, the curcumin is absorbed on the surfaces of the SPI particles. Coating by SSPS does not lead to drastic changes of the particle sizes, except at pH 4, for which large particles are formed due strong electrostatic interactions between SPI and SSPS. The core-shell particles not only have better thermal stability, but also improved controlled release of the curcumin.[26]

A second approach would be to create true composite polysaccharide/plant protein nanoparticles, where also the interior of the nanoparticle is a true polysaccharide/plant protein composite. This approach has not yet been demonstrated convincingly for plant protein–polysaccharide nanoparticles, but an approach developed for zein/caseinate hybrid particles may also be attempted with polysaccharides. For this case, alkaline conditions (pH 11.5) provide a common solvent for both the zein and the caseinate. After acidification, the zein precipitates, with (part of the) caseinate becoming embedded inside the particles due to hydrophobic interactions and hydrogen bonding. The composite interior structure was confirmed by Differential Scanning Calorimetry. Particles produced by this method show a small particle size (d=100 nm) and good storage stability.[41]

2.3 Emulsions and Foams

Proteins from animal sources are commonly used to stabilize emulsions and foams in the food industry such as homogenized and reconstituted milks (O/W emulsions) and dairy creams (foams).[42, 43] As opposed to many proteins derived from animals, plant proteins are mostly hydrophobic. While this may give them better barrier properties than animal proteins, good stabilizers must have both hydrophilic and hydrophobic components:[6] plant proteins can sometimes

be too hydrophobic, lacking the hydrophilic domains required for good stabilization of water–oil or water–air interfaces. For this reason, combinations of hydrophilic polysaccharides with hydrophobic plant protein may be synergistic with respect to surface activity: the more hydrophobic plant protein anchors mainly in the oil phase, while the hydrophilic polysaccharide stays in water phase to provide electrostatic repulsion (if charged) and steric hindrance.[44] Indeed, as shown in Table 2.1, many complexes formed by plant proteins and polysaccharides show excellent capability of stabilizing water–oil or water–air interfaces. We review two strategies to use associative complexes of plant proteins and polysaccharides to stabilize water–oil or water–air interfaces: Pickering stabilization using plant protein/polysaccharide composite colloidal particles, and direct coating of interfaces with plant protein polysaccharide complexes (either as complex coacervates, or by constructing multilayer interfaces).

Various approaches to producing plant protein/polysaccharide colloidal particles were already reviewed in the previous section. Here we specifically review their use for interfacial stabilization. Nanoparticles of the hydrophobic plant protein zein were successfully modified by complexation with an oppositely charged and hydrophilic polysaccharide Gum Arabic.[27] It was shown that the complexation allowed for tuning the balance between hydrophobicity and hydrophilicity of complexes (as deduced from three phase contact angle measurements). Layers of complex particles could be observed to be adsorbed to the surfaces of oil droplets through CLSM. Such particles were found to form gelled emulsions at high oil fractions (>50%) that had good storage stability. Emulsion gels were formed due to bridging attraction between the oil droplets. The gel structure may in fact contribute to the overall emulsion stability since the movement of the oil droplets are restricted by the network.[27] As another example, monodisperse gliadin/chitosan complex particles were synthesized via a facile anti-solvent approach at pH 5. The complex particles effectively absorbed on oil droplet surfaces protecting the droplets against coalescence.[28] Another study compared the stability of emulsions stabilized by particles of single plant protein complexed with different types of polysaccharides.[29] In this study, hydrolyzed rice glutelin and xanthan gum or pectin were found to form smaller particles with better pH stabilities than the same protein complexed with Gum Arabic and alginate. Also,

emulsions containing xanthan gum were found to be more stable at high salt concentration than emulsions with pectin.[29] Covalently attaching polysaccharides to plant proteins is obviously more robust against changes in solution conditions than physical attachment. Indeed, many conjugates have been prepared that have excellent emulsification properties, as shown in Table 2.1. Obtaining good control over the molar mass and architecture of such conjugates however, is another matter.[27]

A second approach for stabilizing interfaces is by coating with (complex) coacervates, or by using complexation to form multilayer interfaces. Again, since many proteins are too hydrophobic to form (complex) coacervates of high water content, the use of this approach has not been reported yet for many plant proteins. Some examples exist (see for example[35]). For another example, complex coacervates formed by soy proteins and chitosan were shown to be effective for encapsulating algal oil. Based on isothermal titration calorimetry measurements, per molecule of soy protein 0.104 molecule of chitosan was enough to achieve optimal complexation pH 6. Rheological measurements show that the complex coacervate behaves as a viscoelastic material. Microcapsules made based on the soy protein chitosan complex coacervates show a better stability than microcapsules made by just soy protein coacervate alone. The stability of the complex coacervate microscapsules could be further improved by transglutaminase crosslinking.[36] Foams can also be stabilized by complex coacervates, and an example of foam stabilization by a plant protein–polysaccharide complex coacervate has recently been given. Foaming properties of a lentil legumin like protein with several polysaccharides (guar gum, pectin and xanthan gum) were investigated by Chen and co-workers.[34] They show that the foaming capacity was not greatly increased by combining the plant proteins with polysaccharides but that foam stability was significantly improved at mildly acidic pH. At pH 3, foams were found to be stabilized by a gel-like interfacial network of complex coacervate. At pH 5, stable foams are formed that are stabilized by a thick and stiff interfacial network formed by aggregates. At pH 7, the protein and polysaccharides are thermodynamically incompatible. This results in phase separation and disruption of the layer around the bubbles.[34] More examples can be found in Table 2.1.

2.4 Conclusions and Outlook

The low solubility of plant proteins are both a challenge and an opportunity for when trying to use plant protein/polysaccharide complexation for interfacial stabilization. The challenge is to either find proper solvents that allow for solution processing of dissolved plant proteins, or to find ways to use the plant proteins in a particulate form, after proper stabilization. The opportunity is that hydrophobic plant proteins, when associated with hydrophilic polysaccharides can be highly amphiphilic, and can be used to stabilize interfaces in various formats: Pickering stabilization using composite plant protein–polysaccharide colloidal particles, complex coacervates of plant proteins with polysaccharides, and multilayers formed by complexation of polysaccharides with interfacially bound plant proteins. The current work is still quite empirical and many papers are oriented towards single specific applications for a single plant protein/polysaccharide combination. We believe the further development of the use of plant protein polysaccharide complexation for interfacial stabilization would benefit from more fundamental research that addresses the more generic challenges and opportunities that we have addressed here by performing comparative characterization of the interfacial activity for ranges of related plant proteins and ranges of related hydrophilic polysaccharides. We hope this would lead to more generic rules that would allow us to use a broad range of complexes of plant proteins and polysaccharide for interfacial stabilization.

References

[1] Wijaya W, Patel AR, Setiowati AD, Van der Meeren P. Functional colloids from proteins and polysaccharides for food applications. Trends in Food Science & Technology. 2017;68:56–69.

[2] Ye A. Complexation between milk proteins and polysaccharides via electrostatic interaction: principles and applications – a review. International Journal of Food Science & Technology. 2008;43(3):406–415.

[3] de Oliveira FC, Coimbra JSdR, de Oliveira EB, Zuñiga ADG, Rojas EEG. Food Protein-polysaccharide Conjugates Obtained via the Maillard Reaction: A Review. Critical Reviews in Food Science and Nutrition. 2016;56(7):1108–1125.

[4] Joye IJ, Nelis VA, McClements DJ. Gliadin-based nanoparticles: Stabilization by post-production polysaccharide coating. Food Hydrocolloids. 2015;43:236–242.

[5] Hosseini SMH, Emam-Djomeh Z, Sabatino P, Van der Meeren P. Nanocomplexes arising

from protein-polysaccharide electrostatic interaction as a promising carrier for nutraceutical compounds. Food Hydrocolloids. 2015;50:16–26.

[6] Dickinson E. Interfacial structure and stability of food emulsions as affected by protein–polysaccharide interactions. Soft Matter. 2008;4(5):932–942.

[7] Rodríguez Patino JM, Pilosof AMR. Protein–polysaccharide interactions at fluid interfaces. Food Hydrocolloids. 2011;25(8):1925–1937.

[8] Azeredo HMC, Waldron KW. Crosslinking in polysaccharide and protein films and coatings for food contact – A review. Trends in Food Science & Technology. 2016;52:109–122.

[9] Le XT, Rioux LE, Turgeon SL. Formation and functional properties of protein–polysaccharide electrostatic hydrogels in comparison to protein or polysaccharide hydrogels. Advances in Colloid and Interface Science. 2017;239:127–135.

[10] Jost V, Stramm C. Influence of plasticizers on the mechanical and barrier properties of cast biopolymer films. Journal of Applied Polymer Science. 2016;133(2).

[11] Souzandeh H, Johnson KS, Wang Y, Bhamidipaty K, Zhong WH. Soy-Protein-Based Nanofabrics for Highly Efficient and Multifunctional Air Filtration. ACS Applied Materials & Interfaces. 2016;8(31):20023–20031.

[12] Shi X, Chen EX, Zhang J, Zeng H, Chen L. Fabrication of ultrathin conductive protein-based fibrous films and their thermal sensing properties. Journal of Materials Chemistry A. 2016;4(13):4711–4717.

[13] Fabian C, Ju YH. A Review on Rice Bran Protein: Its Properties and Extraction Methods. Critical Reviews in Food Science and Nutrition. 2011;51(9):816–827.

[14] Wang W, Tai F, Chen S. Optimizing protein extraction from plant tissues for enhanced proteomics analysis. Journal of Separation Science. 2008;31(11):2032–2039.

[15] van de Velde F, de Hoog EHA, Oosterveld A, Tromp RH. Protein-Polysaccharide Interactions to Alter Texture. Annual Review of Food Science and Technology. 2015;6(1):371–388.

[16] Lin D, Lu W, Kelly AL, Zhang L, Zheng B, Miao S. Interactions of vegetable proteins with other polymers: Structure-function relationships and applications in the food industry. Trends in Food Science & Technology. 2017;68:130–144.

[17] Braudo EE, Plashchina IG, Schwenke KD. Plant protein interactions with polysaccharides and their influence on legume protein functionality A Review. Food / Nahrung. 2001;45(6):382–384.

[18] Wan ZL, Guo J, Yang XQ. Plant protein-based delivery systems for bioactive ingredients in foods. Food & Function. 2015;6(9):2876–2889.

[19] Hu K, McClements DJ. Fabrication of biopolymer nanoparticles by antisolvent precipitation and electrostatic deposition: Zein-alginate core/shell nanoparticles. Food Hydrocolloids. 2015;44:101–108.

[20] Chang C, Wang T, Hu Q, Luo Y. Zein/caseinate/pectin complex nanoparticles: Formation and characterization. International Journal of Biological Macromolecules. 2017;104:117–124.

[21] Xu X, Luo L, Liu C, Zhang Z, McClements DJ. Influence of electrostatic interactions on behavior of mixed rice glutelin and alginate systems: pH and ionic strength effects. Food

Hydrocolloids. 2017;63:301–308.

[22] Cheng CJ, Jones OG. Stabilizing zein nanoparticle dispersions with ι-carrageenan. Food Hydrocolloids. 2017;69:28–35.

[23] Hu K, Huang X, Gao Y, Huang X, Xiao H, McClements DJ. Core–shell biopolymer nanoparticle delivery systems: Synthesis and characterization of curcumin fortified zein–pectin nanoparticles. Food Chemistry. 2015;182:275–281.

[24] Sun C, Xu C, Mao L, Wang D, Yang J, Gao Y. Preparation, characterization and stability of curcumin-loaded zein-shellac composite colloidal particles. Food Chemistry. 2017;228:656–667.

[25] Sun C, Dai L, Gao Y. Binary Complex Based on Zein and Propylene Glycol Alginate for Delivery of Quercetagetin. Biomacromolecules. 2016;17(12):3973–3985.

[26] Chen FP, Ou SY, Tang CH. Core–Shell Soy Protein–Soy Polysaccharide Complex (Nano)particles as Carriers for Improved Stability and Sustained Release of Curcumin. Journal of Agricultural and Food Chemistry. 2016;64(24):5053–5059.

[27] Dai L, Sun C, Wei Y, Mao L, Gao Y. Characterization of Pickering Emulsion Gels Stabilized by Zein/Gum Arabic Complex Colloidal Nanoparticles.

[28] Zeng T, Wu Zl, Zhu JY, Yin SW, Tang CH, Wu LY, et al. Development of antioxidant Pickering high internal phase emulsions (HIPEs) stabilized by protein/polysaccharide hybrid particles as potential alternative for PHOs. Food Chemistry. 2017;231:122–130.

[29] Xu X, Luo L, Liu C, McClements DJ. Utilization of anionic polysaccharides to improve the stability of rice glutelin emulsions: Impact of polysaccharide type, pH, salt, and temperature. Food Hydrocolloids. 2017;64:112–122.

[30] Yang Y, Cui SW, Gong J, Guo Q, Wang Q, Hua Y. A soy protein-polysaccharides Maillard reaction product enhanced the physical stability of oil-in-water emulsions containing citral. Food Hydrocolloids. 2015;48:155–164.

[31] Tamnak S, Mirhosseini H, Tan CP, Ghazali HM, Muhammad K. Physicochemical properties, rheological behavior and morphology of pectin-pea protein isolate mixtures and conjugates in aqueous system and oil in water emulsion. Food Hydrocolloids. 2016;56:405–416.

[32] Zhang B, Guo X, Zhu K, Peng W, Zhou H. Improvement of emulsifying properties of oat protein isolate–dextran conjugates by glycation. Carbohydrate Polymers. 2015;127:168–175.

[33] Pirestani S, Nasirpour A, Keramat J, Desobry S, Jasniewski J. Effect of glycosylation with gum Arabic by Maillard reaction in a liquid system on the emulsifying properties of canola protein isolate. Carbohydrate Polymers. 2017;157:1620–1627.

[34] Jarpa-Parra M, Tian Z, Temelli F, Zeng H, Chen L. Understanding the stability mechanisms of lentil legumin-like protein and polysaccharide foams. Food Hydrocolloids. 2016;61:903–913.

[35] Ducel V, Richard J, Saulnier P, Popineau Y, Boury F. Evidence and characterization of complex coacervates containing plant proteins: application to the microencapsulation of oil droplets. Colloids and Surfaces A: Physicochemical and Engineering Aspects. 2004;232(2):239–247.

[36] Yuan Y, Kong ZY, Sun YE, Zeng QZ, Yang XQ. Complex coacervation of soy protein with chitosan: Constructing antioxidant microcapsule for algal oil delivery. LWT. 2017;75:171–

179.

[37] Kaushik P, Dowling K, McKnight S, Barrow CJ, Adhikari B. Microencapsulation of flaxseed oil in flaxseed protein and flaxseed gum complex coacervates. Food Research International. 2016;86:1–8.

[38] Sağlam D, Venema P, van der Linden E, de Vries R. Design, properties, and applications of protein micro- and nanoparticles. Current Opinion in Colloid & Interface Science. 2014;19(5):428–437.

[39] Lam S, Velikov KP, Velev OD. Pickering stabilization of foams and emulsions with particles of biological origin. Current Opinion in Colloid & Interface Science. 2014;19(5):490–500.

[40] Donsì F, Voudouris P, Veen SJ, Velikov KP. Zein-based colloidal particles for encapsulation and delivery of epigallocatechin gallate. Food Hydrocolloids. 2017;63:508–517.

[41] Pan K, Zhong Q. Low energy, organic solvent-free co-assembly of zein and caseinate to prepare stable dispersions. Food Hydrocolloids. 2016;52:600–606.

[42] Dickinson E. Food emulsions and foams: Stabilization by particles. Current Opinion in Colloid & Interface Science. 2010;15(1):40–49.

[43] McClements DJ. Protein-stabilized emulsions. Current Opinion in Colloid & Interface Science. 2004;9(5):305–313.

[44] Ozturk B, McClements DJ. Progress in natural emulsifiers for utilization in food emulsions. Current Opinion in Food Science. 2016;7:1–6.

Chapter 3

Encapsulation Using Plant Proteins: Thermodynamics and Kinetics of Wetting for Simple Zein Coacervates

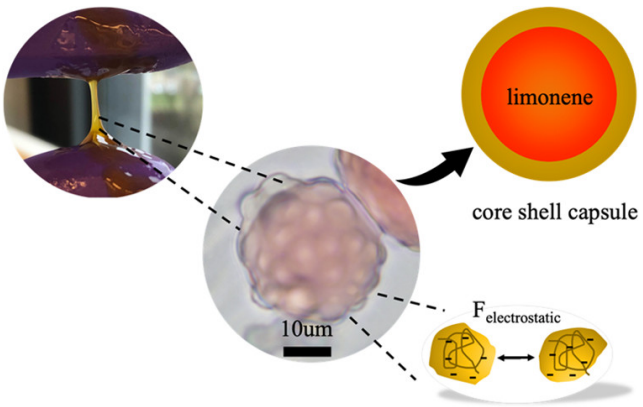

This chapter was published as:
Li, X., Erni, P., Van Der Gucht, J., & De Vries, R. (2020). Encapsulation using plant proteins: Thermodynamics and kinetics of wetting for simple zein coacervates. *ACS Applied Materials & Interfaces*, 12(13), 15802-15809.

Traditionally, complex coacervates of oppositely charged biopolymers have been used to form coatings around oil droplets for encapsulation of oil-soluble payloads. However, many proteins can form coacervates by themselves under certain conditions. Here, we revisit the well-known simple coacervates of prolamins such as zein in mixed solvents to explore whether they can be used for plant-based encapsulation systems. We show that, for zein in mixed water/propylene glycol (PG) solvents, we can encapsulate limonene droplets but only under specific conditions. We illustrate that this limitation is due to the very different physical properties of the simple zein coacervates as compared to those of the more extensively studied complex coacervates. Droplets of simple coacervates of zein can carry a significant net charge, whereas complex coacervates are usually close to being charge-balanced. In particular, we demonstrate that the spreading of zein coacervates at the interface of the droplets is thermodynamically favorable due to their extremely low interfacial tensions in both the dispersed (∼0.24 mN/m) and oil phases (∼0.68 mN/m), but the kinetics of coacervate droplet deposition and the interactions among coacervate droplets that oppose coacervate droplet coalescence are highly pH-dependent, leading to a sharp pH optimum (around pH 8) for capsule formation.

3.1 Introduction

Delivery and release of active ingredients by microcapsules is of great interest among others for pharmaceutical,[1] personal care,[2] and food applications.[3] Many strategies are available to formulate microcapsules. For instance, charged actives can be encapsulated by forming micelles with oppositely charged polymers,[4] and lipophilic molecules can be stabilized by surfactants or formulated as Pickering emulsions.[5] In some cases, the actives have also been covalently attached to the carrier materials.[6]

A classic technique for the microencapsulation of relatively hydrophobic active ingredients is by coating oil droplets with a thick layer of coacervate (the polymer dense phase of a liquid-liquid phase separated polymer system), which is subsequently cured to form a shell.[7, 8] This is an attractive technology since coacervation can bring large amounts of polymers to interfaces and can produce fine capsules with a very high loading efficiency (40-90%).[9]

For both food and nonfood applications, there is a strong interest in microencapsulation techniques that would rely on just abundantly available plant biopolymers and still have competitive performance. For most nonfood applications, the required performance objectives can currently only be achieved using

synthetic polymers. On the other hand, for food applications, the dominant approach to (coacervate-based) microencapsulation still involves the use of animal proteins. A case in point are the well-studied complex coacervates of weakly charged polysaccharides such as Gum Arabic with animal proteins such as gelatin or whey protein.[10]

Many of the most abundant plant storage proteins, such as the prolamins and globulins in leguminous plants, are poorly soluble in water.[11] Additionally, the production of industrial plant protein concentrates and isolates often involve processing steps that lead to irreversible denaturation of (part of) the proteins.[12] As a consequence of these factors, it is difficult to use proteins from these sources to formulate complex coacervates that can be used for microencapsulation. Previous studies show that some purified plant proteins (soy, pea, and wheat proteins) or certain fractions of them can be formulated into complex or simple coacervates for encapsulation.[13] Identifying suitable processing approaches to use the less soluble plant storage proteins for microencapsulation purposes would not only be interesting from the point of view of sustainability but also because their more hydrophobic nature may translate into better barrier properties.

One approach that has been quite extensively studied to use the less soluble plant storage proteins as physical barriers around oil droplets in oil-in-water emulsions is to create colloidal plant protein particles and use these to formulate Pickering emulsions.[14, 15] This requires careful tuning of the hydrophobic/hydrophilic balance of the particles, which has been achieved to some extent by also incorporating more hydrophilic biopolymers.[16] For example, the main storage protein of corn, zein, like other prolamins, is soluble in aqueous ethanol binary solvents due to its unique amino acid composition,[17] and this solubility behavior can be exploited to create colloidal zein particles by precipitation into aqueous (anti)solvents.[18] Velikov and co-workers reported that zein colloids, synthesized by such an anti-solvent precipitation method, can stabilize soybean oil-water interfaces.[5] Furthermore, colloidal stability of the emulsions itself could be improved by coating zein colloids with Gum Arabic.[19] However, Pickering stabilized emulsions usually rely on a large interfacial energy barrier between the oil and water phase plus a precisely tuned amphiphilicity of the

particles. This implies that, with this method, it is still challenging to encapsulate less hydrophobic and somewhat smaller molecules ($M_w \approx$ 100-250 g/mol). Moreover, interfacial layers formed by discrete solid particles remain porous for molecular-size payloads even at the maximum interfacial packing fraction, limiting their suitability as an interfacial permeation barrier.

In the past, it has been found that some plant proteins, under certain conditions, exhibit liquid-liquid phase separation into a protein dense (often called coacervate) and a protein dilute phase (often called excess phase). Simple coacervation is typically found in a narrow range of solution conditions in between one- and two-phase regions where dilute phases coexist with precipitates. For prolamins in mixed solvents, coacervates are found over a narrow range of solvent compositions.[17] Similarly, coacervation of leguminous globulins occurs for a narrow range of pH and salt concentrations.[12]

Therefore, a way forward in using the more hydrophobic plant storage proteins for encapsulation purposes might be to exploit the simple coacervates that they form. While encapsulation by complex coacervates has been studied extensively, encapsulation using simple coacervates has hardly been studied. Encapsulation of oil droplets by simple coacervates of soy glycinin has been discussed previously where core shell capsules were shown to be formed by slowly inducing coacervation.[20]

Complex and simple coacervate droplets however have intrinsically very different physical properties that will translate into a very different behavior in the encapsulation process, and so far, these differences have not been elucidated. For example, at the optimal mass ratio and pH, at which the yield of coacervate is maximal, complex coacervate droplets are nearly neutral,[10] so once they are formed, they have a tendency to aggregate and coalesce. On the other hand, simple coacervate droplets can carry net charges such that they can be kinetically stable and resist coalescence. Also, due to their hydrophobic nature, simple plant protein coacervates may tend to have higher protein contents and hence can have higher viscosities, which may also influence the kinetics of the encapsulation process.

To investigate this issue, we here study the thermodynamics and kinetics of wetting for simple coacervates of zein and demonstrate the encapsulation of a

low molecular weight hydrophobic molecule, limonene. Simple coacervation of zein is well known to occur in ethanol-water binary solvents,[17] but in many cases, ethanol will not be a suitable cosolvent in the encapsulation processes because it is miscible with many low weight hydrophobic molecules to be encapsulated, such as limonene. We therefore investigate propylene glycol as a cosolvent and identify the condition of zein coacervation in mixed propylene glycol-water solvents. Coacervation on oil droplets is induced by slowly adding water, coming from the one-phase region at high propylene glycol.

We show that, for a broad range of conditions, zein coacervate droplets thermodynamically want to wet the interface with the limonene, but that for most conditions, they are kinetically prevented from doing so. We also show, however, that special conditions do exist for which the formation of thick zein coacervate layers around the limonene droplets is kinetically possible.

3.2 Materials and Methods

3.2.1 Materials

Zein from corn (Z-3625), propylene glycol (W294004), (R)-(+)-Limonene (97%, 183164), Nile Red (7385-67-3), and Oil Red O (O0625) were bought from Sigma-Aldrich. Hydrochloric acid (1 and 0.1 N) and sodium hydroxide solutions (1 and 0.1 N) were used to adjust pH and were from Merck. Ethanol absolute (AR) was purchased from Biosolve BV. Milli-Q water was used in all experiments.

3.2.2 Phase Diagram

Eight stock solutions (with different φ_{PG}) were prepared as follows: for each stock solution, 2 g of zein was dissolved in 160, 140, 130, 120, 110, 100, 60, and 20 mL of PG (since it is already known that zein is soluble in pure PG or 80% v/v PG with water).[21] Next, 40, 60, 70, 80, 90, 100, 140, and 180 mL of water were gradually added to the zein solutions, respectively. In this way, the final volume of each stock solution was 200 mL with a constant zein concentration of 1% w/v. The pH of the stock solutions was adjusted to pH 10.0, 8.0, 5.3, and 2.6 using small amounts of hydrochloric acid (1 and 0.1 N) and sodium hydroxide solutions (1 and 0.1 N). The phase diagram is constructed based on both microscopic images

and macroscopic visual observation of the sample vials after spinning at 4500 rpm for 30 min. From optical microscopy, samples are considered to be in the two-phase coacervate region if they show transparent and spherical microscopic droplets. Samples that are completely clear in optical microscopy are considered to be in the one-phase region. Samples that show irregular microscopic particles and aggregates are classified as being in the two-phase precipitated region. Macroscopic visual observation of sample vials after centrifugation is required to be consistent with the microscopic observation: samples in the one-phase region have no sediment and a clear supernatant. Samples in the two-phase coacervate region have a viscous liquid phase, and samples in the two-phase precipitated region have a powdery, solid precipitate.

3.2.3 Coacervate Yield and Protein Fraction

Solutions with 2 g of zein dissolved in 40 mL of 80% v/v PG solvent were prepared. The pH of the zein solutions was adjusted to different values (pH 2.92, 3.47, 4.02, 4.53, 5.17, 6.07, 6.46, 7.13, 7.63, 8.00, 8.50, 9.11, 9.48, and 9.96) using hydrochloric acid (1 and 0.1 N) and sodium hydroxide solutions (1 and 0.1 N). Next, 10 mL of water was added to each solution (this dilution changes the pH by no more than ± 0.1), and all samples were centrifuged at 4500 rpm for 30 min at room temperature to accelerate the sedimentation of the zein coacervate. The zein coacervate was weighed after removing the supernatant, and the samples were freeze-dried to remove water. To completely remove PG, freeze-dried samples were redispersed in 10 mL of 80% v/v ethanol with water, 30 mL of water was added to precipitate zein into colloidal particles, and NaCl was added until a final concentration of 100 mM, which leads to aggregation of the colloidal zein. Next, the supernatant was removed using centrifugation. The process was repeated at least three times to thoroughly remove PG. Finally, samples were freeze-dried. The coacervate yield is the final weight (after freeze drying) divided by the initial amount of zein (2 g), and the mass fraction of protein in the coacervate is determined by dividing the final weight (after freeze drying) by the measured coacervate weight.

3.2.4 Rheology

Rheological measurements were performed with an Anton Paar rheometer 501 equipped with a Peltier element for temperature control. The temperature was controlled at 20 °C. A 25 mm plate-plate geometry with a gap size 0.5 mm was used. The coacervate samples with different pH (pH 7, 8, 9, and 10) were prepared as described previously. In 65% v/v PG, the supernatant was decanted after centrifugation and coacervate samples were transferred onto the plate. We measured viscosity of the coacervate samples as a function of a shear rate from 10^{-6} to 100 s^{-1} (viscosity was not measurable at shear rates around 5 s^{-1} due to wall slip). We performed a gentle pre-shear step (from 10^{-6} to 1 s^{-1}) and waited for 5 min before all measurements to make samples as homogeneous as possible and let samples stick to the plates. The shear stress was monitored to confirm that there is no shear history effect on the viscosity measurements.

3.2.5 Zeta Potential

Zeta potential was measured for zein colloids as a function of pH using a Zetasizer NanoZS apparatus (Malvern Instruments, UK) equipped with a 4 mW He-Ne 88 ion laser (λ = 633 nm). The zein colloids were prepared by an antisolvent precipitation method. The hydrodynamic size of the zein colloids was determined using dynamic light scattering, and a diameter was found to be around 100 nm. The zein colloids were dispersed in Milli-Q water, and various pH values (from pH 3.00 to 9.88) were achieved and adjusted by hydrochloric acid (1 and 0.1 N) and sodium hydroxide solutions (1 and 0.1 N). Each sample was measured three times at 20 °C, and the Smoluchowski equation was used for converting measured mobilities to zeta potentials.

3.2.6 Pendant Drop Measurements

Interfacial tensions between limonene and 65% v/v PG at pH 7, 8, 9, and 10 were measured with a drop tensiometer (Tracker from Teclis) using a reverse needle configuration. For all measurements, the droplet area is constant at 15 mm^2. Each sample was measured 20 times with a data acquisition rate of one measurement per second.

3.2.7 Surface Tension Determination via Capillary Thinning

We obtained the interfacial tensions of coacervate in its excess phase and in the oil phase using capillary thinning experiments, which have been previously described by Dardelle and Erni.[8] Capillary thinning experiments were performed with the zein coacervate prepared at pH 7 as described above. After centrifugation at 4500 rpm for 30 min, we reinjected the coacervate in its supernatant or limonene on a glass surface, and the thinning dynamics of filaments were recorded by a microscope camera and analyzed with ImageJ. For coacervate filaments at 65% v/v PG (pH 7) or limonene, we analyzed five samples by measuring the neck width as a function of time.

3.2.8 Microcapsule Preparation

Typically, 2 g of zein was dissolved in 80 mL of 80% v/v PG (65 mL of PG + 15 mL of water) in a 250 mL beaker, and 1 mL of limonene with Oil Red O predissolved (for staining) was added to be encapsulated. A magnetic stirrer was used to prevent limonene droplets from coalescing. The stir rate was typically at 430 rpm unless specifically mentioned. Hydrochloric acid (1 and 0.1 N) and sodium hydroxide solutions (1 and 0.1 N) were used to adjust the solutions to the desired pH (pH 3, 4, 5, 7, 8, 9, and 10). Then, 20 mL of water was dropwise added by a syringe pump (1 mL/min). pH changes due to the addition of water were less than $\pm$0.1 pH units.

3.2.9 CLSM (Confocal Laser Scanning Microscopy)

We used CLSM to map the distribution of limonene droplets within capsules. Fluorescent images were obtained using an inverted microscope system Eclipse Ti2 from Nikon. Limonene was stained with Nile Red ($\lambda_{ex} \approx$ 550 nm, $\lambda_{em} \approx$ 630 nm). Capsules for CLSM were synthesized at pH 8, as described above.

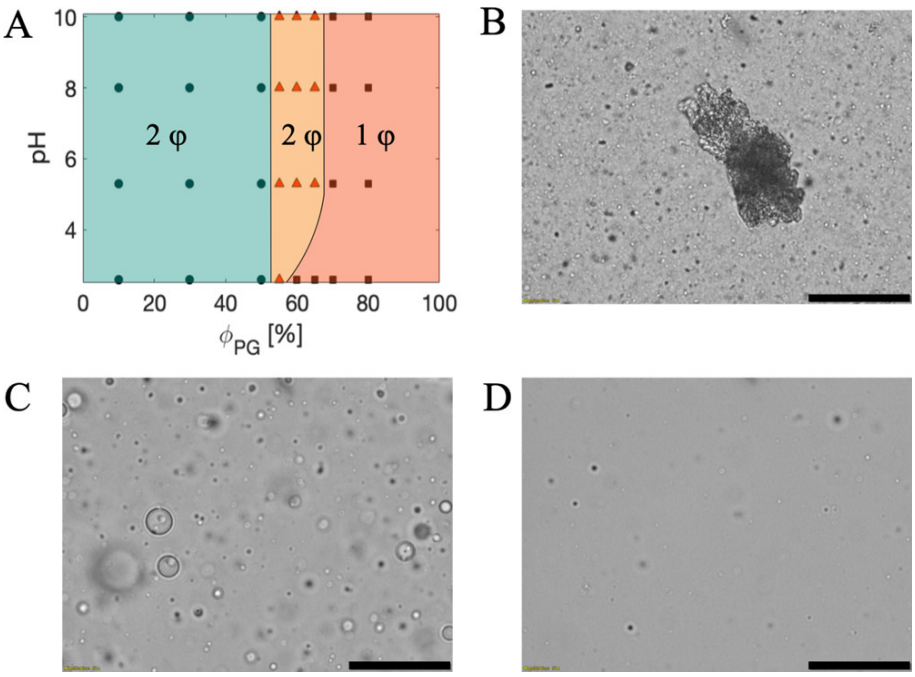

Figure 3.1: (A) Phase diagram for solubility of zein in propylene glycol-water binary solvents. Precipitation (circle), coacervation (triangle), and solution (square) are expressed as different symbols with the coacervate region highlighted in red. Solid lines denote the phase boundaries (note that the transitions are not very sharp). (B-D) Representative optical microscopy images of zein samples at pH 8 with different φ_{PG} of (B) 10%, two-phase, precipitated region; (C) 65%, two-phase, coacervated region; and (D) 80%, one-phase region. Scale bars are 50 μm.

3.3 Results and Discussion

3.3.1 Bulk Coacervate Properties

Ethanol-water, as the mostly used binary solvent, has the optimal condition for zein coacervate around 50% v/v ethanol (Figure 3.14). Zein has different solubility in PG-water. To use simple zein coacervate in a PG-water binary solvent, we made a phase diagram to locate precipitation, coacervation, and solution regions. As Figure 3.1A shows, the PG-water ratio has a strong impact on the solubility of zein. For a φ_{PG} between 0 and 50% v/v, zein precipitates, and between 50 and 70% v/v, we find a zein coacervate. Above 70% v/v, zein becomes soluble.

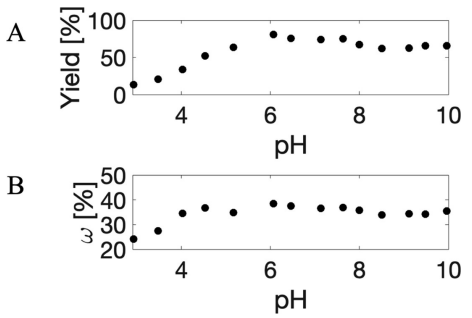

Figure 3.2: (A) Zein coacervate yield at 65% v/v PG and (B) protein mass fraction in coacervate versus pH.

Representative optical microscopy images of zein samples at pH 8 in the different regions are shown in Figure 3.1B-D. In part, because the zein is not completely pure, phase boundaries are not infinitely sharp, and we find narrow transition regions between the different regions (see Figures 3.10 and 3.11). For example, we find both precipitate and coacervate at 55% v/v for pH 2.6, 5.3, 8.0, and 10.0. In the coacervate region, the coacervate yield decreases when the solvent is approaching 70% v/v PG. We choose 65% v/v PG zein coacervates for producing capsules because, for this solvent composition, the supernatant is transparent and it has a good yield of coacervate (by visual observation). In the pH range that we have tested (from pH 2.6 to 10.0), we find that pH has only a minor effect on the solubility and phase behavior of zein. At pH 2.6, the zein coacervate disappears when φ_{PG} is around 60% v/v. This may be attributed to the increasing solubility as a result of the amide groups of glutamine and asparagine being hydrolyzed to carboxyl groups.[17, 22]

Coacervate yield and protein fraction were determined at various pH. As shown in Figure 3.2A, from pH 6 to 10, the decrease of coacervate yield is not significant, but from pH 6 to 4, there is a clear decrease. Figure 3.2B shows the mass fraction of protein in the coacervate. From pH 4 to 10, simple zein coacervate has a high protein mass fraction between 30 and 40%. At pH lower than 4, the protein mass fraction drops.

We measured the viscosity of zein coacervates with different pH at a wide range of shear rates. From Figure 3.3, we can see that zein coacervates have a Newtonian behavior at low shear rates below 10^{-1} s^{-1}. At higher shear rates, we

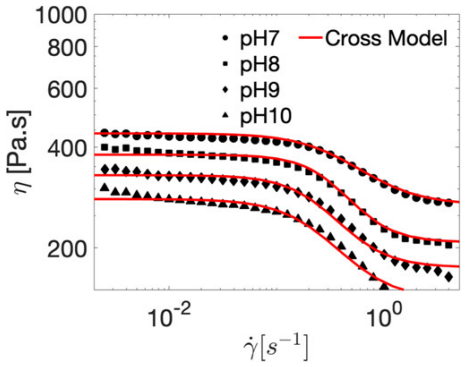

Figure 3.3: Viscosity of zein coacervates (produced from 65% v/v PG) versus shear rate. The red lines show Cross model fits. $\eta = \eta_\infty + (\eta_0 - \eta_\infty)/[1 + (C\dot{\gamma})^m]$ where η is the viscosity, C is the Cross model time constant, $\dot{\gamma}$ is the shear rate, and m is the Cross rate constant.

observe shear thinning followed by a high shear plateau viscosity. The magnitude of the viscosity and the onset of shear thinning are both markedly influenced by pH: at higher pH, when the zein molecules carry a higher net charge, viscosities are lower and shear thinning sets in at lower shear rates. Possibly, the increased net charge on the zein molecules decreases the cohesive energy of the coacervates, leading to the observed changes in the rheology. The absolute values of the viscosity that we found for the zein coacervates in the PG/water binary solvents are orders of magnitude larger than those found, for example, for gelatin-Gum Arabic complex coacervates[8] and simple soy protein coacervates.[23] At least, in part, this is caused by the much larger viscosity of the PG/water binary solvents. An empirical Cross model was used to fit the flow curves, in order to determine the zero-shear viscosities to be used to estimate interfacial tensions.

3.3.2 Surface Properties

We expect that the surface charge will play a significant role in determining how the coacervate droplets will coalesce. We cannot directly determine the electrophoretic mobility of coacervate droplets in 65% v/v PG since the coacervate droplets would have an extremely low mobility due to the high solvent viscosity, and they would most likely also coalesce and sediment during the measurements. Therefore, to obtain estimates of zein zeta potentials, we instead used

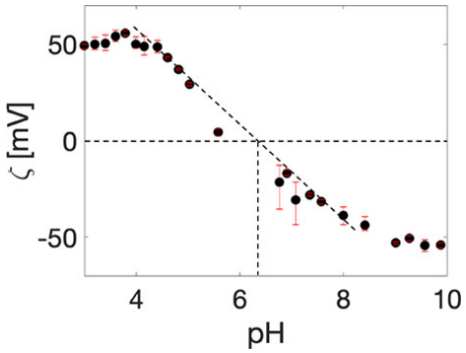

Figure 3.4: Zeta potential of zein colloids in water at various pH. Error bars are indicating variations of three measurements for each sample. A straight line is used to interpolate the data for pH values around the isoelectric point from which we estimate an isoelectric point of pI = 6.2.

zein colloids and measured their zeta potential in water at pH values from pH 3 to 9.88. Needless to say, this zeta potential may deviate from that of zein coacervate droplets in PG/water solvents, but we expect that at least the charge sign as a function of pH and the order of magnitude of the zeta potential should be the same. Results are shown in Figure 3.4. We find that the isoelectric point of zein is around pH 6.2, in agreement with earlier results of Velikov et al. Below the isoelectric point, zein is positively charged. From pH 6.2 to 10, the zeta potential gradually changes from 0 to -60 mV. Below the isoelectric point, from pH 6.2 to 4, there is a relatively sharper increase in the zeta potential from 0 to +60 mV. The absolute values of the zeta potential at pH 4 (+60 mV) and 10 (-60 mV) are very close. However, the coacervate yield at pH 4 is much lower than that at pH 10. This suggests that the zein behavior is not symmetric with respect to the distance to the pI and that zein is more soluble in acidic conditions in the PG/water binary solvent.

From a thermodynamic perspective, whether or not coacervate droplets wet limonene droplets in 65% v/v PG is determined by three interfacial tensions, as described by the spreading parameter S[24]

$$S = \gamma_{LP} - (\gamma_{CP} + \gamma_{CL})$$

where L stands for limonene, P for 65% v/v PG, and C for coacervate. When S

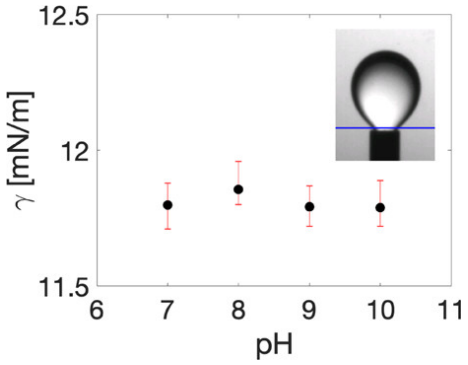

Figure 3.5: Interfacial tension between a limonene droplet and an aqueous PG solution (65% v/v) at different pH values. The inset figure shows the pendant drop setup with a reverse needle geometry.

> 0, coacervate droplets wet the interface completely, and when $S < 0$, coacervate droplets do not wet the interface. From the pendant drop measurements shown in Figure 3.5, we know that γ_{LP} is between 11.5 and 12 mN/m at pH 7, 8, 9, and 10. Due to the high viscosity of the zein coacervate and its low interfacial tension, it is experimentally more difficult to measure the interfacial tensions of zein coacervate with 65% v/v PG and limonene. Based on experience, the interfacial tension between coacervate and its coexisting phase is also expected to be very low. Spruijt and coworkers obtained the interfacial tension between a coacervate of two charged polyelectrolytes and its coexisting aqueous phase on the order of 100 μN/m.[25] Priftis and co-workers measured the interfacial tension of polypeptide coacervates lower than 1 mN/m.[26] Low interfacial tension values (4.2 $\pm$ 0.3 mN/m) between the coacervate and the continuous phase have also been obtained by Bago Rodriguez and co-workers through a series of calculations.[27]

Here, we estimate the interfacial tension (γ_{CP} and γ_{CL}) from capillary thinning dynamics using a method adapted from extensional rheology.[28] Generally, coacervate filaments spontaneously break up in a second fluid if their configuration is out of the static Rayleigh-Plateau stability limit.[29] This process is driven by the interplay of interfacial tension against viscous and elastic stress of the coacervate filament. To apply this method, two conditions need to be met. First,

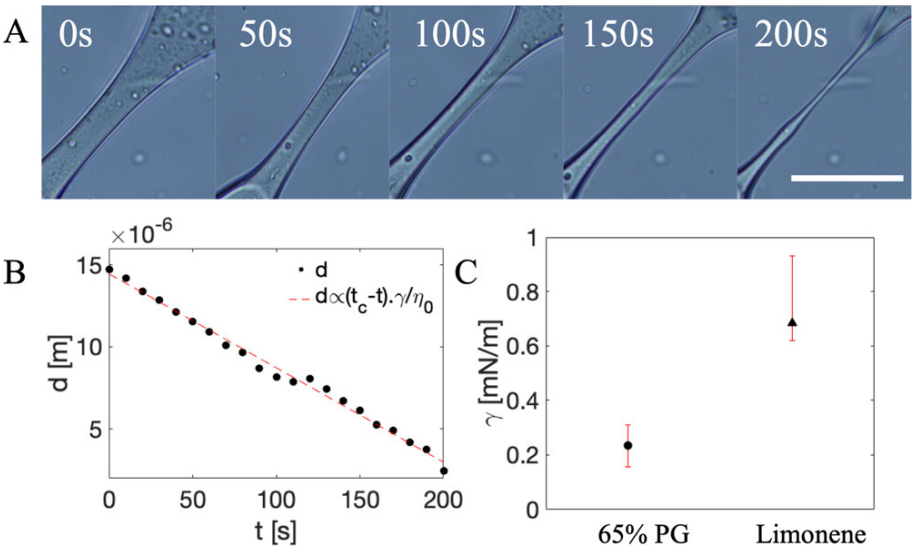

Figure 3.6: (A) Thinning process of a coacervate filament in 65% v/v PG at different time scales; the scale bar is 50 μm. (B) Thinning dynamics of a coacervate filament. Neck width of the filament in panel (A) as a function of time. The dashed line is a linear fit. (C) Calculated interfacial tensions of coacervate filaments in polymer depleted 65% v/v PG phase and limonene. Error bars are showing deviations among five measurements.

the visco-capillary time scale that determines the speed of the thinning process

$$t = \frac{\eta_0 d_0}{\gamma}$$

needs to be experimentally accessible. In this equation, η_0 is the zero-shear viscosity, d_0 is the initial neck width of the filament, and γ is the interfacial tension. This method is particularly interesting for coacervates because their low interfacial tension and their high viscosity[25, 30] will lead to a large visco-capillary time scale. Second, the Ohnesorge number Oh, which balances viscous against inertial forces should be large, that is, inertia should be negligible

$$Oh = \frac{\eta_0}{\sqrt{\Delta\rho\gamma d_0}} \gg 1$$

where $\Delta\rho$ is the buoyant density of the filament in the surrounding fluid.

Results for capillary thinning experiments are shown in Figure 3.6. Repres-

entative microscopy images of the thinning process for a coacervate filament in 65% v/v PG are shown in Figure 3.6A. Linear regression of the thinning dynamics (neck width d versus time) suggests that the coacervate filament behaves as a Newtonian fluid during thinning (Figure 3.6B). This is because if $Oh \gg 1$, then a filament of Newtonian fluid should undergo thinning at a constant velocity of $\nu \sim \gamma/\eta_0$. Any elastic response of the filament would lead to thinning with a non-constant velocity; hence, elasticity can be neglected and we can use the thinning model for a Newtonian fluid

$$\frac{d}{d_0} = f\frac{\gamma}{d_0\eta_0}(t_c - t)$$

where d is the neck width of a filament, γ is the interfacial tension, η_0 is the zero-shear viscosity, and t_c is the critical time scale for filament breakup. For the numerical constant f, we use f = 0.1418 as found from Papageorgiou's similarity solution for a Newtonian fluid undergoing capillary thinning.[31] We use the zero-shear viscosity, η_0 = 440 Pa·s at pH 7, as obtained from the rheology data using the Cross model fit (Figure 3.3). In contrast to capillary breakup extensional rheometry, where the data are fitted such that the rheological properties can be obtained for systems with a known interfacial tension, we use the inverse approach here: based on the independently measured rheological properties, we use the data here to calculate the interfacial tensions of zein coacervate in its coexisting phase (∼0.24 mN/m) and limonene (∼0.68 mN/ m), see Figure 3.6C. Replicates of the filament thinning dynamics in the excess phase or limonene oil are shown in Figures 3.12 and 3.13, respectively. Zein coacervates have a low interfacial tension with their coexisting phases and a slightly higher, but still very low, interfacial tension with the oil phase. Therefore, at pH 7, the spreading parameter S is clearly larger than zero such that complete wetting is thermodynamically favorable.

3.3.3 Capsule Formation

Next, we attempted to create droplets of limonene surrounded by a thick coacervate layer formed by the coalescence of coacervate droplets on the surface of the limonene droplets. First, the oil is dispersed in a one-phase zein solution

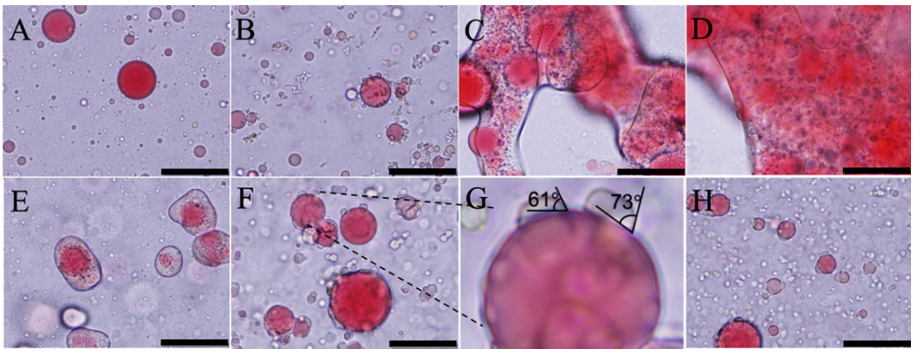

Figure 3.7: Light microscope pictures of capsules at (A) pH 3, (B) 4, (C) 5, (D) 7, (E) 8, (F) 9, and (H) 10. Limonene is stained with Oil Red O. The scale bars are 50 μm. (G) Zoom-in image of a pH 9 sample, showing two examples of contact angles between coacervate and oil droplets measured with ImageJ.

at 80% PG. Coacervation is then induced by slowly adding water, thus moving the system from the one phase region into the coacervate region at 65% PG. The result of this process is shown in Figure 3.7 for a range of pH values. Starting at a low pH, at pH 3, no capsules are observed, just the coexistence of oil droplets and very small coacervate droplets. At pH 4, in addition to coacervate droplets in the bulk, we also observe coacervate droplets that have adsorbed on the oil droplets but which did not spread. Next, at pH 5 and 7, we observe macroscopic coacervate, having engulfed almost all of the oil droplets. Moving further, at pH 8, well-defined capsules of coacervate around oil droplets are formed. Further increasing the pH leads to similar behavior as observed at very low pH: at pH 9 and 10, coacervate droplets attach to the surface of the oil droplets but do not spread.

The nonequilibrium nature of the spreading behavior of the coacervate is further illustrated by the zoom-in image of Figure 3.7G, for pH 9, where we show two examples of coacervate droplets attaching to the oil droplets with finite and very different contact angles (61 and 73°). Clearly, even though thermodynamically favorable, the spreading of the zein coacervate around the oil droplets does not occur easily due to kinetic barriers.

Our results clearly suggest that the electrostatic repulsion between zein coacervate droplets play an important role in determining the kinetics of coacer-

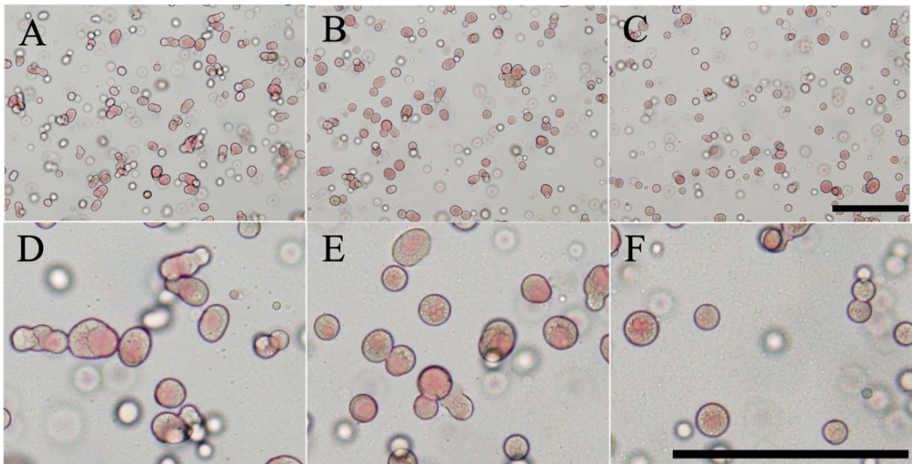

Figure 3.8: Light microscope pictures of capsules produced at pH 8 at a stirring rate of 430 rpm and further stirred for 10 min at the same or higher stirring rates. (A) 430, (B) 760, and (C) 1100 rpm. (D-F) Zoom-in figures of the left, respectively. Scale bars are 200 μm.

vate droplet attachment to and spreading on the oil droplets. For pH values far from the pI, the charge on the coacervate droplets prevent both attachment to the surface of the oil droplets and droplet fusion such that no capsules are formed. For pH values very close to the pI, on the other hand, at a low droplet charge, droplet fusion and spreading is easy and we end up with macroscopic coacervates engulfing the oil droplets. Successful capsule formation requires some droplet fusion while avoiding excessive coalescence, such that there is an optimal charge on the coacervate droplets. In principle, we would therefore expect pH windows for successful capsule formation on both sides of the pI. Here, we have only found such a pH window on the high side of the pI.

3.3.4 Influence of Local Shear Fields in Capsule Formation

Having established that the capsule formation is kinetically determined, we next investigate the role of local shear fields during the capsule formation process. We hypothesize that shear may aid in the coacervate droplet attachment if there are kinetic barriers and may also promote spreading. To test this hypothesis, we first produced capsules, as shown in Figure 3.7, using a fixed stirring speed of 430

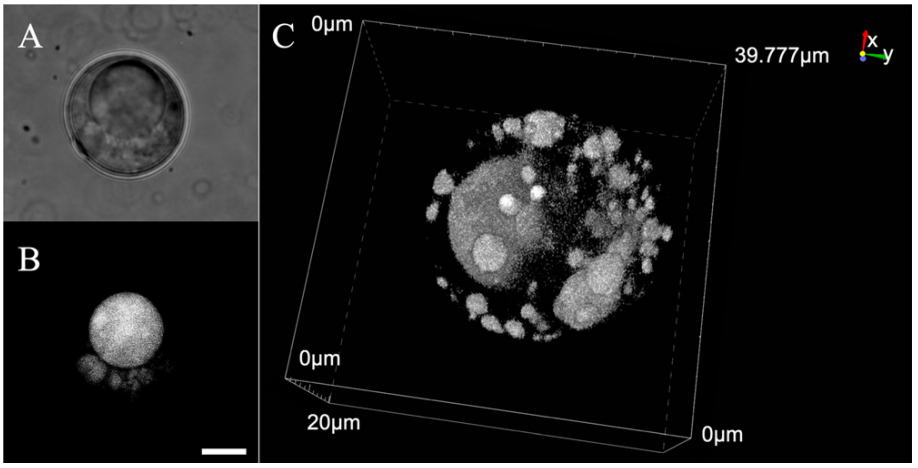

Figure 3.9: (A) Bright-field image of a capsule. (B) Corresponding CLSM image of the capsule in panel (A). Scale bar is 10 μm. (C) Three-dimensional construction of a capsule.

rpm. Next, capsules were stirred 10 more minutes at the same or higher stirring rates (430, 760, and 1100 rpm). Results are shown in Figure 3.8.

We find that capsules become smaller by the additional stirring at higher rates (presumably due to break up), but also more spherical, suggesting that, indeed, kinetic barriers for droplet spreading and coalescence can be overcome by shear forces.

The surface tension of the zein coacervates with the 65% PG solvent is very low (order 10^{-4} N/m), whereas its viscosity is very high (order 100 Pa·s). This implies that a critical capillary number of $Ca \approx 1$ corresponds to very low flow velocities of order 1 μm/s. Hence, even low amounts of shear should, in principle, be able to deform and break the zein coacervate droplets, although the kinetics may be very slow due to the high viscosity. For limonene, on the other hand, the viscosity is much lower than that of the coacervates, and its interfacial tension with the 65% PG solvent is much higher; hence, the coacervate droplets are much more likely to be deformed by shearing than the limonene droplets.

Finally, we used CLSM to more precisely visualize the oil distribution within the capsules. Figure 3.9A shows a bright-field image of a capsule, showing a large oil droplet covered by coacervate. Figure 3.9B shows the corresponding CLSM image from which it is clear that there are in fact multiple oil cores in the capsule.

Figure 3.9C shows a 3D construction of a capsule, indicating that this capsule contains a large oil core and some small oil droplets, which were encapsulated during coacervate coalescence. This multinuclear structure could lead to different release profiles with capsules only containing a single core. If mononucleated capsules are desired, then this could possibly be achieved by increasing the stirring rate.[32]

3.4 Conclusions

We have shown how simple coacervates of zein can be used to create capsules around oil droplets. As opposed to the generally much more hydrophilic animal proteins usually used to formulate complex coacervates for encapsulation, these plant proteins are quite water-insoluble and this may have advantages in terms of barrier properties. Here, we have used zein biopolymers as an example and found that, while thermodynamically, the spreading of zein coacervates droplets on oil droplets is highly favorable, the process is kinetically difficult. As a result of the high protein concentration and the high viscosity of PG, the dynamics of coacervate droplet spreading is extremely slow. In addition, simple zein coacervate droplets carry net charges, leading to electrostatic barriers, preventing droplet attachment to the surface of the oil droplets and the fusion of coacervate droplets. Also, if the droplet charge is too low, then the rapid macroscopic phase separation of the zein ensues and no capsules are formed either.

Nevertheless, by precisely tuning the charge on the coacervate droplets via the pH, it is possible to identify a window of solution conditions for which capsule formation is kinetically possible. We find that capsules can be formed at pH 8 and 65% v/v PG. Furthermore, we showed that high local shear fields can provide hydrodynamic forces to overcome some of the kinetic barriers and lead to smaller, more spherical capsules. Note that many oils (for example, soybean oil, coconut oil, and medium-chain triglycerides) are more hydrophobic than limonene. For all of these, the interfacial tension with PG-water should be higher, making the wetting process even more favorable. With limonene, we have therefore chosen a challenging case such that we expect the procedure should work for a wide range of other oils, too.

While, here, we focused on the thermodynamics and kinetics of the formation of zein coacervate layers around oil droplets, for real applications, the mechanical properties of such capsules will need to be further enhanced by cross-linking. Also, it will be very interesting to see whether, indeed, barrier properties for cross-linked zein capsules are notably different from capsules produced from, e.g., gelatin-Gum Arabic complex coacervates.[7] Finally, since many plant seed storage proteins form simple coacervates, our results point to many new opportunities for using plant proteins for encapsulation.

References

[1] Liao WC, Sohn YS, Riutin M, Cecconello A, Parak WJ, Nechushtai R, et al. The Application of Stimuli-Responsive VEGF- and ATP-Aptamer-Based Microcapsules for the Controlled Release of an Anticancer Drug, and the Selective Targeted Cytotoxicity toward Cancer Cells. Adv Funct Mater. 2016;26:4262.

[2] de Souza HJB, de Barros Fernandes RVB, Borges SV, Felix PHC, Viana LC, Lago AMT, et al. Utility of Blended Polymeric Formulations Containing Cellulose Nanofibrils for Encapsulation and Controlled Release of Sweet Orange Essential Oil. Food Bioprocess Technol. 2018;11:1188.

[3] Lamprecht A, Schäfer U, Leh CM. Influences of process parameters on preparation of microparticle used as a carrier system for O - 3 unsaturated fatty acid ethyl esters used in supplementary nutrition. J Microencapsulation. 2008;18:347.

[4] Nolles A, Westphal AH, De Hoop JA, Fokkink RG, Kleijn JM, Van Berkel WJH, et al. Encapsulation of GFP in Complex Coacervate Core Micelles. Biomacromolecules. 2015;16:1542.

[5] De Folter JWJ, Van Ruijven MWM, Velikov KP. Oil-in-Water Pickering Emulsions Stabilized by Colloidal Particles from the Water-Insoluble Protein Zein. Soft Matter. 2012;8:6807.

[6] Wang K, Arntfield SD. Binding of Carbonyl Flavours to Canola, Pea and Wheat Proteins Using GC/MS Approach. Food Chem. 2014;157:364.

[7] Dardelle G, Jacquemond M, Erni P. Delivery Systems for Low Molecular Weight Payloads: Core/Shell Capsules with Composite Coacervate/Polyurea Membranes. Adv Mater. 2017;29:1.

[8] Dardelle G, Erni P. Three-Phase Interactions and Interfacial Transport Phenomena in Coacervate/Oil/Water Systems. Adv Colloid Interface Sci. 2014;206:79.

[9] Zuidam NJ, Velikov KP. Choosing the Right Delivery Systems for Functional Ingredients in Foods: An Industrial Perspective. Curr Opin Food Sci. 2018;21:15.

[10] De Kruif CG, Weinbreck F, De Vries R. Complex Coacervation of Proteins and Anionic Polysaccharides. Curr Opin Colloid Interface Sci. 2004;9:340.

[11] Carbonaro M, Cappelloni M, Nicoli S, Lucarini M, Carnovale E. Solubility–Digestibility Relationship of Legume Proteins. J Agric Food Chem. 1997;45:3387.

[12] van Megen WH. Solubility Behavior of Soybean Globulins as a Function of PH and Ionic Strength. J Agric Food Chem. 1974;22:126.

[13] Nesterenko A, Alric I, Silvestre F, Durrieu V. Vegetable Proteins in Microencapsulation: A Review of Recent Interventions and Their Effectiveness. Ind Crops Prod. 2013;42:469.

[14] Liu F, Tang CH. Soy Protein Nanoparticle Aggregates as Pickering Stabilizers for Oil-in-Water Emulsions. J Agric Food Chem. 2013;61:8888.

[15] Liang HN, Tang C. Pea Protein Exhibits a Novel Pickering Stabilization for Oil-in-Water Emulsions at PH 3.0. LWT - Food Sci Technol. 2014;58:463.

[16] Li X, de Vries R. Interfacial Stabilization Using Complexes of Plant Proteins and Polysaccharides. Curr Opin Food Sci. 2018;21:51.

[17] Shukla R, Cheryan M. Zein: the Industrial Protein from Corn. Ind Crops Prod. 2001;13:171.

[18] Filippidi E, Patel AR, Bouwens ECM, Voudouris P, Velikov KP. All-Natural Oil-Filled Microcapsules from Water-Insoluble Proteins. Adv Funct Mater. 2014;24:5962.

[19] Dai L, Sun C, Wei Y, Mao L, Gao Y. Characterization of Pickering Emulsion Gels Stabilized by Zein/Gum Arabic Complex Colloidal Nanoparticles. Food Hydrocolloids. 2018;74:239.

[20] Lazko J, Popineau Y, Legrand J. Soy Glycinin Microcapsules by Simple Coacervation Method. Colloids Surf, B. 2004;37:1.

[21] Lawton JW. Zein: A History of Processing and Use. Cereal Chem. 2002;79:1.

[22] Li Y, Li J, Xia Q, Zhang B, Wang Q, Huang Q. Understanding the Dissolution of α-Zein in Aqueous Ethanol and Acetic Acid Solutions. J Phys Chem B. 2012;116:12057.

[23] Lui DYM, Litster JD, White ET. Precipitation of Soy Proteins : Particle Formation and Protein Separation. AIChE J. 2007;53:2.

[24] Torza S, Mason SG. Three-Phase Interactions In Shear and Electrical Fields. J Colloid Interface Sci. 1970;33:67.

[25] Spruijt E, Sprakel J, Cohen Stuart MA, Van Der Gucht J. Interfacial Tension between a Complex Coacervate Phase and Its Coexisting Aqueous Phase. Soft Matter. 2010;6:172.

[26] Priftis D, Farina R, Tirrell M. Interfacial Energy of Polypeptide Complex Coacervates Measured via Capillary Adhesion. Langmuir. 2012;28:8721.

[27] Bago Rodriguez AM, Binks BP, Sekine T. Emulsion Stabilisation by Complexes of Oppositely Charged Synthetic Polyelectrolytes. Soft Matter. 2018;14:239.

[28] McKinley GH. Visco-Elasto-Capillary Thinning and Break-Up of Complex Fluids. Annu Rheol Rev. 2005; p. 1.

[29] Mora S, Phou T, Fromental JM, Pismen LM, Pomeau Y. Capillarity Driven Instability of a Soft Solid. Phys Rev Lett. 2010;105:1.

[30] Liu Y, Winter HH, Perry SL. Linear Viscoelasticity of Complex Coacervates. Adv Colloid Interface Sci. 2017;239:46.

[31] Papageorgiou DT. On the Breakup of Viscous Liquid Threads. Phys Fluids. 1995;7:1529.

[32] Lemetter CYG, Meeuse FM, Zuidam NJ. Control of the Morphology and the Size of Complex Coacervate Microcapsules during Scale-Up. AIChE J. 2009;55:1487.

3.5 Appendix

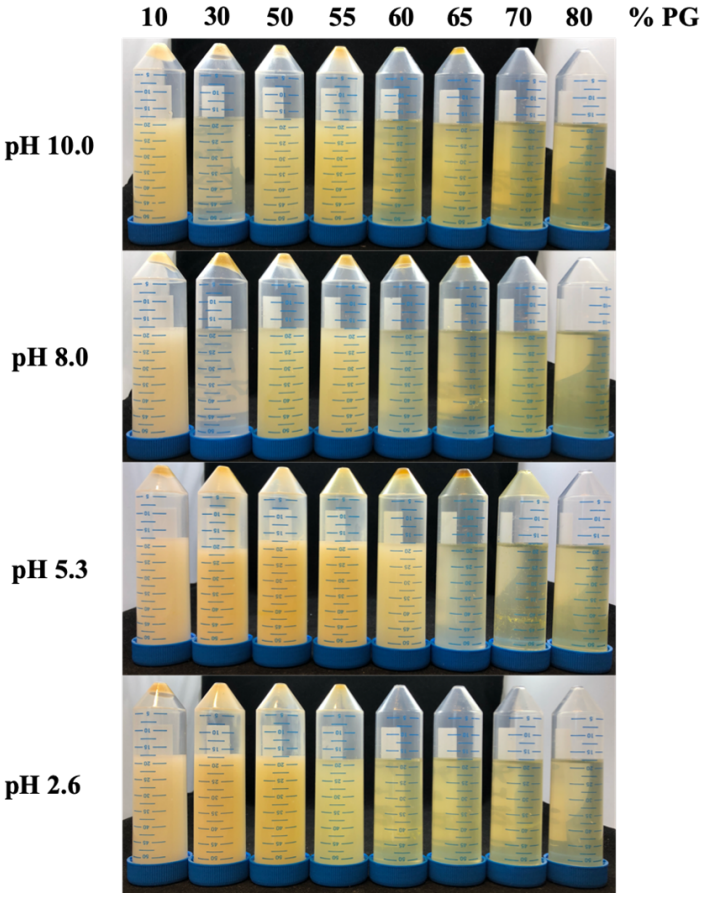

Figure 3.10: Sample vials for determining the phase diagram. The φ_{PG} and pH are indicated in the figure, from left to right (10, 30, 50, 55, 60, 65, 70, 80%), from top to bottom (pH 10.0, 8.0, 5.3, 2.6).

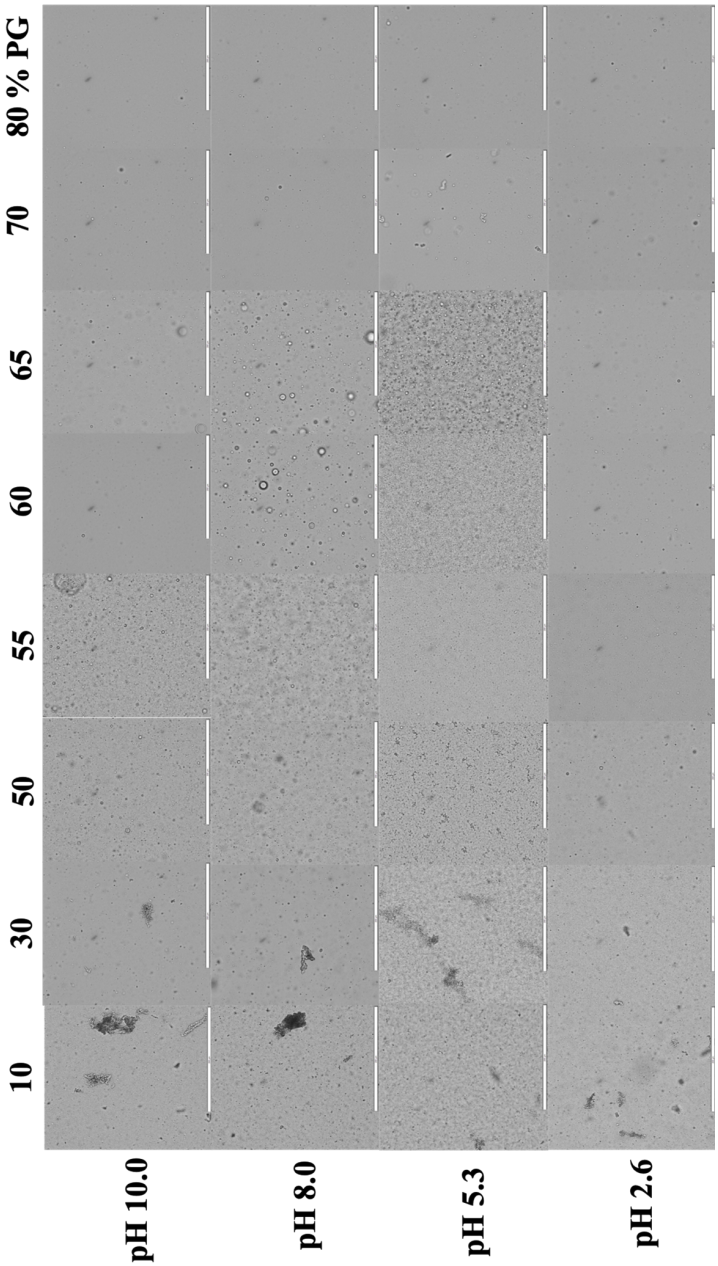

Figure 3.11: Microscopic images for determining the phase diagram. The φ_{PG} and pH are indicated in the figure. The scale bar is 200 μm.

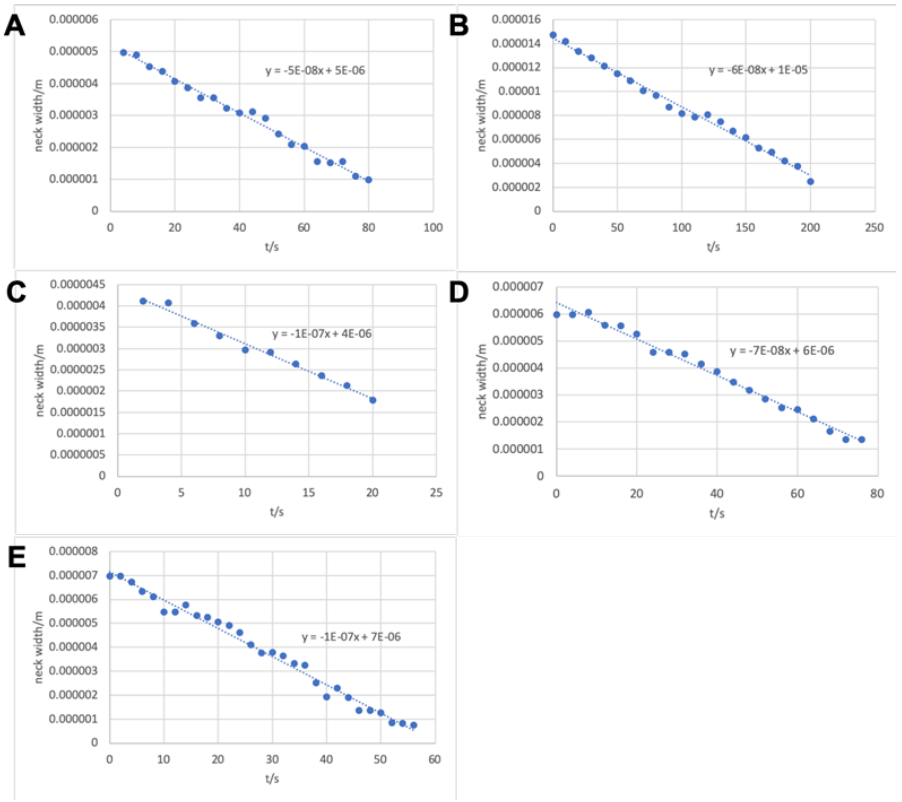

Figure 3.12: Coacervate filament thinning dynamics in excess phase at pH 7, measured neck width as a function of time. Different panels are replicates.

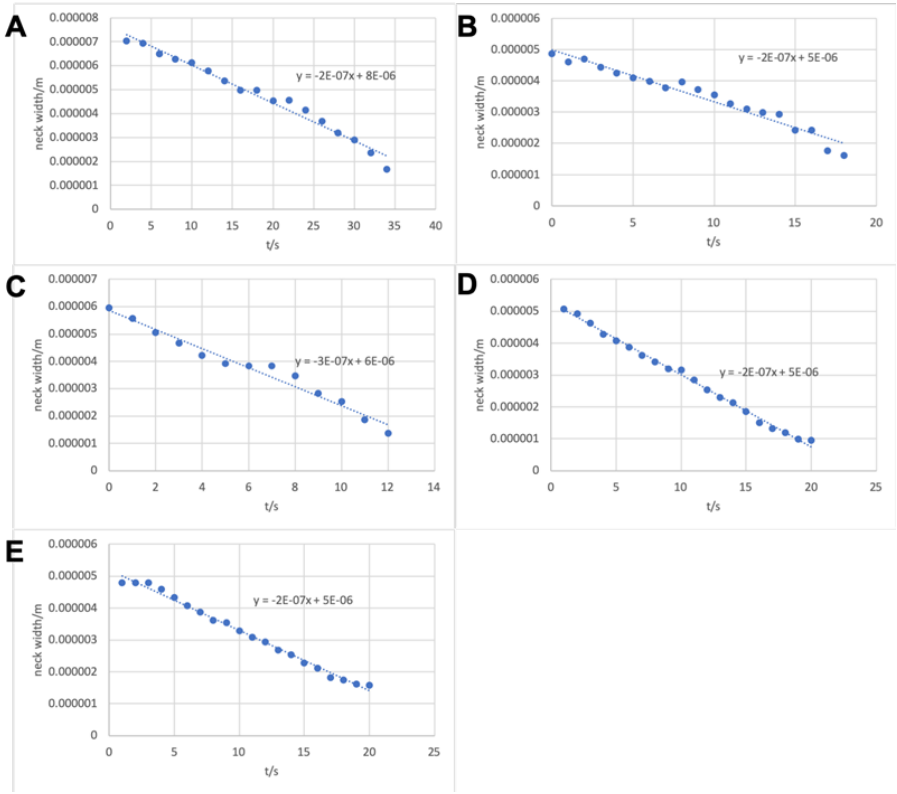

Figure 3.13: pH 7 coacervate filament thinning dynamics in limonene, measured neck width as a function of time. Different panels are replicates.

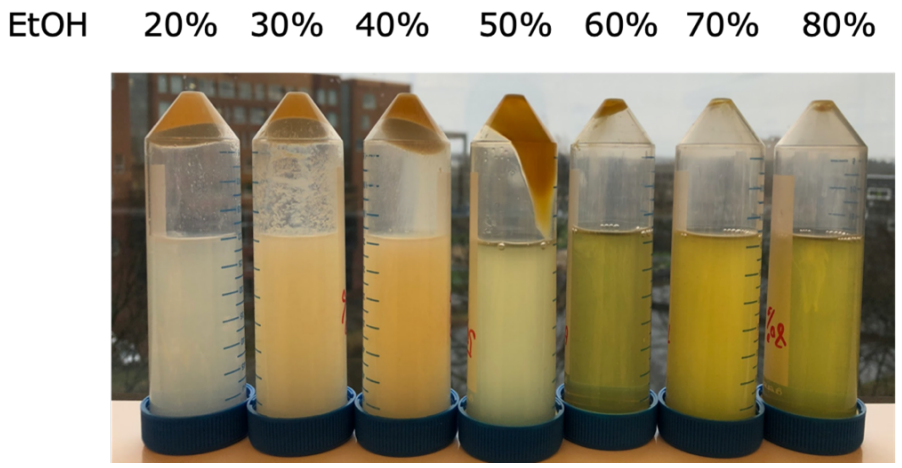

Figure 3.14: Sample vials of zein in ETOH (ethanol)/water binary solvents at pH 8. Protein concentration was kept in constant for all vials. The φ_{ETOH} is indicated in the figure, from left to right (20, 30, 40, 50, 60, 70, 80%).

Chapter 4

Core-Shell Microcapsules from Unpurified Legume Flours

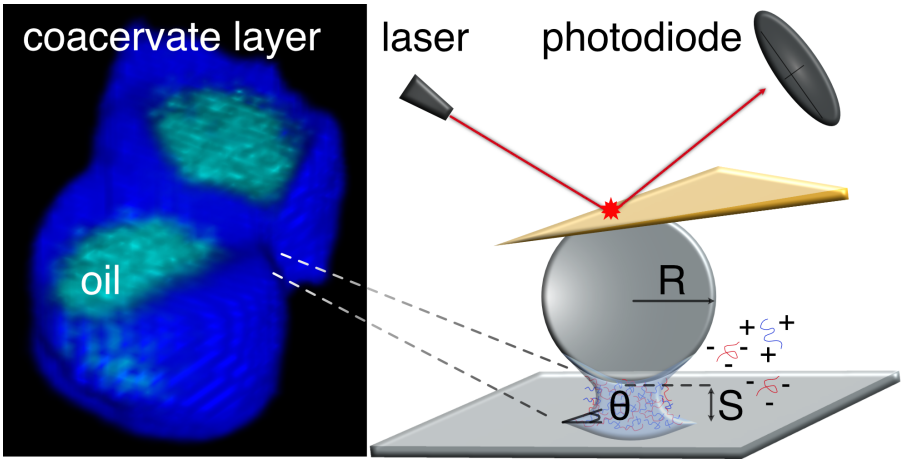

This chapter was published as:
Li, X., Van Der Gucht, J., Erni, P., & De Vries, R. (2021). Core-Shell Microcapsules from Unpurified Legume Flours. *ACS Applied Materials & Interfaces*, 13(31), 37598-37608.

Plant-based ingredients are key building blocks for future sustainable advanced materials. Functionality is typically higher for highly purified plant-based ingredients, but this is at the expense of their sustainability value. Here, a method is introduced for creating a soft functional material, with structural elements ranging from the nanometer to the millimeter scale, directly from legume flours. Globulins from soy and pea flours are extracted in their native state at acidic pH and mixed with Gum Arabic, resulting in liquid-liquid phase separation into a dilute phase and a viscoelastic complex coacervate. Interfacial tensions of the coacervates, determined via AFM-based probing of capillary condensation, are found to be very low (γ = 48.5 and 32.3 μN/m for resp. soy and pea), thus promoting the deposition of a shell of coacervate material around oil droplets. Despite the complex nature of the starting material, the dependence of interfacial tensions on salt concentrations follows a scaling law previously shown to hold for model complex coacervates. Curing of the coacervate material into a strong and purely elastic hydrogel is shown to be possible via simple heating, both in bulk, and as a shell around oil droplets, thus providing proof of principle for the fabrication of precise core-shell microcapsules directly from Legume flours.

4.1 Introduction

For future sustainable materials, increasing attention is being directed to plants as a source of raw starting material.[1, 2, 3, 4] Either these can be converted into biobased chemicals via microbial fermentation, such as fuel from biomass conversion,[5, 6] or one can try to directly utilize polymers from plants to fabricate plant-based materials for medical applications, functional coatings, drug delivery, food and nutrition.[7, 8, 9] One of the challenges with the latter approach is the complexity of plant-based ingredients. For clear structure-property relations and rational materials design one would expect that it would be best to work with purified plant polymers, but extracting pure polymers from raw plant-based ingredients is both complex and costly.[10] Additionally, and maybe even more importantly, such purification efforts use only part of the plant materials and often require substantial water and energy. Hence they are at odds with the sustainability value of plant-based materials. Therefore, there is an urgent need for more sustainable methods to extract the target ingredients from plants[11] or easier ways to create well defined functional materials starting directly from raw plant materials.[12, 13]

A case in point are core-shell microcapsules, which consist of a polymer shell with a cargo encapsulated as the core. They have a wide range of applications in

pharma, food- and personal care.[14, 15, 16] One of the approaches to fabricate core-shell microcapsules is via coacervation: liquid-liquid phase separation in polymer solutions where one of the phases is highly concentrated in polymer and the other phase is extremely dilute in polymer. The concentrated coacervate phase typically still contains a significant fraction of solvent and hence has a very low interfacial tension with the excess phase. As a consequence, coacervates typically wet a wide range of materials. By slowly moving from the one-phase region into the two-phase region, it is possible to deposit a coacervate shell around, for example, oil droplets. Core-shell capsules are created by subsequently curing such coacervate liquid shells into an elastic material.[17]

A specific case of coacervation is complex coacervation, where electrostatic attraction between oppositely charged polymers drives coacervation. These phenomena were first systematically studied by De Jong and Bungenberg in 1932[18] and have since then been investigated for many types of mixtures of oppositely charged water soluble macromolecules, such as proteins, colloids and polysaccharides.[19] As for coacervates in general, complex coacervates have a high polymer content (typically between 10 and 40% w/w) while remaining liquid. They have very low interfacial tensions with their excess phases (of order 100 μN/m).[20] These features make complex coacervates appealing not only to fabricate core-shell capsules for drugs, nutrients and flavors,[21] but also, for example, as underwater adhesives and coatings.[22]

For many applications of core-shell microcapsules, naturally sourced polymers (proteins and polysaccharides) are preferred if they can provide same functionalities as their counterparts from synthetic routes.[23] But often, the latter is not the case. Nevertheless, gelatin has been widely used at an industrial scale for core-shell microcapsules fabricated via complex coacervation.[17] For reasons of sustainability and consumer preference, many researchers are now attempting to use just plant-based proteins and polysaccharides for fabricating core-shell microcapsules via complex coacervation. Indeed, several plant proteins, such as soy, pea, canola and flaxseed proteins, show the potential to form complex coacervates with a variety of polysaccharides, for instance, Gum Arabic, alginate, chitosan and pectin.[24, 25] However, using plant proteins to formulate complex coacervates at a large scale, for use in industrial applications is still

challenging.[9] Challenges include the often rather poor solubility of commercial protein isolates from major plant protein sources, such as leguminous plants, and their low functionality, which is at least in part due to current plant protein purification methods, that lead to a large degree of protein denaturation and aggregation. Hence they are often difficult to dissolve down to the single protein level, which is essential for obtaining homogeneous complex coacervates rather than co-precipitates.

In a recent study,[10] Tanger et al. compared three commonly used extraction methods for pea proteins: alkali extraction followed by isoelectric precipitation, micellar precipitation and salt extraction followed by dialysis. They show that both solubilization and precipitation steps have an impact on the protein conformation. Proteins are denatured in the solubilization step, while irreversible and reversible aggregation occur at the precipitation step. Alkali extraction with isoelectric precipitation is the most efficient and common method in industry.[26] However, the isoelectric precipitation causes most irreversible aggregates, as also reported elsewhere.[27] The other two methods use the salting-in effect, which dissolves proteins in high salt conditions. For micellar precipitation, the solution with high salt concentration is quickly diluted in cold water, and proteins tend to form micelles and precipitates. These proteins can be resolubilized at a high salt concentration, which is not favorable for complex coacervation. The last one is the mildest method among the three, but the dialysis step takes much longer time and costs more, which make this method often only used in labs, but less preferred in industry. Not surprisingly therefore, many studies on complex coacervation of plant proteins and polysaccharides have been performed not with industrially available protein isolates, but rather with plant proteins purified to a high degree using more gentle lab-scale methods.[28, 29, 30] Since many of these studies have been motivated by practical/technical/medical applications, so scalability is an important aspect, which our work presented here addresses.

Understanding the effect of compositional parameters, extraction pathways and physicochemical interactions on the structural and mechanical characteristics of the resulting coacervates is key for the rational design of coacervate capsules that are suitable as delivery systems in the applications outlined above.

The main innovation we present here, to allow for core-shell capsule formation directly from legume flours, is to use acid-extraction of the proteins from the legume flour rather than alkali extraction. The latter inevitably leads to protein denaturation that is incompatible with the formation of homogeneous complex coacervates. In the acidic environment, the plant proteins can directly form complex coacervates with weakly anionic polymers, such as Gum Arabic.[31] Because globulins, the main fraction from leguminous seed proteins, carry positive net charges below their isoelectric points (mostly below 5), and most polysaccharides are anionic polymers in a wide pH range. Thus, the narrow window for their complex coacervation is typically located at low pH. Furthermore, by never exposing the proteins to pH close to their isolectric point (around pH 5), they retain their native and soluble state suitable for making homogeneous complex coacervates. In view of their extremely low interfacial tensions, quantitation of the interfacial behavior of complex coacervates, which is crucial for their application in core-shell microcapsule fabrication, is challenging. Previously, it has been shown that Colloidal Probe Atomic Force Microscopy (CP-AFM) allows for a detailed analysis of the capillary condensation of model coacervates. This capillary condensation occurs in the nano-scale gap between colloids and a nearby macroscopically flat surface.[32, 20, 33, 34] Surprisingly, we find that the CP-AFM technique works equally well for the highly impure mixtures that we use here. As methodological innovation, we show that dissipation due to coacervate viscosity makes a non-negligible contribution to the force at finite retraction speeds, and we show how to correct for this effect to obtain more accurate determinations of the coacervate interfacial tensions.

4.2 Results and Discussion

We choose two industrial legume crops, soy and pea, as representative plant protein sources to show suitability of the processing methodology for the variability coming with different protein sources. First we show that neither commercial pea- and soy protein isolates nor proteins alkali-extracted from pea- and (defatted) soy flour are suitable for making homogeneous complex coacervates with Gum Arabic. Next we analyze in detail the acid extraction of proteins from pea-

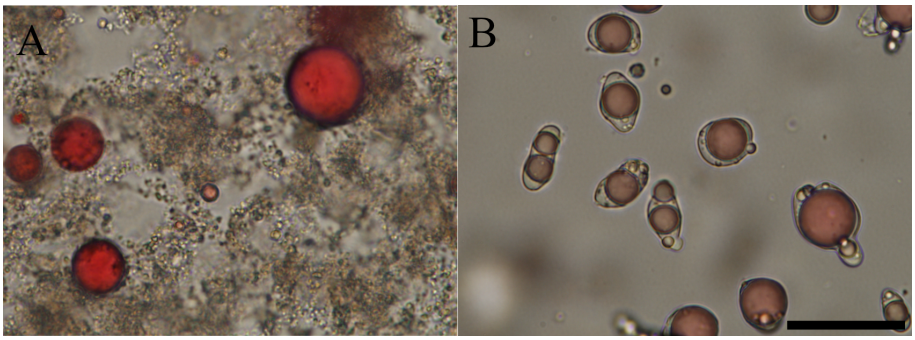

Figure 4.1: Representative optical microscope images showing the complex formation and interfacial affinity of (A) Alkali extracted pea protein with chitosan at pH 5.8, (B) Acid extracted soy protein with Gum Arabic at pH 3. Oil phase was dyed with Oil Red O. The scale bar is 50 μm.

and soy flours, study complex coacervation of the extracted proteins with Gum Arabic, and study the interfacial properties as well as the mechanical properties of the coacervates (both before and after heating). Finally we demonstrate core-shell microcapsule formation, and the successful heat-induced curing of the shells.

4.2.1 Comparison Study on Complex Formation

While in principle one could try to make complex coacervates at either side of the isoelectric point of plant proteins (around pH 5 for the pea- and soy proteins that we consider here), in practice one is limited by the availability of suitable polysaccharides that have opposite signs of the charge (as compared to the proteins) at these pH values. Quite a few plant polysaccharides are available (such as Gum Arabic, or pectins) that still have a weak negative charge at low pH, say at pH 3. These are ideal for complex coacervate formation with the pea- and soy proteins, that are positively charged at low pH. Here we use Gum Arabic, which has been very well characterized with respect to its complex coacervation behavior with proteins at low pH.[19] Note that weakly charged rather than highly charged polysaccharides are optimal, since the latter induce solid-liquid phase separation (or precipitation) rather than liquid-liquid phase separation (or complex coacervation).[19, 35] At higher pH values, above the isoelectric point

of the plant proteins, the proteins are negatively charged. Very few polysaccharides exist that are weakly positively charged at relatively high pH, as required to form complex coacervates with plant proteins, which are negatively charged at pH values above their isolectric points. One of the few that is available is chitosan, which is a chemically modified version of the natural polysaccharide chitin. However, chitosan is only soluble at pH values below about 6.[36] This then leaves a rather narrow window of pH values, in between the solubility limit of chitosan and the isoelectric point of the plant proteins, where complex coacervates of chitosan and plant proteins may potentially form. For exploring complex coacervation of pea- and soy proteins above their isoelectric point, we here use chitosan at pH 5.8, a pH in between the pea- and soy protein isoelectric point and the solubility limit of the chitosan. In addition, although polysaccharides can still interact with proteins close to the isoelectric point, their weak interactions usually lead to the formation of soluble complexes even if the protein can still remain high solubility.[37] Therefore, the pH range close to the isoelectric point is not considered in our study.

First we study the complexation behavior of commercial isolates of pea- and soy protein. As shown in Figure 4.13, the commercial protein isolates are not completely soluble, neither at pH 3, nor at pH 5.8: the solutions remain turbid. Microscopy images of mixtures of these protein dispersions at pH 3 with Gum Arabic, and mixtures of the protein dispersions at pH 5.8 with Chitosan, are shown in Figure 4.14. For both cases, we observe solid precipitates rather than liquid complex coacervates. This may very well be related to the presence of the larger protein aggregates, that will have very different complexation behaviour with the polysaccharides as compared to molecularly dispersed proteins.

Next we compare the complexation with these commercially available protein isolates to proteins directly extracted from soy and pea flours. We again consider the two cases of positively charged proteins at pH 3 and negatively charged proteins at pH 5.8. First we use alkali extraction (at pH 8) of proteins from soy and pea flour, followed by a change of pH to pH 5.8 to ensure (marginal) solubility of the oppositely charged chitosan. Figure 4.1A shows a typical example of alkali extracted proteins complexing with chitosan at pH 5.8: we find the formation of solid precipitates that have little affinity for the water oil interface. Next,

Table 4.1: Protein yield from extraction

Type	Protein content in flour [%]	Protein content in extract [%]	Extracted protein from total protein content in flour [%]	Literature comparison [%]
soy	53.6	52.6	53.9	60-70 (from alkali extraction)[38]
pea	11.6	29.9	43.2	80 (from alkali extraction)[39]

we use acid extraction (at pH 3), followed directly by mixing with Gum Arabic. As shown in Figure 4.1B, for this case we find complex coacervates that homogeneously wet the water oil interface, to form core-shell capsules. The molecular weight and isoelectric point of the same proteins from different sources (commercial, alkali-extracted, and acid extracted) are expected to be identical or close because they are essentially the same molecules. Here, their distinctive complexation behaviors with oppositely charged polymers were mainly affected by the extraction pathways, which influence the solubility of the proteins at the desired pH for complex formation.

4.2.2 Extraction Efficiency

Protein extraction efficiency is a key concern for industrial applications, hence we compare the extraction efficiency of acid extraction at pH 3 with the more typically used alkali extraction. Results are given in Table 4.1. The protein yield from soy flour, and pea flour is 53.9% and 43.2%, respectively. While for soy this is similar to alkali extraction, protein extraction yields for alkali extraction applied to pea flour can be much higher than this.[39] The same authors do report for pea flour that similar extraction yields can be obtained for both alkali and acid extraction, if the extraction pH is lowered down to 1.5. We here choose not to do so, in order not to loose the advantage of not having to adjust pH, which would amount to an extra process step.

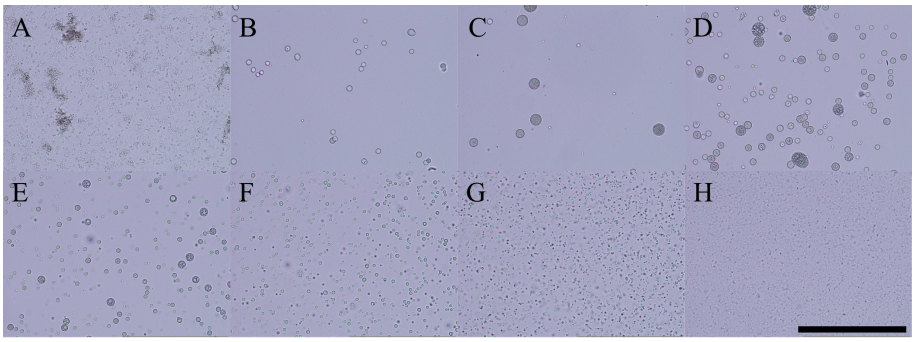

Figure 4.2: Micrographs of mixtures of soy extract and Gum Arabic with different polymer ratios at pH 3. These ratios are: soy extract:Gum Arabic=(A)1:0.1, (B)1:0.3, (C)1:0.5, (D)1:0.7, (E)1:1, (F)1:1.5, (G)1:2, (H)1:5. The scale bar is 200 μm.

4.2.3 Complex Formation at Different Polymer Ratios

Optimal wetting at the oil-water interface occurs if the coacervate droplets approach electroneutrality (in terms of the charges on the oppositely charged macroions.[19, 40] In view of the complex composition of our protein extracts, it is difficult to predict which composition that will be the case. Therefore, we tested a wide range of polymer ratios. For both soy and pea flour extracts we observe similar behaviors. Microscopy images are shown in (Figure 4.2 and Figure 4.15). At low Gum Arabic content, we mainly observe small aggregates. As the ratio of Gum Arabic to protein extract increases, ever larger coacervate droplets appear until finally, at high Gum Arabic content, droplets become smaller again.

The precise locations of the optimal ratios at pH 3 were determined more quantitatively by measuring the transmittance of samples (observed after a fixed waiting time) as a function of the Gum Arabic to protein extract ratio. The large complex coacervate droplets around the optimal ratio will sediment quickly, such that a maximum in transmittance corresponds to the optimal ratio. Results are shown in Figure 4.3. It is found that the optimal weight ratio for soy extract/Gum Arabic is from 1:0.7 to 1:0.3, and from 1:0.3 to 1:0.1 for pea extract/Gum Arabic. Pea extract requires less Gum Arabic for complex coacervation because pea extract has less protein than soy extract. Furthermore, we noticed that the pea extract/Gum Arabic complex coacervate near its optimal ratios needed around three hours to sediment while for the soy extract/Gum

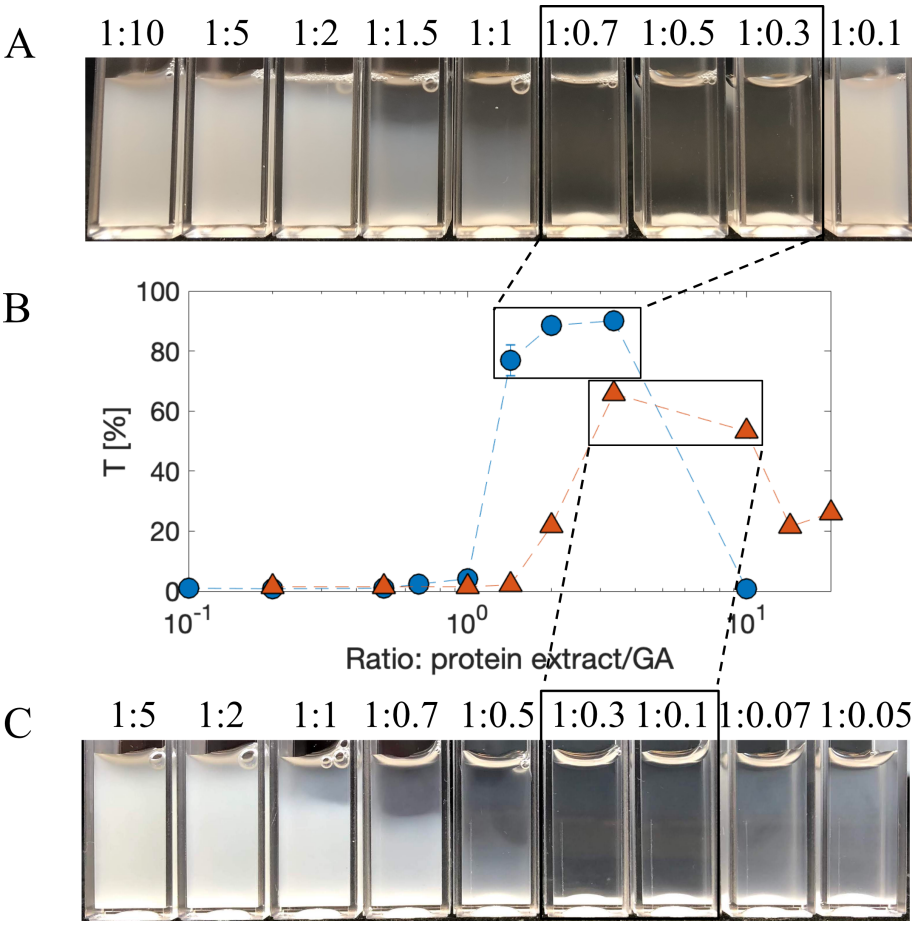

Figure 4.3: (A) Mixed solutions of soy extract and Gum Arabic in different ratios (soy extract:Gum Arabic) at pH 3. (B) Measured transmittance (λ=500 nm) as function of polymer ratio. Circles and triangles represent soy and pea mixed solutions, respectively. Error bars show the standard deviation of triplicates, if invisible, error bars are smaller than symbols. The optimal ratios are highlighted in boxes. (C) Mixed solutions of pea extract and Gum Arabic at pH 3 with their ratios being indicated in the same manner (pea extract:Gum Arabic).

Arabic complex coacervate this only took half an hour, pointing to slower coalescence and smaller droplet size at optimal amounts of Gum Arabic for the case of the pea extracts.

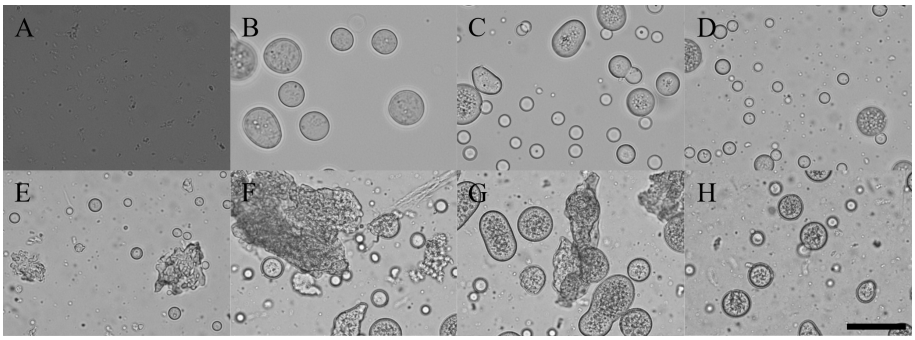

Figure 4.4: Micrographs of soy extract/Gum Arabic complex coacervate at different pH (A)2.43, (B)2.75, (C)3, (D)3.25, (E)3.5, (F)3.75, (G)4, (H)5. The scale bar is 50 μm.

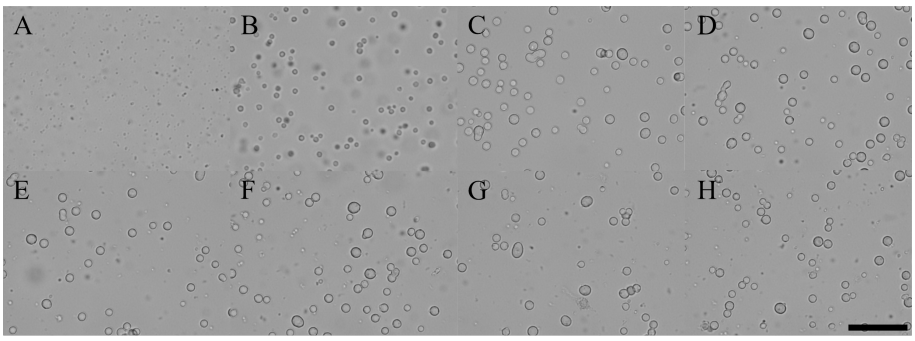

Figure 4.5: Micrographs of pea extract/Gum Arabic complex coacervate at different pH (A)2.5, (B)2.75, (C)3, (D)3.25, (E)3.5, (F)3.75, (G)4, (H)5. The scale bar is 50 μm.

4.2.4 Complex Formation at Different pH

The condition of electroneutrality and the resulting optimal mass ratio of course sensitively depends on pH, since this sets the charges on the macroions. To investigate pH dependence, we fix the mass ratio at the optimal value found for pH 3, and explore the pH dependence at this mass ratio. We find distinctly different behaviours for the two types of protein extracts. As shown in Figure 4.4, for the soy extract/Gum Arabic coacervate system, spherical coacervate droplets start appearing at pH 2.75. The droplets remain transparent and spherical up to pH 3.25. At pH values above pH 3.5, we observe solid aggregates coexisting with some (spherical and transparent) coacervate droplets. The coexistence of different type of complexes strongly suggests that in our protein extracts different pro-

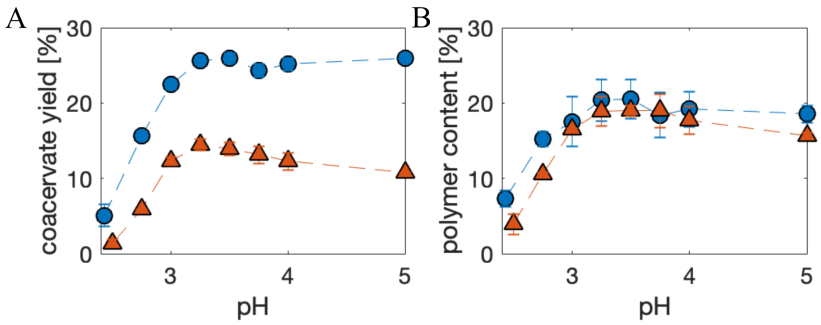

Figure 4.6: Coacervate yields (A) and polymer contents in coacervates (B) as a function of pH. Coacervate yields are determined by the mass of polymers in coacervates divided by the total polymer mass in solutions. Polymer contents are obtained by the mass of polymers in coacervates divided by the total coacervate mass. Circles and triangles represent soy- and pea extract/Gum Arabic coacervates, respectively. Error bars show the standard deviation of triplicates.

tein fractions (with different charge intensity and solubility properties[27, 41]) may form segregated complexes. In contrast to the soy protein extracts, for the pea extracts, as shown in Figure 4.5, upon complexation with Gum Arabic, coacervate droplets start forming from pH 2.75 but this time no obvious large aggregates are found until at least pH 5. Rather than being caused by differences in electrostatic interactions, we believe the difference between the behaviour of the two types of extracts is caused by differences in solubility of proteins in the extracts. As we show in Figure 4.16, the pH 3 soy protein extracts start showing precipitation when brought to pH 4, while for the pea protein extracts, this does not occur until at least pH 5.

As shown in Figure 4.6A, we have also determined coacervate yields and the total (bio)polymer content of the coacervates as a function of pH. We find that, starting from low pH, both increase up to pH 3 and then stay roughly constant. For both the soy- and pea protein extracts, the total polymer content in the coacervates reaches a maximum of around 20%, which is similar to values reported for many other coacervate systems consisting of proteins from animal sources[42] or synthetic polymers.[22] The coacervate yield is much higher for coacervates of Gum Arabic with the soy- than with the pea protein extracts (Fig-

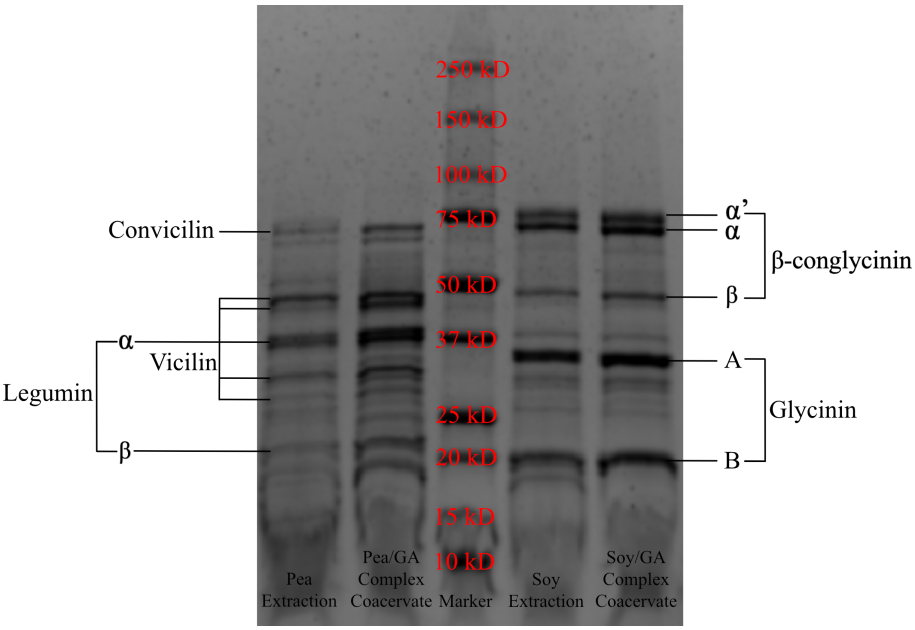

Figure 4.7: SDS-PAGE of the pea extract, pea extract/Gum Arabic complex coacervate (left) and the soy extract, soy extract/Gum Arabic complex coacervate (right).

ure 4.6A), hence the coacervates with the pea protein extracts feature significantly more biopolymer dissolved in the continuous phase. Presumably this reflects both the higher protein solubility and the lower fraction of protein extracted for the case of pea.

4.2.5 Protein Composition

To investigate which protein fractions are extracted and contribute to complex coacervation at the optimal ploymer ratios and pH, Polyacrylamide Gel Electrophoresis (SDS-PAGE) was used to study soy and pea extracts, as well as their coacervates with Gum Arabic (Figure 4.7). Glycinin and β-conglycinin are two major components of soy globulins, and these two components together take up around 60% of the total soy protein content.[38] They are found in both the soy extracts and the coacervates, with no apparent change of their relative abundance. In pea protein fractions, globulins take up 70-80% of the total protein content.[26] Globulins in pea consist of three main fractions: legumin, vicilin and

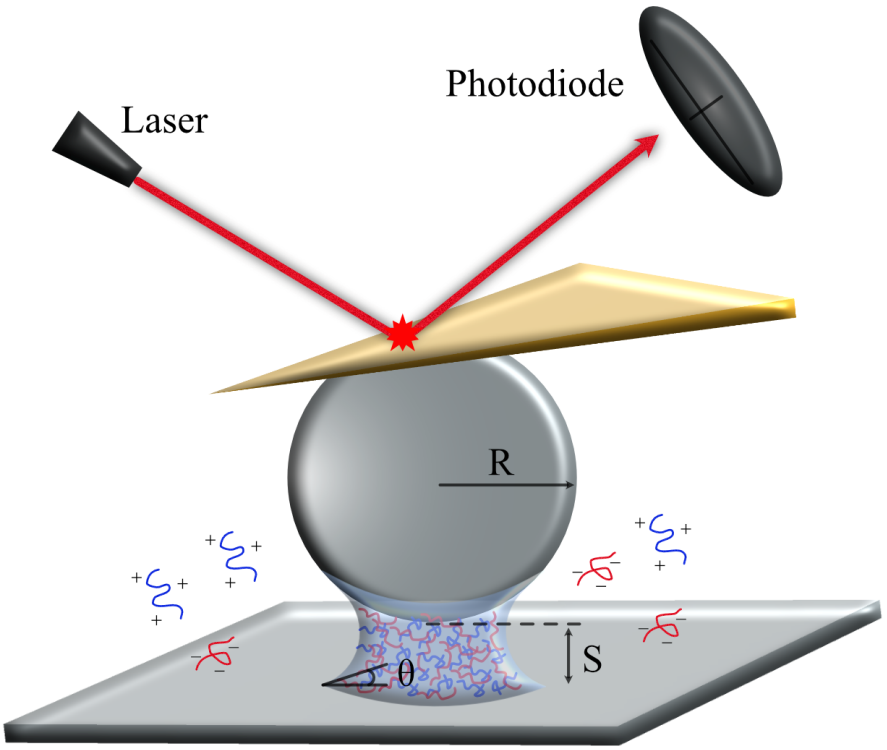

Figure 4.8: Artistic illustration of the capillary bridge geometry, with the complex coacervate condensed between the sphere and the substrate. Reproduced from[20] with permission from The Royal Society of Chemistry.

convicilin. All are found in the pea protein extracts as well as in the coacervates. As is clear from Figure 4.7, also for pea, the relative abundance of the proteins appears to be essentially the same in the protein extract and in its coacervates. Hence, all major protein fractions from soy and pea flours are successfully extracted, and efficiently used in complex coacervation in our process.

4.2.6 Salt- and Concentration Dependence of Interfacial Tension

After studying the complex coacervation behavior of the soy- and pea extracts with Gum Arabic, we next focus on the major physical property determining core-shell capsule formation: the extremely low interfacial tensions γ of the co-

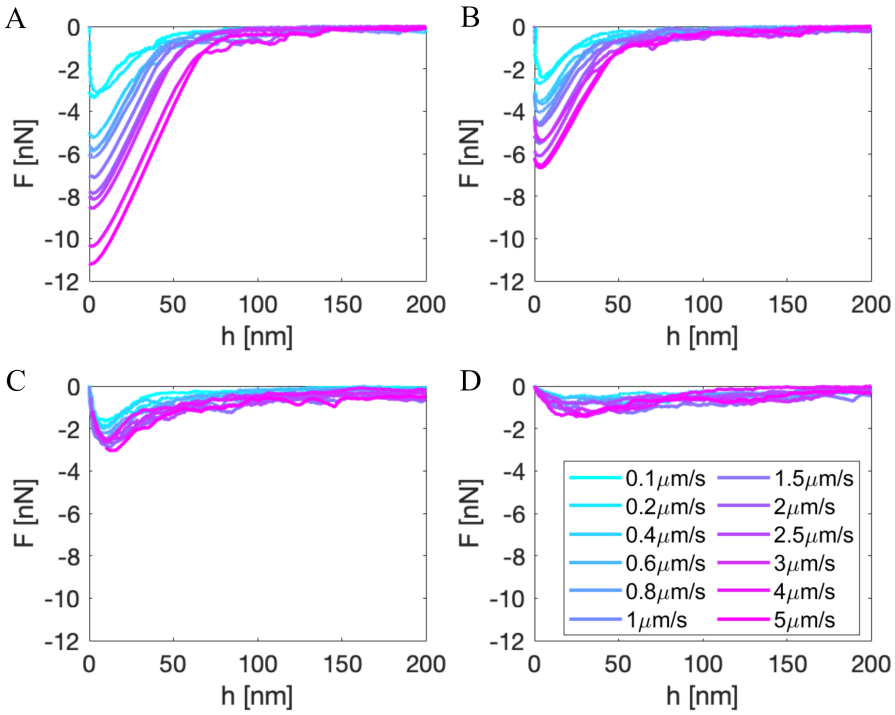

Figure 4.9: Retraction force–distance curves of soy extract/Gum Arabic coacervates at different retraction rates (from 0.1 μm/s to 5 μm/s) and different salt concentrations, (A) 0 mM, (B) 30 mM, (C) 60 mM and (D) 90 mM.

acervates with their excess phases which typically leads to full wetting of coacervates at oil-water interfaces.[43] In addition to viscous forces and external flow, it is this interfacial tension that largely determines the capsule size and morphology.[44, 17] However, because of their extremely low values, measuring the γ between coacervate phases and their coexisting aqueous phases is difficult.

In recent years, several creative techniques[32, 20, 33, 34, 45, 46, 17] have been developed to measure the extremely low γ of coacervates. We here use the Colloid-Probe Atomic Force Microscope based method developed by Sprakel et al., which has also been adopted by other groups.[33, 34] Details of the technique are explained elsewhere,[32, 20, 34] but in brief, a coacervate bridge is formed between the colloid probe and substrate by either capillary condensation in the polymer dilute phase or by direct contact with a substrate pre-coated with co-

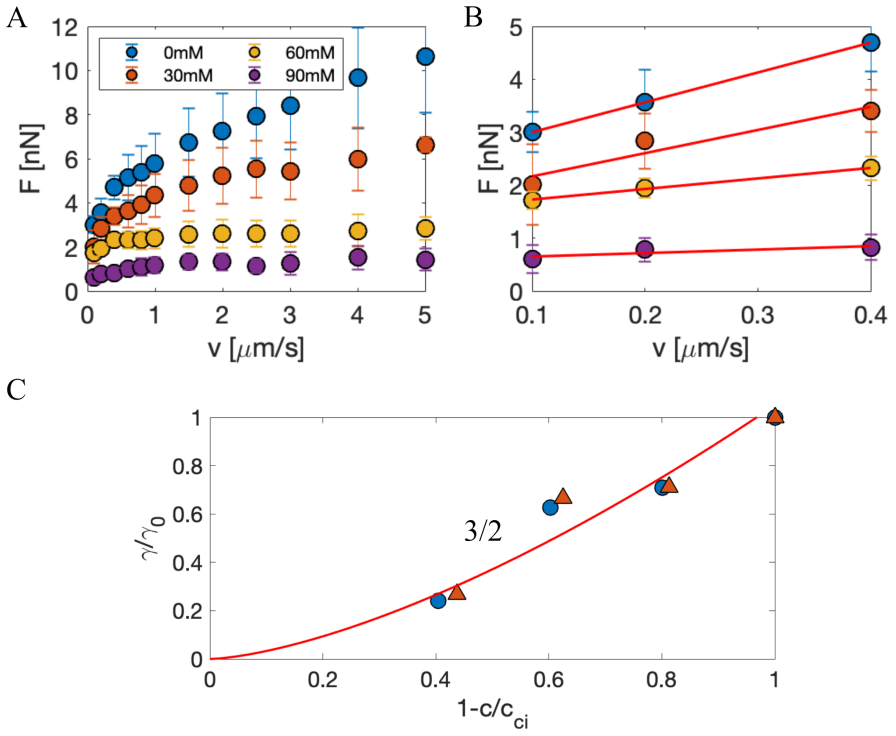

Figure 4.10: (A) Peak forces as a function of retraction rates for soy extract/Gum Arabic coacervates at different salt concentrations, error bars show the standard deviation of 20 measurements. (B) A zoom-in figure of panel A at low retraction rates (form 0.1 μm/s to 0.4 μm/s) with linear fits. (C) Normalized interfacial tensions of soy (circles) and pea (triangles) extract/Gum Arabic coacervates as a function of the normalized separation from their critical salt concentrations, soy(151 mM) and pea(160 mM). The solid line is a power law fit with an exponent of 3/2 as predicted by Spruijt et al.[20]

acervates. A schematic is shown in Figure 4.8. In practice, retraction of the colloid probe increases the surface area of the capillary bridge and leads to an increase of the interfacial energy and a measurable force response, from which the surface tension can be inferred.

So far this technique has been applied to relatively well defined model systems. Here we show that it is also very suitable to precisely measure interfacial tensions in our more complex mixed systems. We follow Sprakel et al. in using capillary condensation as our means of creating the capillary bridges: these

form spontaneously when immersing the colloid probe in the excess phase that surrounds the dense coacervate droplets, and bringing the colloid probe close to the interface.

First we perform controls to rule out forces due to mechanisms other than capillary bridge formation, following the same reasoning as Sprakel et al. and Spruijt et al.[32, 20] No bridging is found in solutions with either only Gum Arabic, or only protein extract due to the absence of phase separation in those cases. Next, the range of the attraction range found for mixtures of Gum Arabic and protein extracts (100 nm) is many times that of interactions such as a depletion interaction.[47] Similarly, van der Waals attractions are ruled out because no hysteresis is observed in pure water or salt solutions. Hence we conclude that the long range attractions we observe in mixtures of Gum Arabic and extracts of soy- and pea- proteins can be attributed to the capillary bridge.

Next we have measured force–distance curves for soy- and pea extract/Gum Arabic coacervates for a wide range of retraction rates (from 0.1 to 5 μm/s) and four salt concentrations (0, 30, 60, 90 mM). Results for soy extract/Gum Arabic coacervates are shown in Figure 4.9. For the equivalent results for pea extract/Gum Arabic coacervates, see Figure 4.17 and Figure 4.18). Two features are very prominent in Figure 4.9: the magnitude of the force strongly decreases with increasing salt concentrations, and the magnitude of the force also increases significantly with increasing retraction rates.

The former behaviour is expected, as the salt screens the electrostatic interactions that drive coacervate formation. Too much salt eventually leads to the disappearance of the coacervates and hence to a vanishing surface tension. A rate-dependence of the force has been reported before[34, 45] while in other cases no dependence on retraction rates was found. It was already pointed out before[17] that at high retraction rates, the bulk coacervate viscosity will make a rate-dependent contribution to the force response that cannot be neglected. Hence, we have modified the analysis of the force curves to also account for the (rate dependent) effect of coacervate viscosity on the observed forces.

First, peak forces F are plotted against retraction rates for different salt concentrations (Figure 4.10A). Two regions can clearly be distinguished: at low retraction rates (< 0.4 μm/s), F increases linearly. At high rates (> 0.4 μm/s), curves

start to level off. We observe that this trend is similar to what is observed for a shear thinning fluid behavior obtained using macroscale rheology, with the slope of the force versus rate curve representing viscosity. Hence, by analogy, we identify the low retraction rate regime as the linear, Newtonian regime.

To eliminate the viscosity effect which depends on retraction rates, we obtain the peak force F for zero retraction rate by using a linear fit (Figure 4.10B). When the retraction rate is zero, the peak force F solely comes from the interfacial tension γ. Furthermore, for simplicity, we assume that the peak force F occurs at zero separation (S=0) for all measurements. A well-known solution[33] for the sphere-plate geometry is:

$$F = 4\pi\gamma R cos\theta \tag{4.1}$$

where R is the probe radius, θ is the contact angle between coacervates and the substrate. We assume the contact angle is small and cos$\theta \approx$1, since the coacervates wet both the substrate and probe.

Interfacial tensions γ of soy- and pea extract/Gum Arabic coacervates are calculated from Equation 4.1. We find that the soy- and pea extract/Gum Arabic coacervates have, respectively, γ = 48.5 and 32.3 μN/m in the absence of salt. As expected, with increasing salt the interfacial tensions decrease and eventually vanish (Figure 4.10C). The salt-dependence of model-complex coacervates has previously been explained semi-quantitatively using the Voorn-Overbeek model for bulk coacervates and a Flory-Huggins-like expression for the interfacial tension of polymer solutions by Spruijt et al.[20] (and elaborated by Qin et al.[48]). The main prediction is that the interfacial tension should vanish at increasing salt concentrations according to a power law with an exponent 3/2. The critical salt concentrations (soy: 151 mM, pea: 160 mM) determined via using this scaling exponent is very consistent with observations on bulk coacervate samples, soy and pea extract/Gum Arabic complex coacervate solutions become transparent above their critical salt concentrations. It is surprising that this model also very nicely captures the salt dependence of the interfacial tension for our multicomponent complex coacervates with crude soy- and pea protein extracts.

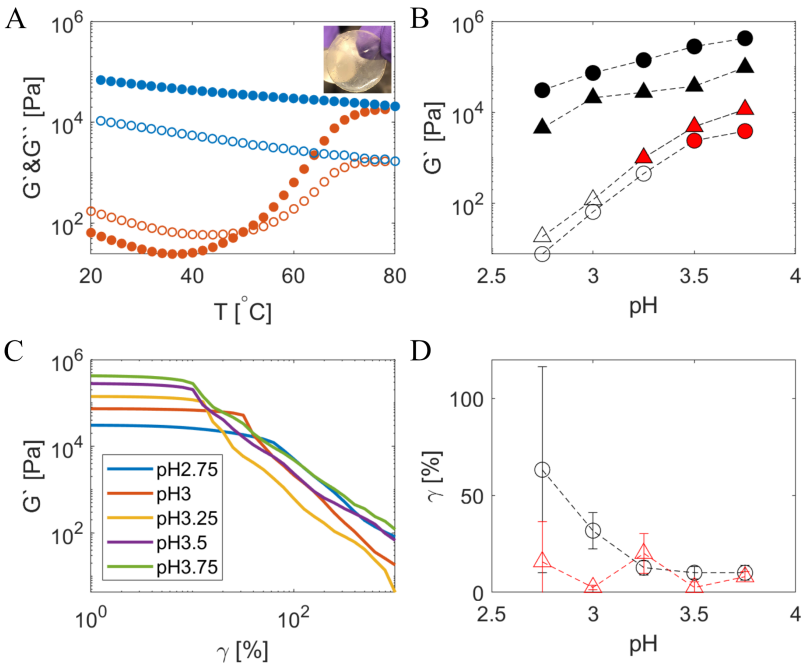

Figure 4.11: (A) Evolution of the linear viscoelastic properties upon imposing a typical temperature ramp. A representative temperature ramp on soy extract/Gum Arabic coacervates at pH 3. Open and solid symbols represent loss modulus (G'') and storage modulus (G'). Orange and blue colors indicate the heating and cooling process, respectively. Inset shows an example of the crosslinked coacervate probed using a 25 mm cone plate geometry on a rheometer. (B) G' of soy (circles) and pea (triangles) extract/Gum Arabic coacervates before (open) and after (filed) crosslinking. The red color indicates the samples have $G' > G''$ even before crosslinking. (C) Strain amplitude sweep experiments of soy extract/Gum Arabic coacervates at different pH after crosslinking. (D) Strain-at-break as a function of pH. Soy- and pea extract/Gum Arabic coacervates are represented by circles and triangles, respectively. Error bars are corresponding to the widths of the strain-at-break peaks ($\Delta G'/\Delta \gamma$) at half prominence.

4.2.7 Heat Induced Crosslinking of Coacervates

The ultra low interfacial tensions of the coacervates favor the wetting of the coacervates at the oil-water interface and the formation of a continuous layer. For actual applications of coacervate core-shell particles as microcapsules, usually a curing step is needed in which the coacervate material is solidified.[17] The so-

lidification is necessary to prevent the microcapsules from agglomerating and to enhance their stability. Many globular proteins exhibit thermal gelation, and in the present case this can be used as a clean-label strategy for microcapsule curing. We first study the thermal gelation behavior of bulk soy- and pea extract/Gum Arabic coacervates and their mechanical properties by macroscale rheology.

Figure 4.11A shows a typical measurement of the linear viscous and elastic moduli G'' and G' during heating and subsequent cooling of the protein-polysaccharide complex coacervates. At 20 °C, the complex coacervate remains liquid, with G'' being higher than G'. This is in fact a desired property for coacervates to be applied as coatings. At the start of the heating process, both G'' and G' first decrease, further enhancing the spreading of the coacervates at interfaces. At a temperature between 40 to 60 °C, the elastic moduli G' finally exceed the viscous moduli G'', and the coacervates have gelled. Both G' and G'' reach plateau values at 80 °C. After cooling, the elastic modulus G' is around 10^5 Pa, which is one order of magnitude larger than the viscous modulus G''. Hence, we find that heat-induced gelation is a potentially convenient process to cure the coacervates, since this forms strong and irreversible gels.

We have also investigated the influence of pH on gel strength. Results are shown in Figure 4.11B. Before heating, the G' of pea extract/Gum Arabic coacervates is slightly higher than that of the soy extract/Gum Arabic coacervates. When increasing the pH, the elastic moduli G' of both coacervates increase, and start exceeding the viscous moduli G'' for pH $>$ 3.5 for the soy protein extracts, and for pH $>$ 3.25 for the pea extracts. This is the result of enhanced electrostatic interactions and decreasing solubility of the protein components. This pH-induced liquid to solid transition could be used as an initial solidification step for the coacervate phase. After crosslinking, the final G' of both coacervates at each pH is more than two orders of magnitude larger than their initial strength. Disulfide bridge formation (between thiol groups of cysteine residues) may play a role in determining the strength of heat-induced gels of globular proteins. We speculate that the higher elastic moduli G' of the cured soy extract/Gum Arabic coacervates as compared to those for pea is due to the higher cysteine content of the soy proteins, as compared to the pea proteins.[49] Nevertheless, our speculation is not definitive considering the complex nature of the coacervate systems

in our work. Alting et al. have shown that strong gels can be formed even in the absence of any disulfide bridges.[50] Therefore, the exact gelation mechanism still requires further study.

The nonlinear rheology, in particular the fracture behaviour, is also a key property determining the usefulness of these coacervates for core-shell microcapsules. Typical strain sweeps of (heated) soy extract/Gum Arabic coacervates are shown in Figure 4.11C. The critical strains for both soy- and pea extract/Gum Arabic coacervates are summarized in Figure 4.11D. We find that soy extract/Gum Arabic coacervates have better fracture resistance than pea extract/Gum Arabic coacervates at pH 2.75 and 3. Their fracture resistance decreases with increasing pH. In contrast, for pea extract/Gum Arabic coacervates, the critical strains for fracture are relatively pH-independent. This difference may very well be due to the lower solubility of the soy proteins (Figure 4.16). Indeed, the soy protein precipitates that form at higher pH values might concentrate stresses in the hydrogels that promote fracture.

On balance, we conclude that increasing pH after coacervate spreading at oil-water interfaces may provide a way to obtain yet more rigid capsules after heating, although for the case of soy this may be at the expense of the fracture strength.

4.2.8 Capsule Morphology and Stability

Finally, we present preliminary results on microcapsules prepared using the soy- and pea protein flours. Capsule morphology before heat-induced crosslinking was observed by using Confocal Laser Scanning Microscopy (CLSM). Figure 4.12A and B show three dimensional reconstructions of oil droplets encapsulated by soy extract/Gum Arabic coacervates. A thick coacervate layer (a few micrometers) around oil droplets can clearly be recognized (Figure 4.12A). From Figure 4.12B, which emphasizes the internal structure of the capsules, it is clear that some capsules can have multiple oil cores. Although not explored here, the capsule size and core density could be further controlled by tuning the coacervate viscosity and flow applied during capsule formation.[17, 51]

Salt stability is a crucial parameter for the cured core-shell microcapsules. Before crosslinking (Figure 4.12C), soy extract/Gum Arabic coacervate capsules

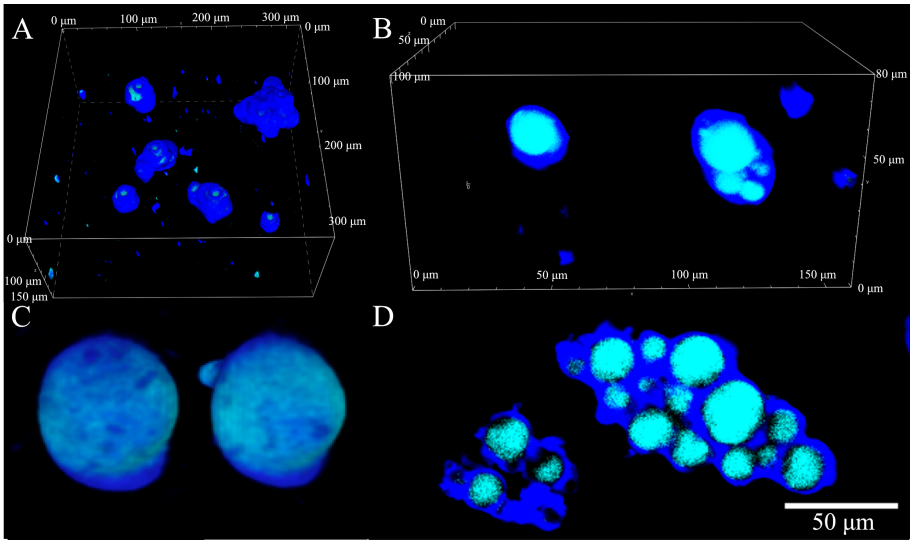

Figure 4.12: CLSM of the core-shell capsules made from soy extract/Gum Arabic coacervates. (A) A three dimensional reconstruction of core-shell capsules formed around pH 3, scales are labelled on the rectangular box. (B) Capsules formed in the same condition as in panel A, and the MaxIP render mode was used to accentuate the internal structure of the capsules. Scales are labelled on the rectangular box. (C) Capsules before crosslinking at 200 mM NaCl. (D) Capsules after crosslinking at 500 mM NaCl. The light blue color corresponds to the oil phase, and dark blue represents the coacervate phase.

dissolve in 200 mM NaCl after around 3 hours, which is above the critical salt concentration determined from CP-AFM measurements. Only a small amount of proteins or Gum Arabic, which can act as emulsifiers, stay at the oil-water interface. In contrast, capsules crosslinked via heat-induced gelation remain stable at 500 mM NaCl for at least 3 hours (Figure 4.12D). Furthermore, the crosslinked capsules also show good stability at neutral pH, for storage times of up to at least several weeks (Figure 4.19). Very similar results were found for capsules formulated with pea extract/Gum Arabic coacervates (Figure 4.20).

4.3 Conclusion

We have demonstrated a straightforward two-step approach to formulate plant-based complex coacervates, directly using legume flours rather than protein isol-

ates. We find the soluble proteins can be effectively extracted from legume flours in an acidic environment and spontaneously form complex coacervates in this acidic environment after adding weakly negatively charged polysaccharides such as Gum Arabic. In line with the sustainable formulation of the coacervates, we demonstrate that simple heating is enough to cure core-shell capsules prepared with these coacervates, and no chemical crosslinking is necessary. In conclusion, we show that the sustainable fabrication of advanced microstructures is possible starting from raw ingredients, and that resource intensive purification of plant biopolymers is not a prerequisite for creating such structures.

4.4 Experimental Section

Materials. Soybean flour (S9633), Nile Blue A perchlorate (370088), Oil Red O (O0625), Gum Arabic (51198), Chitosan (448869) and (R)-(+)-Limonene (97%, 183164) were bought from Sigma-Aldrich. Pea flour (yellow pea) and a medium-chain triglyceride (NEOBEE M-5) were gifts from AM Nutrition and Stepan Company, respectively. In the comparison test, soy protein isolate (SUPRO) was bought from Solae, and pea protein isolate (NUTRALYS F85) was bought from Roquette. Sodium metabisulfite (97%+) was bought from Acros Organics. HCl and NaOH (1 and 0.1 N) solutions purchased from Merck were used to control pH. Milli-Q water was used in all experiments.

Protein Extraction and Yield Determination. Typically, a mixture of 10% w/w soy or pea flour with sodium metabisulfite (15 mM) (prevent disulfide aggregates)[27] was prepared in demineralized water (100 mL). pH was adjusted to 2.7 with 1 M HCl, and the mixture was then vigorously stirred for 1 hour. pH was controlled between 2.7 and 2.9 during this process. The resulting mixture was centrifuged at 10000 g for 30 minutes, collect the supernatant, which contains soluble components (mostly protein and carbohydrate) from the corresponding flour. The supernatant was then freeze dried for storage and later use. The nitrogen content of flours and extracts was measured by the Dumas method. A general nitrogen-to-protein conversion factor of 6.25 was used to calculate the protein content for both soy and pea.

Optimal Ratio Determination. The optimal ratios for soy- and pea ex-

tract/Gum Arabic complex coacervates at pH 3 were determined by sweeping a wide range of polymer ratios. Specifically, for soy extract/Gum Arabic complex coacervates, a stock solution of soy extracts (pH 3, 0.005 g/mL) was prepared. We mixed the soy stock solution (10 mL) with Gum Arabic solutions (10 mL, pH 3) with different concentrations (0.0005, 0.0015, 0.0025, 0.0035, 0.005, 0.0075, 0.01, 0.025 and 0.05 g/mL). The final concentration of soy extracts was kept constant for all samples. The mixed solutions were also controlled at pH 3. All samples were observed in both micro- and macroscopic ways. A bright filed light microscope was used to check the mixed solutions. We transferred each sample (2 mL) into cuvette cells and left them to stand still for around 30 minutes. After that, the turbidity of the solutions was determined by the transmittance of a visible light (λ=500 nm) measured by a spectrophotometer (Evolution 220 Thermo Scientific). For pea extract/Gum Arabic complex coacervates, mixed solutions were prepared in the same manner, but in different concentrations. We mixed the pea extract stock solution (10 mL, pH 3, 0.02 g/mL) with Gum Arabic solutions (10 mL, pH 3) with different concentrations (0.001, 0.0014, 0.002, 0.006, 0.01, 0.014, 0.02, 0.04 and 0.1 g/mL). Moreover, longer waiting time for transmittance measurements was required for pea samples, which was around 3 hours.

Optimal pH Determination. The optimal pH for soy- and pea extracts forming complex coacervates with Gum Arabic were determined at the following fixed polymer ratios: soy extract:Gum Arabic=1:0.7, pea extract:Gum Arabic=1:0.3. Their total polymer concentrations were kept constant (11.9 mg/mL). Stock solutions of soy extract, pea extract and Gum Arabic were prepared at pH between 2.4 and 2.5. After mixing, solutions were in these two fixed ratios, we slowly raised the pH from 2.5 to 2.75, 3, 3.25, 3.5, 3.75, 4 and 5. At each pH, microscopic images were taken. Furthermore, a total volume of 30 mL solutions for each pH were transferred to three centrifuge tubes with an equal volume. All samples were centrifuged at 4500 rpm at room temperature for 30 minutes. The coacervate phase was freeze dried to determine the coacervate yield and polymer content. Finally, the solubility of individual soy and pea extracts (1 mg/mL) at different pH (3, 3.5, 4 and 5) was studied.

SDS-PAGE. The protein composition of soy and pea extracts and their complex coacervates with Gum Arabic was studied by SDS-PAGE. Gel electrophoresis

was conducted using commercial SDS/polyacrylamide gels (4-20% Mini-PROTEAN TGX precast gels, BioRad). Reference protein marker was purchased from BioRad. GelCode Blue Safe Protein Stain (Thermo Scientific) was used for staining.

CP-AFM and Salt Dependence of Interfacial Tensions. Force measurements were performed on an Atomic Force Microscope (ForceRobot 300, JPK). An AFM cantilever with a spherical silica particle (d=8 μm) was sealed in a liquid chamber by a rubber ring on a silicon wafer as the substrate. Both the AFM probe and substrate were cleaned via plasma and rinsed with water prior to measurements. Complex coacervates of soy and pea extracts with Gum Arabic were prepared at pH 3 and with fixed polymer ratios (soy extract:Gum Arabic=1:0.7, pea extract:Gum Arabic=1:0.3). The total polymer concentration was kept constant and extremely low (1.1875 mg/mL). Different salt concentrations (0, 30, 60, 90 mM) were tested for both coacervates. The chamber was filled with freshly prepared complex coacervate solutions and incubated about half an hour to reach equilibrium. Two surfaces (substrate and probe) were brought into direct contact (S=0) as the reference height, which was used to determine the absolute separation. The probe and substrate were kept in contact for 10 s for capillary bridge nucleation and growth. The probe was retracted at different velocities ranging from 0.1 μm/s to 5 μm/s, and force distance curves were recorded. We conducted 20 measurements for each retraction velocity. The vertical tip position was calibrated from cantilever bending by using the JPK data processing software. The cantilever deflection was converted to force by using Hooke's law, $F=k\Delta x$. k is the spring constant of the cantilever, which was calibrated by a contact based method in air. In this study, the spring constant was at 0.203 N/m.

Coacervate Crosslinking and Rheology. Heat induced crosslinking of soy- and pea extract/Gum Arabic coacervates and their mechanical properties were studied by rheology. Complex coacervates of soy and pea extracts with Gum Arabic were prepared at their optimal ratios and various pH (from 2.75 to 3.75). Rheological measurements were performed on an Anton Paar 501 rheometer equipped with a 25 mm cone-plate geometry and a Peltier temperature control unit. A solvent trap with tetradecane was used to prevent water evaporation. The continuous coacervate phase was obtained by centrifugation (4500 rpm, 30min) and subsequently loaded on the rheometer. First, a temperature

ramp was conducted to induce gelation, the temperature was increased from 20 to 80 °C in 1 hour, kept at 80 °C for 5 min, finally decreased to 20 °C with the same rate. G' and G'' were monitored at 0.5% stain and 6.28 rad/s. Then, the fracture resistance was tested via an amplitude sweep until 1000% strain at 6.28 rad/s and 20 °C.

Capsule Preparation and CLSM. First, stock solutions of soy and pea extracts were prepared at pH 2.6, and Gum Arabic stock solutions were prepared at pH 2.9. Then, we prepared mixed solutions (40 mL) with fixed polymer ratios (soy extract:Gum Arabic=1:0.7, pea extract:Gum Arabic=1:0.3) and a constant total polymer concentration (11.9 mg/mL). We added mixed oil (0.5 mL, 80 vol% NEOBEE M5 + 20 vol% limonene) to the mixed solutions followed by an emulsification step by using ULTRA-TURRAX. pH of the mixed solutions was slowly raised to around 3 to induce complex coacervation and form capsules. The obtained capsules were further crosslinked by heating in a preheated water bath at 80 °C for 1 hour. Capsule stability was tested by adding NaCl and adjusting to neutral pH. CLSM was conducted on an inverted microscope system Eclipse Ti2 from Nikon. Two excitation wavelengths, 488 nm and 640 nm, were used to probe the local environments of Nile Blue dyed oil phase and proteins, respectively.

References

[1] Amar Kumar Mohanty, Manjusri Misra, and LT Drzal. Sustainable bio-composites from renewable resources: opportunities and challenges in the green materials world. *Journal of Polymers and the Environment*, 10(1):19–26, 2002.

[2] Dieter Klemm, Friederike Kramer, Sebastian Moritz, Tom Lindström, Mikael Ankerfors, Derek Gray, and Annie Dorris. Nanocelluloses: a new family of nature-based materials. *Angewandte Chemie International Edition*, 50(24):5438–5466, 2011.

[3] Brian P Mooney. The second green revolution? production of plant-based biodegradable plastics. *Biochemical Journal*, 418(2):219–232, 2009.

[4] M Ramesh, K Palanikumar, and K Hemachandra Reddy. Plant fibre based bio-composites: Sustainable and renewable green materials. *Renewable and Sustainable Energy Reviews*, 79:558–584, 2017.

[5] Pierre Gallezot. Conversion of biomass to selected chemical products. *Chemical Society Reviews*, 41(4):1538–1558, 2012.

[6] Yan Lin and Shuzo Tanaka. Ethanol fermentation from biomass resources: current state and prospects. *Applied microbiology and biotechnology*, 69(6):627–642, 2006.

[7] Siavash Iravani and Rajender S Varma. Plants and plant-based polymers as scaffolds for tissue engineering. *Green Chemistry*, 21(18):4839–4867, 2019.

[8] Yong Zhang, Lili Cui, Xiaoxia Che, Heng Zhang, Nianqiu Shi, Chunlei Li, Yan Chen, and Wei Kong. Zein-based films and their usage for controlled delivery: Origin, classes and current landscape. *Journal of controlled release*, 206:206–219, 2015.

[9] Xiufeng Li and Renko de Vries. Interfacial stabilization using complexes of plant proteins and polysaccharides. *Current Opinion in Food Science*, 21:51–56, 2018.

[10] Caren Tanger, Julia Engel, and Ulrich Kulozik. Influence of extraction conditions on the conformational alteration of pea protein extracted from pea flour. *Food Hydrocolloids*, page 105949, 2020.

[11] Qinhui Xing, Konstantina Kyriakopoulou, Martin de Wit, Remko M Boom, and Maarten AI Schutyser. Effect of tube wall material on electrostatic separation of plant raw-materials. *Journal of Food Process Engineering*, 44(1):e13575, 2021.

[12] Remco Kornet, Justus Veenemans, Paul Venema, Atze Jan van der Goot, Marcel Meinders, Leonard Sagis, and Erik van der Linden. Less is more: Limited fractionation yields stronger gels for pea proteins. *Food Hydrocolloids*, 112:106285, 2021.

[13] Simha Sridharan, Marcel BJ Meinders, Johannes H Bitter, and Constantinos V Nikiforidis. Pea flour as stabilizer of oil-in-water emulsions: Protein purification unnecessary. *Food Hydrocolloids*, 101:105533, 2020.

[14] Wei-Ching Liao, Yang Sung Sohn, Marianna Riutin, Alessandro Cecconello, Wolfgang J Parak, Rachel Nechushtai, and Itamar Willner. The application of stimuli-responsive vegf- and atp-aptamer-based microcapsules for the controlled release of an anticancer drug, and the selective targeted cytotoxicity toward cancer cells. *Advanced Functional Materials*, 26(24):4262–4273, 2016.

[15] Hugo Junior Barboza de Souza, Regiane Victória de Barros Fernandes, Soraia Vilela Borges, Pedro Henrique Campelo Felix, Lívia Cássia Viana, Amanda Maria Teixeira Lago, and Diego Alvarenga Botrel. Utility of blended polymeric formulations containing cellulose nanofibrils for encapsulation and controlled release of sweet orange essential oil. *Food and Bioprocess Technology*, 11(6):1188–1198, 2018.

[16] A Lamprecht, U Schäfer, and C-M Lehr. Influences of process parameters on preparation of microparticle used as a carrier system for o-3 unsaturated fatty acid ethyl esters used in supplementary nutrition. *Journal of microencapsulation*, 18(3):347–357, 2001.

[17] Gregory Dardelle and Philipp Erni. Three-phase interactions and interfacial transport phenomena in coacervate/oil/water systems. *Advances in colloid and interface science*, 206:79–91, 2014.

[18] HG Bungenberg De Jong. Die koazervation und ihre bedeutung für die biologie. *Protoplasma*, 15(1):110–173, 1932.

[19] Cornelus G De Kruif, Fanny Weinbreck, and Renko de Vries. Complex coacervation of proteins and anionic polysaccharides. *Current opinion in colloid & interface science*, 9(5):340–349, 2004.

[20] Evan Spruijt, Joris Sprakel, Martien A Cohen Stuart, and Jasper van der Gucht. Interfacial

tension between a complex coacervate phase and its coexisting aqueous phase. *Soft Matter*, 6(1):172–178, 2010.

[21] G Dardelle, M Jacquemond, and P Erni. Delivery Systems for Low Molecular Weight Payloads: Core/Shell Capsules with Composite Coacervate/Polyurea Membranes. *Adv. Mater.*, 29:1, 2017.

[22] Marco Dompé, Francisco J Cedano-Serrano, Mehdi Vahdati, Larissa van Westerveld, Dominique Hourdet, Costantino Creton, Jasper van der Gucht, Thomas Kodger, and Marleen Kamperman. Underwater adhesion of multiresponsive complex coacervates. *Advanced Materials Interfaces*, 7(4):1901785, 2020.

[23] Yiping Cao and Raffaele Mezzenga. Design principles of food gels. *Nature Food*, 1(2):106–118, 2020.

[24] Sumudu N Warnakulasuriya and Michael T Nickerson. Review on plant protein–polysaccharide complex coacervation, and the functionality and applicability of formed complexes. *Journal of the Science of Food and Agriculture*, 98(15):5559–5571, 2018.

[25] Alla Nesterenko, Isabelle Alric, Françoise Silvestre, and Vanessa Durrieu. Vegetable proteins in microencapsulation: A review of recent interventions and their effectiveness. *Industrial crops and products*, 42:469–479, 2013.

[26] ACY Lam, A Can Karaca, RT Tyler, and MT Nickerson. Pea protein isolates: Structure, extraction, and functionality. *Food Reviews International*, 34(2):126–147, 2018.

[27] Wim H Van Megen. Solubility behavior of soybean globulins as a function of ph and ionic strength. *Journal of agricultural and food chemistry*, 22(1):126–129, 1974.

[28] V Ducel, J Richard, P Saulnier, Yves Popineau, and F Boury. Evidence and characterization of complex coacervates containing plant proteins: application to the microencapsulation of oil droplets. *Colloids and Surfaces A: Physicochemical and Engineering Aspects*, 232(2-3):239–247, 2004.

[29] Shuanghui Liu, Yuan-Long Cao, Supratim Ghosh, Derick Rousseau, Nicholas H Low, and Michael T Nickerson. Intermolecular interactions during complex coacervation of pea protein isolate and gum arabic. *Journal of agricultural and food chemistry*, 58(1):552–556, 2010.

[30] Shuanghui Liu, Nicholas H Low, and Michael T Nickerson. Effect of ph, salt, and biopolymer ratio on the formation of pea protein isolate- gum arabic complexes. *Journal of Agricultural and Food Chemistry*, 57(4):1521–1526, 2009.

[31] Denis Renard, Laurence Lavenant-Gourgeon, Marie-Christine Ralet, and Christian Sanchez. Acacia s enegal gum: continuum of molecular species differing by their protein to sugar ratio, molecular weight, and charges. *Biomacromolecules*, 7(9):2637–2649, 2006.

[32] J Sprakel, NAM Besseling, FAM Leermakers, and MA Cohen Stuart. Equilibrium capillary forces with atomic force microscopy. *Physical review letters*, 99(10):104504, 2007.

[33] Seonghye Lim, Dustin Moon, Hyo Jeong Kim, Jeong Hyun Seo, In Seok Kang, and Hyung Joon Cha. Interfacial tension of complex coacervated mussel adhesive protein according to the hofmeister series. *Langmuir*, 30(4):1108–1115, 2014.

[34] Dimitrios Priftis, Robert Farina, and Matthew Tirrell. Interfacial energy of polypeptide complex coacervates measured via capillary adhesion. *Langmuir*, 28(23):8721–8729, 2012.

[35] Fatih Comert and Paul L Dubin. Liquid-liquid and liquid-solid phase separation in protein-polyelectrolyte systems. *Advances in colloid and interface science*, 239:213–217, 2017.

[36] Qing-Xi Wu, Dong-Qiang Lin, and Shan-Jing Yao. Design of chitosan and its water soluble derivatives-based drug carriers with polyelectrolyte complexes. *Marine drugs*, 12(12):6236–6253, 2014.

[37] R De Vries, F Weinbreck, and CG De Kruif. Theory of polyelectrolyte adsorption on heterogeneously charged surfaces applied to soluble protein–polyelectrolyte complexes. *The Journal of chemical physics*, 118(10):4649–4659, 2003.

[38] Dora YM Lui, Edward T White, and James D Litster. Dissolution behavior of soy proteins and effect of initial concentration. *Journal of agricultural and food chemistry*, 55(6):2467–2473, 2007.

[39] Barry G Swanson. Pea and lentil protein extraction and functionality. *Journal of the American Oil Chemists' Society*, 67(5):276–280, 1990.

[40] Paul Dubin and Russell J Stewart. Complex coacervation. *Soft Matter*, 14(3):329–330, 2018.

[41] T Ya Bogracheva, N Yu Bespalova, and AL Leont'ev. Isolation of 11s and 7s globulins from seeds of glycine max. *Applied Biochemistry and Microbiology*, 32(4):429–433, 1996.

[42] Fanny Weinbreck, Roland HW Wientjes, Hans Nieuwenhuijse, Gerard W Robijn, and Cornelus G de Kruif. Rheological properties of whey protein/gum arabic coacervates. *Journal of Rheology*, 48(6):1215–1228, 2004.

[43] Xiufeng Li, Philipp Erni, Jasper Van Der Gucht, and Renko De Vries. Encapsulation using plant proteins: Thermodynamics and kinetics of wetting for simple zein coacervates. *ACS applied materials & interfaces*, 12(13):15802–15809, 2020.

[44] S Torza and SG Mason. Three-phase interactions in shear and electrical fields. *Journal of colloid and interface science*, 33(1):67–83, 1970.

[45] Samim Ali and Vivek M Prabhu. Characterization of the ultralow interfacial tension in liquid–liquid phase separated polyelectrolyte complex coacervates by the deformed drop retraction method. *Macromolecules*, 52(19):7495–7502, 2019.

[46] Louise M Jawerth, Mahdiye Ijavi, Martine Ruer, Shambaditya Saha, Marcus Jahnel, Anthony A Hyman, Frank Jülicher, and Elisabeth Fischer-Friedrich. Salt-dependent rheology and surface tension of protein condensates using optical traps. *Physical review letters*, 121(25):258101, 2018.

[47] Wout Knoben, NAM Besseling, and MA Cohen Stuart. Long-range depletion forces induced by associating small molecules. *Physical review letters*, 97(6):068301, 2006.

[48] Jian Qin, Dimitrios Priftis, Robert Farina, Sarah L Perry, Lorraine Leon, Jonathan Whitmer, Kyle Hoffmann, Matthew Tirrell, and Juan J De Pablo. Interfacial tension of polyelectrolyte complex coacervate phases. *ACS Macro Letters*, 3(6):565–568, 2014.

[49] Mandy Claessens, Wim Calame, André D Siemensma, Marleen A van Baak, and Wim HM Saris. The effect of different protein hydrolysate/carbohydrate mixtures on postprandial glucagon and insulin responses in healthy subjects. *European journal of clinical nutrition*, 63(1):48–56, 2009.

[50] Arno C Alting, Harmen HJ de Jongh, Ronald W Visschers, and Jan-Willem FA Simons. Phys-

ical and chemical interactions in cold gelation of food proteins. *Journal of Agricultural and Food Chemistry*, 50(16):4682–4689, 2002.

[51] CYG Lemetter, FM Meeuse, and NJ Zuidam. Control of the morphology and the size of complex coacervate microcapsules during scale-up. *AIChE Journal*, 55(6):1487–1496, 2009.

4.5 Appendix

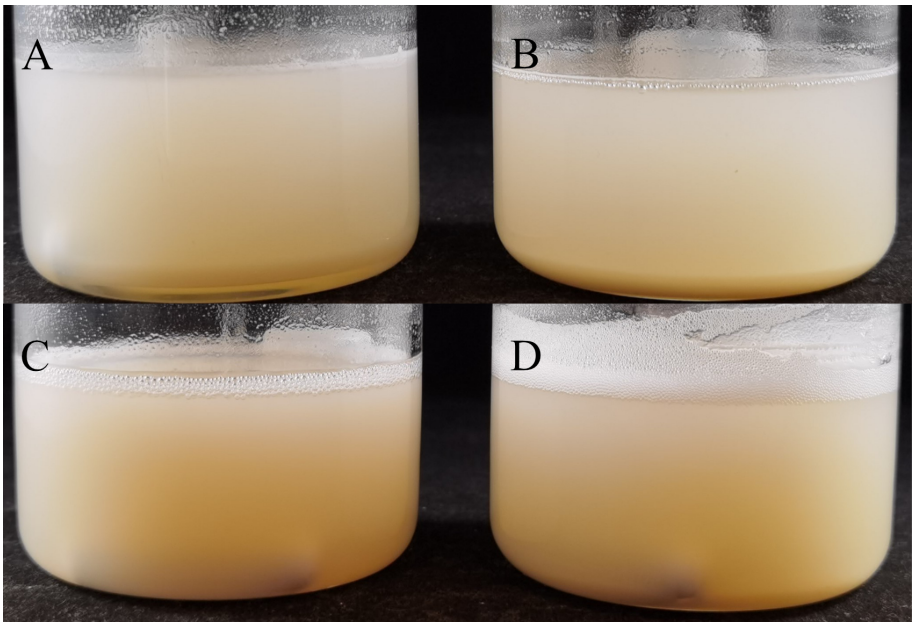

Figure 4.13: Aqueous solutions of commercial plant protein isolates (1 wt%). Soy protein isolates at (A)pH 3 and (B)pH 5.8, pea protein isolates at (C)pH 3 and (D)pH 5.8.

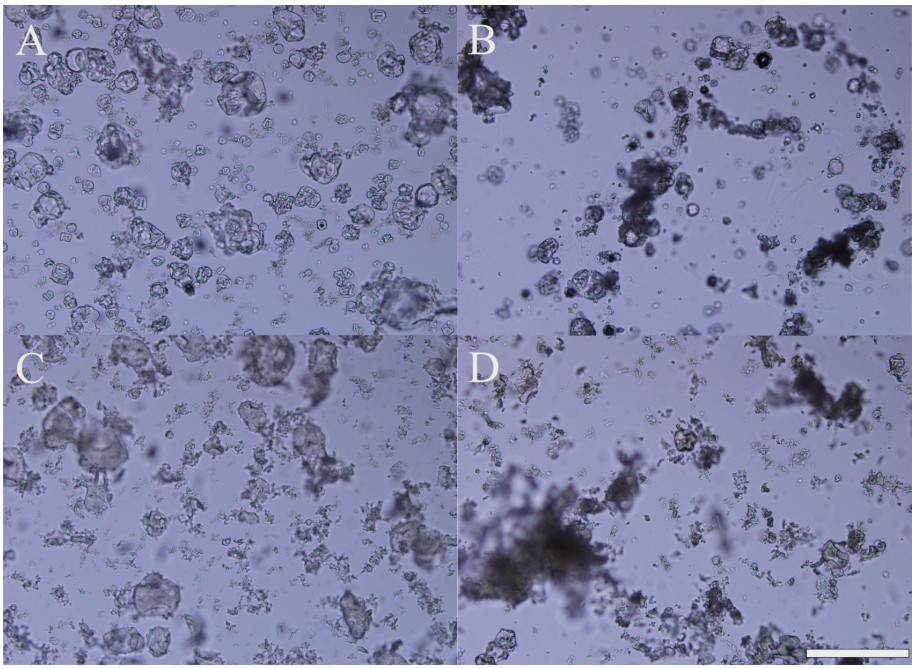

Figure 4.14: Micrographs of mixtures of commercial plant protein isolates with polysaccharides. Soy protein isolate with (A) Gum Arabic at pH 3 or with (B) chitosan at pH 5.8. Pea protein isolate with (C) Gum Arabic at pH 3 or with (D) chitosan at pH 5.8. The scale bar is 200 μm.

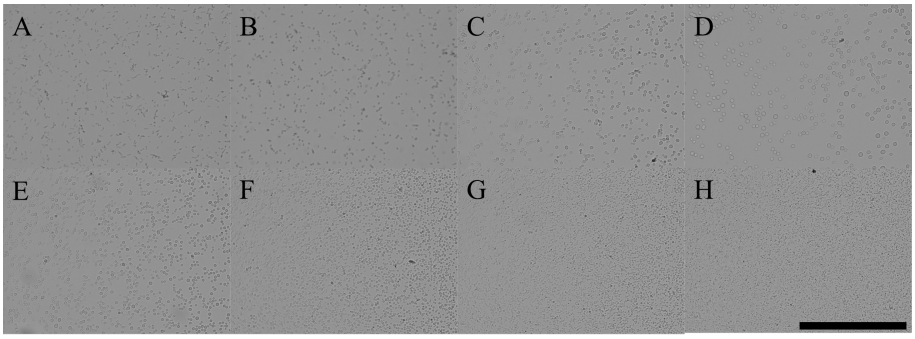

Figure 4.15: Micrographs of pea extracts and Gum Arabic with different polymer ratios at pH 3. These ratios are pea extract:Gum Arabic=(A)1:0.05, (B)1:0.07, (C)1:0.1, (D)1:0.3, (E)1:0.5, (F)1:0.7, (G)1:1, (H)1:2. The scale bar is 200 μm.

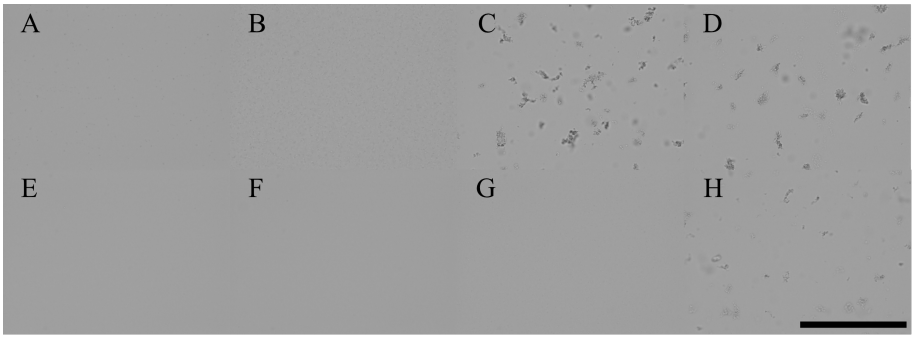

Figure 4.16: Micrographs of soy and pea extracts at different pH, (A) and (E) pH 3, (B) and (F) pH 3.5, (C) and (G) pH 4, (D) and (H) pH 5. The scale bar is 200 μm.

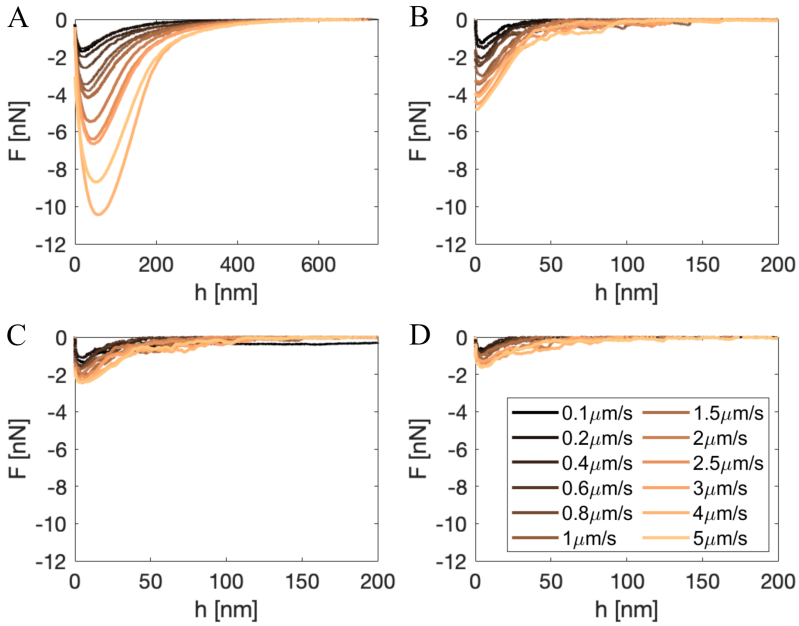

Figure 4.17: Retraction force–distance curves of pea extract/Gum Arabic complex coacervates at different retraction rates (form 0.1 μm/s to 5 μm/s) and different salt concentrations, (A) 0 mM, (B) 30 mM, (C) 60 mM and (D) 90 mM.

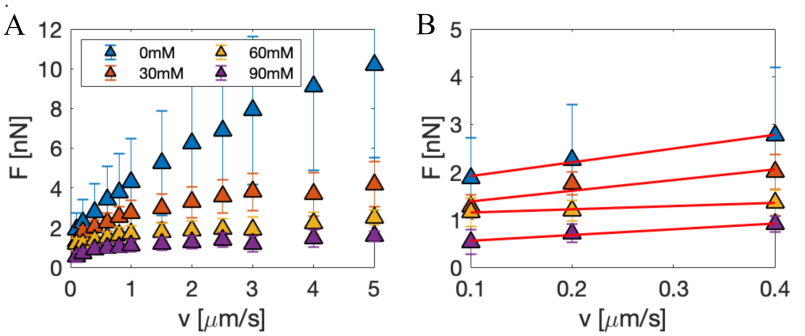

Figure 4.18: (A) Peak force as a function of retraction rates for pea extract/Gum Arabic coacervates at different salt concentrations, error bars show the standard deviation of 20 measurements. (B) A zoom-in figure of panel A at low retraction rates (form 0.1 μm/s to 0.4 μm/s) with linear fits.

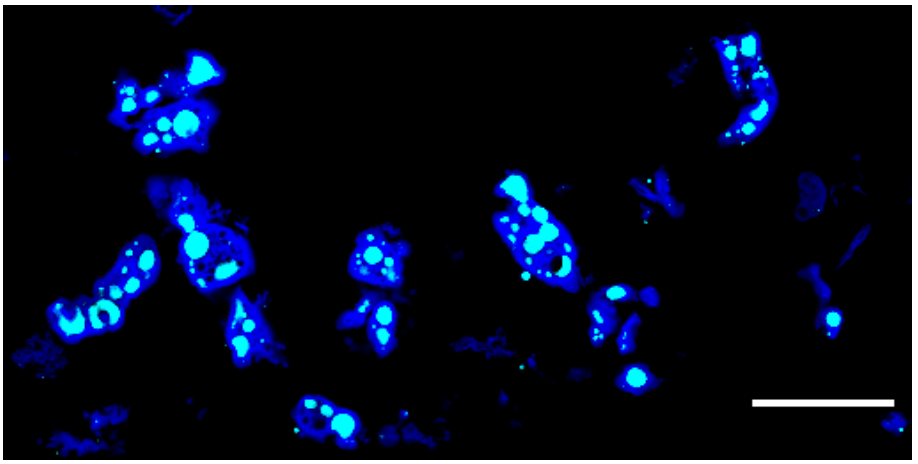

Figure 4.19: CLSM of soy extract/Gum Arabic complex coacervate core-shell capsules near pH 7. The scale bar is 100 μm. The light blue color corresponds to the oil phase, dark blue represents the coacervate phase.

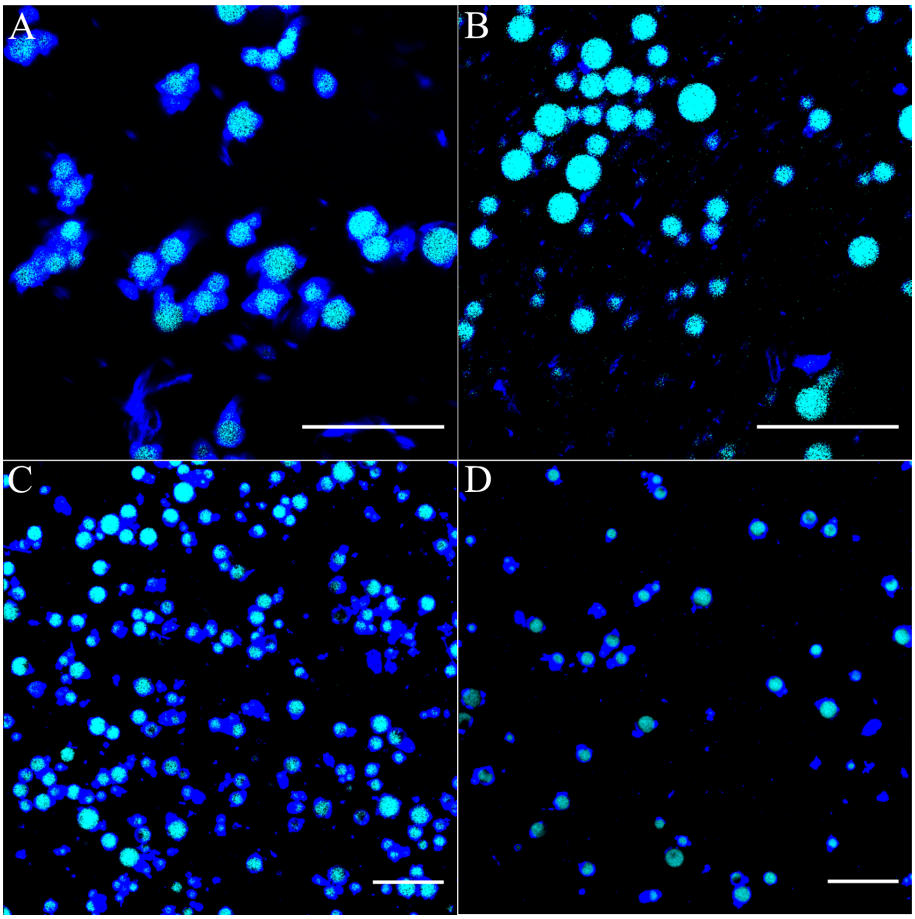

Figure 4.20: CLSM of core-shell capsules made from pea extract/Gum Arabic complex coacervates. (A) Core-shell capsules formed around pH 3, before crosslinking (B) Capsules without crosslinking, at 200 mM salt. (C) Capsules after crosslinking, at 500 mM salt. (D) Capsules after crosslinking, near pH 7. Scale bars correspond to 100 μm. The light blue color corresponds to the oil phase, dark blue represents the coacervate phase.

Chapter 5

Active Microrheology of Protein Condensates Using Colloidal Probe-AFM

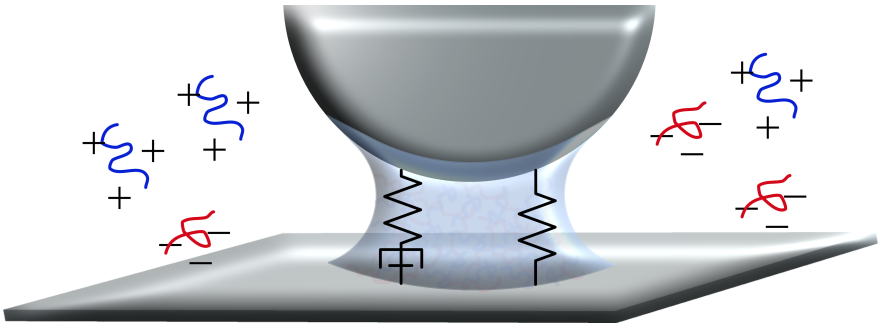

Manuscript in preparation as:
Li, X., Van Der Gucht, J., Erni, P., & De Vries, R. Active Microrheology of Protein Condensates Using Colloidal Probe-AFM.

Protein condensates resulting from liquid-liquid phase separation exhibit intrinsically different mechanical properties at different length and time scales. Understanding their mechanical properties is vital to elucidate the underlying physics of phenomena involving such condensates, from how cells regulate biochemical processes in protein droplets to industrial applications based on protein condensates. Here, a microrheology technique based on Colloidal Probe Atomic Force Microscopy is introduced to simultaneously investigate the interfacial and viscoelastic properties of a model protein condensate. An equivalent mechanical model is built to describe the amplitude ratio and phase lag between the driving force and resulting stress response of the capillary bridge between the probe and substrate under sinusoidal modulation at different frequencies. The experimental data and mechanical model allow us to distinguish three characteristic frequency domains of the model protein condensate: an interfacial tension-dominated domain at low frequencies, a transition domain at intermediate frequencies, and an elasticity-dominated domain at high frequencies.

5.1 Introduction

Protein condensates, also known as coacervates in colloid science and chemistry, are the polymer-rich phase of liquid-liquid phase separation (LLPS) formed by assembling one or several macromolecules via various interactions, including electrostatic interactions,[1, 2] cation-π interactions,[3] and hydrophobic effects.[4] Protein condensates usually exhibit intrinsically different mechanical properties at different length and time scales.[5, 6, 7] They are predominantly viscous fluids but also exhibit elasticity at short time scales. Their interfacial tension with the co-existing phase greatly influences the mobility and shape transformation of protein condensates at short length scales, below their capillary length, which is typically in the order of 100 μm or smaller. At larger length scales, the influence of interfacial tension on shapes of condensate droplets can be be neglected.

The mechanical properties of protein condensates play a vital role in the many technological applications and biological systems in which protein condensates occur. For example, protein condensates formed via LLPS have been studied for applications in designing underwater adhesives,[8, 9] coatings,[10] and core-shell microcapsules.[11, 12] When they serve as adhesives, high viscosity can ensure better adhesion strength. For coatings and microcapsules, the ultra-low interfacial tensions of protein condensates with their co-existing phases favor their wetting and spreading on a third phase. More recently, protein condensates have also received increasing attention in biology in connection to so-

called membraneless organelles (MLOs): intracellular structures that include nucleoli,[13] P granules,[14, 15] and stress granules.[16] These are liquid compartments composed of nucleic acids and various proteins. Many protein condensates are designed as *in vitro* models to study the biophysics of MLOs.[17, 18, 19] Numerous studies have shown that the mechanical properties of such compartments are highly relevant to their functionalities.[20, 21] For example, when they act as a biochemical reactor, they can localize the molecules of interest and physically separate them from other (macro-)molecules in the cell to facilitate the reaction.[22, 23, 24] The fluidity enables protein condensates to carry on rapid transportation and exchange of their contents within the compartment or with the surrounding environment. Moreover, it has been shown that the liquid state protein condensates can undergo a liquid-gel or liquid-glass transition due to the formation of crosslinking knots or simply aging.[25, 26, 27, 28] Both processes can kinetically arrest bio-activities, and they are usually irreversible in physiological conditions. An increasing number of studies hint that the liquid to solid transition of MLOs could be linked to pathological protein aggregation.[29, 30, 31, 32] Therefore, investigating the mechanics of protein condensates will provide insights in designing functional materials as well as deepen our understanding of the physics of living cells.

Characteristic length scales relevant for MLOs, as well as many technological applications of protein condensates, are well below the capillary length such that we always have to take into account interfacial tension and viscoelasticity simultaneously. Therefore, it is highly useful to have a microrheology technique that can bring the viscoelastic and interfacial properties of protein condensates together and investigate their interplay at different time scales. Colloidal Probe Atomic Force Microscopy (CP-AFM) has already shown its ability to measure the ultra-low interfacial tensions for segregative and associative LLPS systems.[33, 34, 35] In previous studies, CP-AFM was used to measure the pull-off force upon retracting a capillary bridge formed between the probe and substrate. The pull-off force has been attributed to the increase of interfacial energy. In these studies, a low retraction velocity was used to avoid any influence of the coacervate viscoelasticity on the measurement. Investigating the viscoelasticity of the capillary bridge consisting of protein condensates by only performing

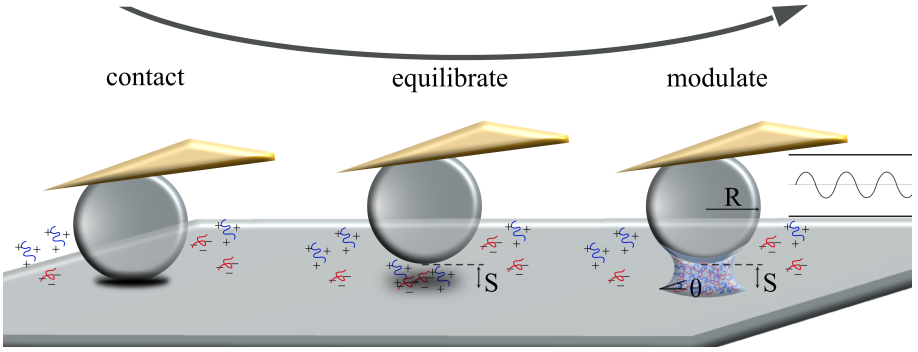

Figure 5.1: Artist's impression of the capillary bridge composed of protein condensates formed via capillary condensation, where a spherical probe with a radius of R is attached to an AFM cantilever and placed above a flat substrate at a separation of S, θ is the contact angle between the condensate and substrate.

retraction measurements is challenging due to the nonlinear effect of rheology and capillary thinning at large separations, where the extensional rheology flow terms must be taken into account.

Here, we report on a CP-AFM based microrheology technique that can be used to probe the viscoelastic and interfacial properties of protein condensates simultaneously. We use a model protein condensate consisting of oppositely charged natural polyelectrolytes (Gum Arabic and soy globulins: glycinin and β-conglycinin) as a model system. The complexity of this model system is not only proving the robustness of this method but also close to real MLOs and applications based on protein condensates which typically involve multiple polymers. As shown in Figure 5.1, a capillary bridge consisting of protein condensates between the probe and substrate is formed, which is deformed by applying sinusoidal modulation at different frequencies. The stress response is obtained by monitoring the cantilever deflection. Depending on the selection of cantilevers, this technique can probe the stress response from milliseconds to seconds with piconewton and nanometer precision on force and position, respectively. We analyze our data using a mechanical model that elucidates the contrasting roles of viscoelasticity and interfacial tension in determining the mechanical response.

5.2 Results and Discussion

5.2.1 Capillary bridge formation.

The capillary bridge consisting of protein condensates between the probe and substrate is formed via capillary condensation following the method previously introduced by Sprakel et al.[33] The capillary condensation process occurs spontaneously if the probe and substrate are close enough when they are immersed in the polymer-dilute phase, and the protein condensate wets both surfaces. As explained by Sprakel et al., the formation of the capillary bridge follows two steps: nucleation and growth. The former occurs very rapidly due to the ultra-low interfacial tension, whereas the diffusion of polymers limits the latter. Therefore, after an initial contact to trigger the capillary condensation, we lift the probe to constant separations above the substrate for some time to let the capillary bridge grow and equilibrate. We find that 30 s is adequate for the capillary bridge to saturate at all separations we have studied (from 40 to 70 nm). This was established by comparing the pull-off forces with the same retraction velocity after different waiting periods. We find that keeping the probe at a constant separation above the substrate with nanometer precision longer than 30 s often leads to inaccurate measurements due to drift issues and some external interference, such as noise and vibration.

5.2.2 Modeling.

A mechanical model (Figure 5.2A) is built to analyze the stress response of the capillary bridge between the probe and substrate under sinusoidal modulation and to quantitatively interpret our experimental data. In the model, the motion of the probe is controlled by a cantilever with stiffness k_l and a capillary bridge consisting of three elements: k_p, b_p, and k_m. We treat the protein condensate as a Maxwell fluid by combining the spring constant k_p and damping coefficient b_p in a series, representing the condensate's elasticity and viscosity, respectively. The capillary force acting on the probe due to the interfacial tension is modelled as an elastic contribution with a spring constant k_m, parallel to the Maxwell elements. For simplicity, we neglect the variations of b_p, k_p, and k_m upon the small separation change during modulation. We also assume b_p and k_p are independent from

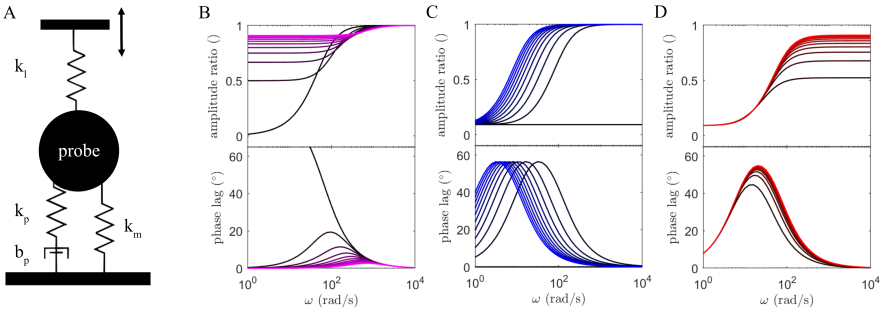

Figure 5.2: (A) Equivalent mechanical model for the CP-AFM setup. Amplitude ratio (top) and phase lag (bottom) calculated from the mechanical model: (B) b_p = 0.0015072 N.s/m and k_p = ∞, k_m is ranging from 0 to 1 N/s (from dark to light purple). (C) k_m = 0.01 N/m and k_p = ∞, b_p is ranging from 0 to 0.01 N.s/m (from dark to light blue). (D) k_m = 0.01 N/m and b_p = 0.0015072 N.s/m, k_p is ranging from 0.1 to 1 N/m (from dark to light red).

the modulation frequency ω. We study the stress response of the capillary bridge under sinusoidal modulation by looking into the amplitude ratio and phase lag between the resulting cantilever deflection and drive piezo. From this model, we can predict the experimentally measured amplitude ratio and phase lag (details of the derivation process are provided in SI):

$$C = 1 - \frac{k_l}{k_l + k_m + \frac{i\omega b_p k_p}{i\omega b_p + k_p} - \omega^2 m} \tag{5.1}$$

where

$$\textit{amplitude ratio} = |C| \tag{5.2}$$

$$\textit{phase lag} = angle(C) \tag{5.3}$$

where i is the imaginary unit, m is the effective mass of the cantilever with resonance frequency f, which can be determined by $m = k_l/(2\pi f)^2$. The amplitude ratio and phase lag are obtained from the absolute value and phase angle of Equation 5.1, respectively.

To elucidate the role of each mechanical element in determining the amp-

litude ratio and phase lag when the capillary bridge is under sinusoidal modulation, we plot the mechanical model (Equation 5.2 and 5.3) as a function of angular frequency by varying each element one by one while keeping the other two as constants. Figure 5.2B shows that when k_p and b_p are kept as constants, increasing k_m will result in a higher amplitude ratio in the low-frequency domain, and the phase lag will significantly decrease with the peak being shifted to higher frequencies. This indicates that the interfacial tension dominates the stress response and provides an instant stress response which significantly reduces phase lag at low frequencies. Figure 5.2C shows that an increase of b_p does not affect the initial amplitude ratio at low frequencies. However, a higher b_p leads to an early increase in the amplitude ratio and phase lag in the low-frequency domain. This suggests that the amplitude ratio is not only caused by elastic elements (k_p and k_m), but that viscosity can also lead to an increase of the amplitude ratio. A similar finding was reported by Friedenberg and Mate before for a pure Newtonian fluid (low molecular weight PDMS).[36] The increase of the amplitude ratio at higher frequencies was attributed to compliance of the soft cantilever. Figure 5.2D shows that k_p only starts playing a role in the stress response in the high-frequency domain. At high frequencies, the material elasticity takes over the stress response, determining the amplitude ratio and significantly reducing the phase lag.

This mechanical model contains three adjustable parameters (k_m, b_p, and k_p) to fit the experimental data. To obtain these parameters from our experimental data, we first fix k_m by fitting the amplitude ratio at low frequencies as it is the only parameter that determines the amplitude ratio in the low-frequency domain. Next, b_p is determined based on where the amplitude ratio starts increasing after k_m is set. k_p is adjusted to fit the amplitude ratio at high frequencies. Finally, we check and ensure that the parameters used to fit the amplitude ratio data also fit the phase lag data.

5.2.3 Experimental output and data analysis using FFT (Fast Fourier Transform).

Next, we analyze the experimental data of protein condensates under sinusoidal modulation and extract the amplitude and phase information. The typical exper-

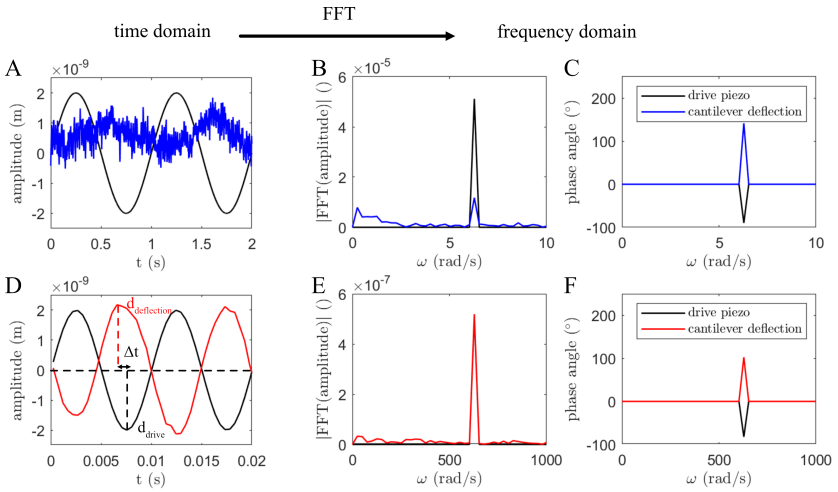

Figure 5.3: Illustration of the experimental output at two specific angular frequencies (first row 6.28 rad/s, and second row 628 rad/s) in time domain (A and D), as well as in frequency domain (B,C and E,F) after performing FFT. Two data groups are selected from the protein condensate at pH 3 with a probe-substrate separation at 50 nm. (A) and (D) Amplitude of the drive piezo d_{drive} (black) and cantilever deflection $d_{deflection}$ (blue or red) as a function of time. Δt is the time difference, and the phase lag is determined by $\omega\Delta t$. Dashed lines are drawn to guide the eye. (B) and (E) Absolute value of the amplitude of the drive piezo and cantilever deflection obtained from performing FFT as a function of angular frequency. (C) and (F) Phase angle of the drive piezo and cantilever deflection obtained from performing FFT versus angular frequency. The colors are consistent for each row.

imental output and data analysis using FFT are shown in Figure 5.3, where the responses of the same protein condensate modulated at two angular frequencies are compared. It can be clearly seen that the cantilever deflection at 6.28 rad/s has a smaller amplitude and more obvious phase lag than at 628 rad/s. To quantitatively determine the amplitude and phase angle (ϕ) of the drive piezo and cantilever deflection, FFT is performed to transform the experimental data from the time domain to the frequency domain. The amplitude ratio is determined as the amplitude of the cantilever deflection divided by the amplitude of the drive piezo at the modulation frequency (Figure 5.3B and E). As shown in Figure 5.3C and F, the phase lag is obtained by $\varphi = \phi_{deflection}$-$\phi_{drive}$-180°, because the direction of the cantilever deflection is opposite to the drive piezo.

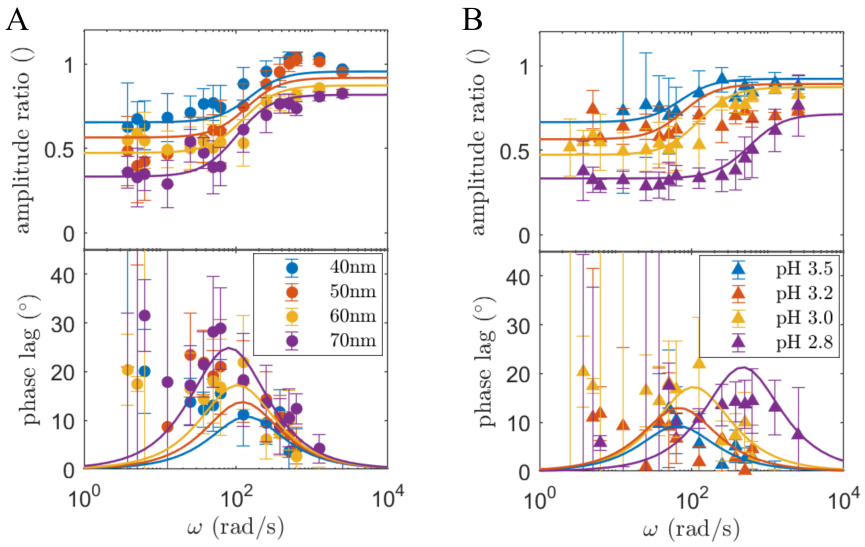

Figure 5.4: (A) Amplitude ratio (top) and phase lag (bottom) as a function of angular frequency for the measurements performed on the same protein condensate at pH 3 with different probe-substrate separations (stated in the legend). (B) Amplitude ratio (top) and phase lag (bottom) as a function of angular frequency for the measurements performed on protein condensates at different pH (stated in the legend) with a constant probe-substrate separation at 60 nm. Fits to the mechanical model are plotted as solid lines in the same color with the corresponding experimental data.

5.2.4 Amplitude ratio and phase lag at different separations and pH.

To understand the effect of changing the probe-substrate separation on the stress response, we summarize the amplitude ratio and phase lag of the same protein condensate under sinusoidal modulation at different separations (Figure 5.4A). The amplitude ratios start from nonzero values at low frequencies and increase to values equal or close to one as the modulation frequency increases. Based on our model, the force response at low frequencies is attributed to the interfacial tension between the capillary bridge and the surrounding aqueous phase. The capillary force arising from the interfacial tension decreases with increasing separation and will eventually vanish at a critical separation as the capillary bridge no longer exists. This critical separation is about 100 nm in our case with this particular protein condensate and probe size ($R \approx 4$ μm). It is also noticed that

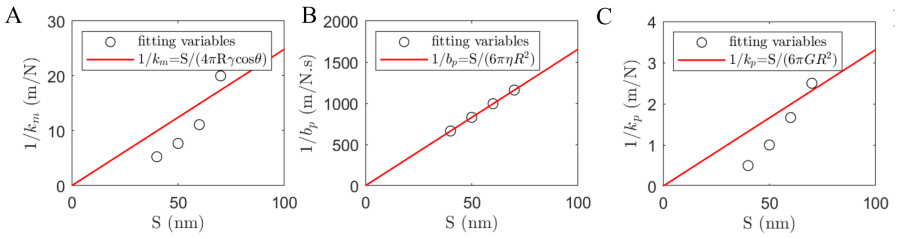

Figure 5.5: Reciprocals of the fitting elements (A: $1/k_m$, B: $1/b_p$, and C: $1/k_p$) as a function of the probe-substrate separation S. Red solid lines represent predictions.

the phase lag has more significant variations at angular frequencies lower than 10 rad/s. This may be related to the instability of the soft cantilever in long-time measurements. Nevertheless, it is clear that the larger separation causes an increase of the phase lag. We attribute this to the smaller k_m at larger separations. As the frequency increases to around 100 rad/s, the elasticity of the protein condensate starts dominating the stress response. At high frequencies, the phase lag is reduced to close to 0° when the cantilever deflection is synchronized with the drive piezo without time lag. Moreover, larger separations eventually result in smaller amplitude ratios at the high-frequency domain, indicating a smaller k_p at larger separations.

The parameter values we obtained by fitting the mechanical model to our experimental data are shown in Figure 5.5. We can semi-quantitatively relate the parameters of the mechanical model, to the viscoelasticity and interfacial tension through scaling models. First, we expect the spring constant (k_m) representing the interfacial tension to scale as Equation 5.4 (derived from [36]), from which γ=80 μN/m is obtained. This value is close to the independently measured interfacial tension (48.5 μN/m) of this system in chapter 4.

$$1/k_m = S/(4\pi R\gamma cos\theta) \tag{5.4}$$

Next, a scaling estimate for the damping coefficient (b_p) representing the viscosity is:

$$1/b_p = S/(6\pi\eta R^2) \tag{5.5}$$

Equation 5.5 is a model from fluid dynamics,[37, 38] which describes a rigid sphere oscillating in a fluid above a rigid plane is highly damped. η=0.2 Pa.s shows the best fit to the parameter values obtained from the experimental data. However, this value is two orders of magnitude lower than the complex viscosity obtained from bulk rheology measurements. The reasons for this difference is still unknown.

Finally, we expect the spring constant k_p representing the condensate elasticity is related to the elastic modulus G of the condensate by the following approximate relation:

$$1/k_p = S/(6\pi G R^2) \tag{5.6}$$

k_p used for plotting the mechanical model in Figure 5.4A is found to be close to the approximate relation (Equation 5.6) when G=100 Pa. Interestingly, this is close to the elastic modulus of the protein condensate at around 6 rad/s (Figure 5.7).

We have also established the dependence of the mechanical parameters on the pH, a key variable determining the molecular interactions in the condensate. As shown in Figure 5.4B, the mechanical model again shows excellent agreement with the experimental data. From pH 2.8 to 3.5, the protein condensate with higher pH starts from a higher amplitude ratio in the low-frequency domain, indicating a higher interfacial tension. As the frequency increases, the protein condensate with a higher interfacial tension also exhibits higher viscoelasticity. This trend agrees with the bulk rheology data (Figure 5.7), which shows that the protein condensate is transformed from a flexible liquid state to a more compact and condensed viscoelastic structure with increasing pH. Although the interfacial tension and viscoelasticity of protein condensates all increase at higher pH, our microrheology technique suggests that changing pH from 2.8 to 3.5, especially from 2.8 to 3.0, reduces the frequency domain dominated by the interfacial tension.

Likewise, the fitting elements (k_m, b_p and k_p) used to plot the model in Figure 5.4B can also be translated into the physical properties of protein condensates by using the Equations (5.4, 5.5 and 5.6) above. These results are shown in Figure 5.8.

5.3 Conclusions

We have demonstrated a CP-AFM based microrheology technique to simultaneously study the interfacial and viscoelastic properties of protein condensates at different time scales. We show that the stress response of the capillary bridge under sinusoidal modulation can be described by a simplified mechanical model assuming that the viscoelastic elements of protein condensates are independent of frequency. Our results indicate that there are three characteristic frequency domains of the model protein condensate. The interfacial tension dominates the stress response at low frequencies. The viscosity of protein condensates results in more phase lag at medium frequencies. The protein condensate behaves as a purely elastic material at high frequencies. This work should pave the way for studying the physical properties of MLOs in biology as well as industrial applications based on protein condensates.

5.4 Methods

Materials. Soy protein extracts (SPEs) were prepared from soybean flour (Sigma-Aldrich, S9633) in an acidic environment and freeze-dried for storage following the work in chapter 4. Gum Arabic (GA) (51198) was purchased from Sigma-Aldrich. NaOH and HCl (1 and 0.1 N) solutions bought from Merck were used to adjust pH. Milli-Q water was used in all experiments.

Protein condensate preparation. An aqueous suspension of the protein condensate consisting of SPEs and GA was prepared at a constant polymer ratio (SPEs:GA=1.375:1) in pH ranging from 2.8 to 3.5. The particular polymer ratio in this pH range for protein condensate formation was determined in chapter 4. The total polymer concentration was kept at 1.1875 mg/mL for all samples prepared for CP-AFM microrheology measurements.

CP-AFM microrheology measurements. All microrheology measurements were performed on ForceRobot 300 (JPK), a type of Atomic Force Microscope designed for force spectroscopy. We glued a spherical silica particle ($R \approx 4$ μm) on an AFM cantilever with a spring constant around 0.1 N/m, calibrated using a contact based method. Silicon wafers were used as the substrate. We used a rubber ring to create a chamber between the probe holder and substrate to per-

form measurements in liquids. The AFM probe and substrate were processed by plasma cleaner to remove contaminants and subsequently rinsed with water to deactivate their surfaces. The protein condensate suspensions were always freshly prepared and equilibrated in the chamber for about one hour prior to microrheology measurements. In a typical measurement, the probe was first brought into direct contact with the substrate (S=0) to determine the absolute separation and induce the capillary condensation. Then the probe was slowly lifted to a fixed separation with a constant velocity (0.01 μm/s). The probe was kept at the constant separation for 30 s to let the capillary bridge grow and saturate. After that, the probe was modulated to deform the capillary bridge with a constant amplitude (2 nm) in a wide range of angular frequencies (from 2.512 to 2512 rad/s). Ten measurements were performed at each frequency, and each measurement contains 25 periods of sinusoidal modulation.

We conducted two groups of experiments in this study. In the first group, the influence of the probe-substrate separation on the stress response was tested on the same protein condensate at pH 3 with different separations (40, 50, 60, and 70 nm). In the second group, we studied the stress response of the protein condensates at different pH (2.8, 3.0, 3.2, and 3.5) with a fixed separation of 60 nm.

Bulk rheology measurements. Bulk rheology measurements were conducted on an Anton Paar rheometer 301 with a 25 mm cone plate geometry. The temperature was maintained at 20 °C by a Peltier temperature control unit, and a solvent trap was used to keep water from evaporation during measurements. Protein condensates at different pH (2.8, 3.0, 3.2, and 3.5) were prepared in the same way as the samples for microrheology measurements but with a total polymer concentration ten times higher (11.875 mg/mL). The continuous phase of the protein condensate was separated from the aqueous phase by centrifugation (4500 rpm, 30 min) and loaded on the rheometer for measurements. Dynamic frequency sweeps were performed on protein condensates from 0.1 to 100 rad/s with a constant strain amplitude at 1%.

References

[1] Jasper Van der Gucht, Evan Spruijt, Marc Lemmers, and Martien A Cohen Stuart. Polyelectrolyte complexes: Bulk phases and colloidal systems. *Journal of colloid and interface science*, 361(2):407–422, 2011.

[2] Cornelus G De Kruif, Fanny Weinbreck, and Renko de Vries. Complex coacervation of proteins and anionic polysaccharides. *Current opinion in colloid & interface science*, 9(5):340–349, 2004.

[3] Sangsik Kim, Hee Young Yoo, Jun Huang, Yongjin Lee, Sohee Park, Yeonju Park, Sila Jin, Young Mee Jung, Hongbo Zeng, Dong Soo Hwang, et al. Salt triggers the simple coacervation of an underwater adhesive when cations meet aromatic π electrons in seawater. *ACS nano*, 11(7):6764–6772, 2017.

[4] Xiufeng Li, Philipp Erni, Jasper Van Der Gucht, and Renko De Vries. Encapsulation using plant proteins: Thermodynamics and kinetics of wetting for simple zein coacervates. *ACS applied materials & interfaces*, 12(13):15802–15809, 2020.

[5] Louise M Jawerth, Mahdiye Ijavi, Martine Ruer, Shambaditya Saha, Marcus Jahnel, Anthony A Hyman, Frank Jülicher, and Elisabeth Fischer-Friedrich. Salt-dependent rheology and surface tension of protein condensates using optical traps. *Physical review letters*, 121(25):258101, 2018.

[6] Evan Spruijt, Martien A Cohen Stuart, and Jasper van der Gucht. Linear viscoelasticity of polyelectrolyte complex coacervates. *Macromolecules*, 46(4):1633–1641, 2013.

[7] Evan Spruijt, Joris Sprakel, Marc Lemmers, Martien A Cohen Stuart, and Jasper Van Der Gucht. Relaxation dynamics at different time scales in electrostatic complexes: time-salt superposition. *Physical review letters*, 105(20):208301, 2010.

[8] Marco Dompé, Francisco J Cedano-Serrano, Olaf Heckert, Nicoline van den Heuvel, Jasper van der Gucht, Yvette Tran, Dominique Hourdet, Costantino Creton, and Marleen Kamperman. Thermoresponsive complex coacervate-based underwater adhesive. *Advanced Materials*, 31(21):1808179, 2019.

[9] Russell J Stewart, Ching Shuen Wang, and Hui Shao. Complex coacervates as a foundation for synthetic underwater adhesives. *Advances in colloid and interface science*, 167(1-2):85–93, 2011.

[10] Kristopher D Kelly and Joseph B Schlenoff. Spin-coated polyelectrolyte coacervate films. *ACS applied materials & interfaces*, 7(25):13980–13986, 2015.

[11] Gregory Dardelle, Marlène Jacquemond, and Philipp Erni. Delivery systems for low molecular weight payloads: core/shell capsules with composite coacervate/polyurea membranes. *Advanced Materials*, 29(23):1606099, 2017.

[12] Gregory Dardelle and Philipp Erni. Three-phase interactions and interfacial transport phenomena in coacervate/oil/water systems. *Advances in colloid and interface science*, 206:79–91, 2014.

[13] Denis LJ Lafontaine, Joshua A Riback, Rümeyza Bascetin, and Clifford P Brangwynne. The nucleolus as a multiphase liquid condensate. *Nature Reviews Molecular Cell Biology*, 22(3):165–182, 2021.

[14] Geraldine Seydoux. The p granules of c. elegans: a genetic model for the study of rna–protein condensates. *Journal of molecular biology*, 430(23):4702–4710, 2018.

[15] Paulina Strzyz. Controlling phase separation of p granules. *Nature Reviews Molecular Cell Biology*, 18(1):4–4, 2017.

[16] Chih-Yung Lee and Geraldine Seydoux. Dynamics of mrna entry into stress granules. *Nature cell biology*, 21(2):116–117, 2019.

[17] Ming-Tzo Wei, Shana Elbaum-Garfinkle, Alex S Holehouse, Carlos Chih-Hsiung Chen, Marina Feric, Craig B Arnold, Rodney D Priestley, Rohit V Pappu, and Clifford P Brangwynne. Phase behaviour of disordered proteins underlying low density and high permeability of liquid organelles. *Nature chemistry*, 9(11):1118–1125, 2017.

[18] Dan Bracha, Mackenzie T Walls, and Clifford P Brangwynne. Probing and engineering liquid-phase organelles. *Nature biotechnology*, 37(12):1435–1445, 2019.

[19] Tiemei Lu and Evan Spruijt. Multiphase complex coacervate droplets. *Journal of the American Chemical Society*, 142(6):2905–2914, 2020.

[20] N Amy Yewdall, Alain AM André, Tiemei Lu, and Evan Spruijt. Coacervates as models of membraneless organelles. *Current Opinion in Colloid & Interface Science*, page 101416, 2020.

[21] Simon Alberti, Amy Gladfelter, and Tanja Mittag. Considerations and challenges in studying liquid-liquid phase separation and biomolecular condensates. *Cell*, 176(3):419–434, 2019.

[22] Karina K Nakashima, Mahesh A Vibhute, and Evan Spruijt. Biomolecular chemistry in liquid phase separated compartments. *Frontiers in molecular biosciences*, 6:21, 2019.

[23] Jessica Sheu-Gruttadauria and Ian J MacRae. Phase transitions in the assembly and function of human mirisc. *Cell*, 173(4):946–957, 2018.

[24] Xiaolei Su, Jonathon A Ditlev, Enfu Hui, Wenmin Xing, Sudeep Banjade, Julia Okrut, David S King, Jack Taunton, Michael K Rosen, and Ronald D Vale. Phase separation of signaling molecules promotes t cell receptor signal transduction. *Science*, 352(6285):595–599, 2016.

[25] Louise Jawerth, Elisabeth Fischer-Friedrich, Suropriya Saha, Jie Wang, Titus Franzmann, Xiaojie Zhang, Jenny Sachweh, Martine Ruer, Mahdiye Ijavi, Shambaditya Saha, et al. Protein condensates as aging maxwell fluids. *Science*, 370(6522):1317–1323, 2020.

[26] Priyanka Dogra, Ashish Joshi, Anupa Majumdar, and Samrat Mukhopadhyay. Intermolecular charge-transfer modulates liquid–liquid phase separation and liquid-to-solid maturation of an intrinsically disordered ph-responsive domain. *Journal of the American Chemical Society*, 141(51):20380–20389, 2019.

[27] Yalin Liu, Brian Momani, H Henning Winter, and Sarah L Perry. Rheological characterization of liquid-to-solid transitions in bulk polyelectrolyte complexes. *Soft Matter*, 13(40):7332–7340, 2017.

[28] Charles E Sing and Sarah L Perry. Recent progress in the science of complex coacervation. *Soft Matter*, 16(12):2885–2914, 2020.

[29] Simon Alberti and Anthony A Hyman. Biomolecular condensates at the nexus of cellular stress, protein aggregation disease and ageing. *Nature Reviews Molecular Cell Biology*, 22(3):196–213, 2021.

[30] Douglas M Fowler, Atanas V Koulov, William E Balch, and Jeffery W Kelly. Functional

amyloid–from bacteria to humans. *Trends in biochemical sciences*, 32(5):217–224, 2007.

[31] Simon Alberti and Dorothee Dormann. Liquid–liquid phase separation in disease. *Annual review of genetics*, 53:171–194, 2019.

[32] Shana Elbaum-Garfinkle. Matter over mind: Liquid phase separation and neurodegeneration. *Journal of Biological Chemistry*, 294(18):7160–7168, 2019.

[33] J Sprakel, NAM Besseling, FAM Leermakers, and MA Cohen Stuart. Equilibrium capillary forces with atomic force microscopy. *Physical review letters*, 99(10):104504, 2007.

[34] Evan Spruijt, Joris Sprakel, Martien A Cohen Stuart, and Jasper van der Gucht. Interfacial tension between a complex coacervate phase and its coexisting aqueous phase. *Soft Matter*, 6(1):172–178, 2010.

[35] Dimitrios Priftis, Robert Farina, and Matthew Tirrell. Interfacial energy of polypeptide complex coacervates measured via capillary adhesion. *Langmuir*, 28(23):8721–8729, 2012.

[36] Matthew C Friedenberg and C Mathew Mate. Dynamic viscoelastic properties of liquid polymer films studied by atomic force microscopy. *Langmuir*, 12(25):6138–6142, 1996.

[37] Desmond F Moore. *The friction and lubrication of elastomers*, volume 9. Pergamon, 1972.

[38] A Tonck, JM Georges, and JL Loubet. Measurements of intermolecular forces and the rheology of dodecane between alumina surfaces. *Journal of colloid and interface science*, 126(1):150–163, 1988.

5.5 Appendix

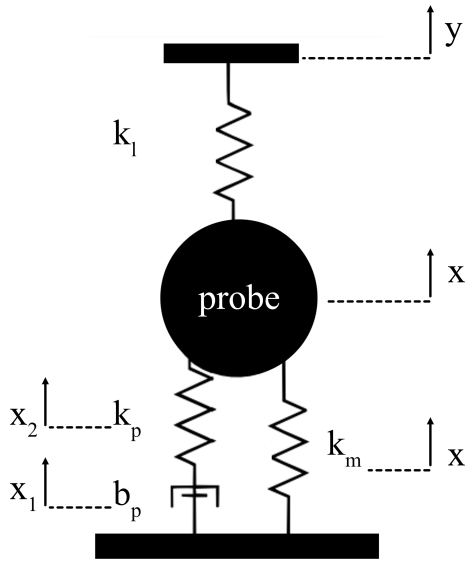

Figure 5.6: Equivalent mechanical model for the CP-AFM setup.

Figure 5.6 shows the mechanical model that describes the CP-AFM microrheology measurements. Above the probe, y denotes the displacement of the drive piezo at the top of the spring with a spring constant k_l. x donates the position of the cantilever (or probe) with an effective mass m. Therefore, the cantilever deflection is $y - x$. Below the probe, the capillary bridge is decomposed into three mechanical elements: k_m (spring constant for the interfacial tension), k_p (spring constant for the protein condensate's elasticity), and b_p (damping coefficient for the protein condensate's viscosity). There are two forces acting on the probe: the spring (top) exerts a force given by $k_l(y - x)$, and the capillary bridge exerts a force given by $k_m x + b_p \dot{x_1}$ or $k_m x + k_p x_2$. Newton's law gives

$$m\ddot{x} = k_l(y - x) - k_m x - b_p \dot{x_1} \tag{5.7}$$

where

$$b_p \dot{x_1} = k_p x_2 \tag{5.8}$$

and

$$x_1 + x_2 = x \tag{5.9}$$

We apply sinusoidal modulation with an angular frequency ω to the system through the drive piezo. Therefore, according to Euler's formula, the displacement of the drive piezo can be expressed as

$$y = Ae^{i\omega t} \tag{5.10}$$

and the motion of the mechanical elements of the capillary bridge are

$$x = Be^{i\omega t} \tag{5.11}$$

$$x_1 = B_1 e^{i\omega t} \tag{5.12}$$

$$x_2 = B_2 e^{i\omega t} \tag{5.13}$$

Then, Equation 5.7, 5.8, and 5.9 can be expressed as

$$-m\omega^2 Be^{i\omega t} = k_l(A - B)e^{i\omega t} - k_m Be^{i\omega t} - i\omega b_p B_1 e^{i\omega t} \tag{5.14}$$

$$i\omega b_p B_1 e^{i\omega t} = k_p B_2 e^{i\omega t} \tag{5.15}$$

$$(B_1 + B_2)e^{i\omega t} = Be^{i\omega t} \tag{5.16}$$

Moving $e^{i\omega t}$ away from Equation 5.14, 5.15, and 5.16 gives

$$k_l A + B(m\omega^2 - k_l - k_m) - i\omega b_p B_1 = 0 \tag{5.17}$$

$$i\omega b_p B_1 = k_p B_2 \tag{5.18}$$

$$B_1 + B_2 = B \tag{5.19}$$

Equation 5.19 can also be written as

$$B_2 = B - B_1 \tag{5.20}$$

Substituting B_2 in Equation 5.18 by Equation 5.20 gives

$$i\omega b_p B_1 = k_p(B - B_1) \tag{5.21}$$

Move B_1 to the left, then we have

$$B_1 = \frac{k_p B}{k_p + i\omega b_p} \tag{5.22}$$

Substituting B_1 in Equation 5.17 by Equation 5.22 gives

$$k_l A + B(m\omega^2 - k_l - k_m) - \frac{i\omega b_p k_p B}{i\omega b_p + k_p} = 0 \tag{5.23}$$

$$B[m\omega^2 - k_l - k_m - \frac{i\omega b_p k_p}{i\omega b_p + k_p}] = -k_l A \tag{5.24}$$

$$B = \frac{k_l A}{k_l + k_m + \frac{i\omega b_p k_p}{i\omega b_p + k_p} - \omega^2 m} \tag{5.25}$$

The cantilever deflection is

$$d = y - x = (A - B)e^{i\omega t} = CAe^{i\omega t} \tag{5.26}$$

where C is the ratio of the amplitude of the cantilever deflection to that of the drive piezo. Then we can derive

$$C = 1 - \frac{k_l}{k_l + k_m + \frac{i\omega b_p k_p}{i\omega b_p + k_p} - \omega^2 m} \tag{5.27}$$

where

$$\textit{amplitude ratio} = |C| \tag{5.28}$$

and

$$phase\ lag = angle(C) \tag{5.29}$$

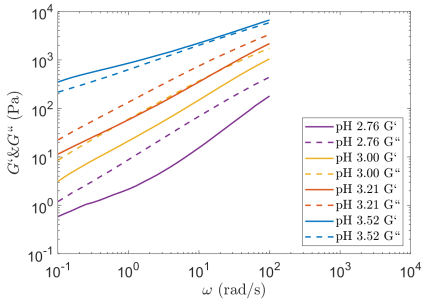

Figure 5.7: Frequency sweeps (bulk rheology) of SPEs/GA protein condensates at different pH. Solid lines represent storage moduli (G'), and dashed lines represent loss moduli (G'').

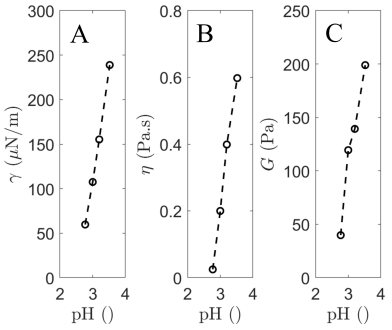

Figure 5.8: Physical properties of SPEs/GA protein condensates obtained from the fitting variables as a function of pH: (A) interfacial tension, (B) viscosity, and (C) elastic modulus. Dashed lines are drawn to guide the eye.

Chapter 6

General Discussion

This thesis aimed to design coacervate-based core-shell microcapsules using polymers from plant sources and understand the underlying physics governing capsule formation. In previous chapters, we explored various polymer sources from plants for coacervate formulations and studied their interfacial and viscoelastic properties at different length and time scales by (micro-)rheology. In the current chapter, we first highlight the key findings in addressing the research questions and application problems we have raised from previous chapters. Then, we place our findings in a broader context and discuss what open questions remain. Finally, we look beyond, pointing out future directions for research and applications.

6.1 Plant Proteins for Coacervate Formulations

The aim of this thesis was to define the bottlenecks of using plant proteins in coacervate formulations for designing core-shell microcapsules and find solutions to address them. We know coacervation is a liquid-liquid phase separation phenomenon that leads to a polymer-rich phase coexisting with a polymer-dilute phase.[1, 2] The continuous polymer-rich phase remains as a fluid after bulk phase separation while maintaining a high content in polymers (10 to 40%). To maintain the fluidity, the polymers involved in coacervation need to have an excellent affinity to the solvents so that they can still keep the solvent molecules around their polymer chains. Traditionally, coacervates are formulated in aqueous solvents, and water-soluble hydrophilic polymers are used to form them. Therefore, the more hydrophilic proteins from animal sources, such as whey protein and gelatin,[3, 4, 5, 6] are widely studied and used in research and applications. In contrast, using the less soluble plant proteins in coacervate formulations is mainly in the research phase. This is primarily because plant proteins are generally more sensitive to extraction and purification conditions. For example, the proteins in plant protein isolates are usually highly denatured and aggregated.[7, 8] In this case, it is difficult to re-disperse them at a molecular level, which is necessary for coacervation. However, previous studies show evidence that plant proteins or particular protein fractions from plant sources can indeed be used in coacervate formulations when they are extracted and purified as native proteins.[9, 10] Therefore, choosing suitable proteins or processing methods to keep the proteins in their native states or resolubilize them is the key to scale-up their use in coacervate formulations in industry.

In order to select suitable plant protein candidates that can be formulated into coacervates, we have reviewed the recent progress on using various plant proteins for interfacial stabilization in chapter 2. We find plant proteins, as solid particles, are more often used to stabilize Pickering emulsions instead of formulating coacervates for designing core-shell microcapsules. Several plant protein particles show a high interfacial affinity, and more hydrophilic polysaccharides can be used to formed complexes with plant proteins to improve their interfacial properties further. However, the current work is still very empirical and often only focuses on a single combination of proteins and polysaccharides for specific

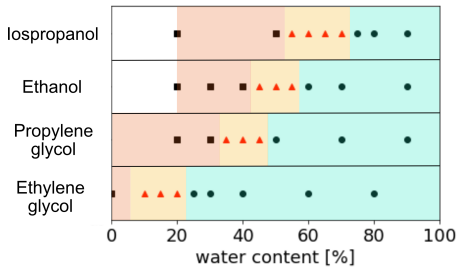

Figure 6.1: Phase diagram for solubility of zein in different binary solvents as a function of water content. Solution (square), coacervation (triangle), and precipitation (circle) are presented as different symbols, where the coacervation region is highlighted in red. The blank areas are not studied.

applications. More generic studies on plant protein/polysaccharide complexes with tunable amphiphilicity will significantly help the design and selection of plant-based delivery systems for different payloads.

In chapter 3, we studied prolamins, which are a type of storage proteins present in many cereal seeds, including corn (zein), wheat (gliadin), and barley (hordein). Prolamins are rich in glutamine and proline. They usually have very low solubility in water but are soluble in some binary solvents containing water, such as a mixture of water and ethanol.[11, 12, 13] Previous studies show that prolamins can form simple coacervates by changing the solvent ratio of the binary solvents.[12] We used a well-known prolamin, zein, as an example and studied its phase behavior in a few different binary solvents (Figure 6.1). We found that the state of zein can be adjusted from solution to coacervation and eventually precipitation with the increasing water content in the binary solvent. The co-solvents that are miscible with water with increasing hydrophobicity require a higher water content to reach the coacervate region. In our case, propylene glycol was chosen to be combined with water instead of the classic combination of water and ethanol because ethanol has high miscibility with a wide range of flavor molecules and is often used as a co-solvent for flavor molecules.

Unlike the more conventionally studied complex coacervates, which are usually adjusted to charge neutrality for forming capsules, zein simple coacervate droplets carry significant net charges at pH far away from the isoelectric point and low salt concentrations. The net charges opposing the coacervate droplet

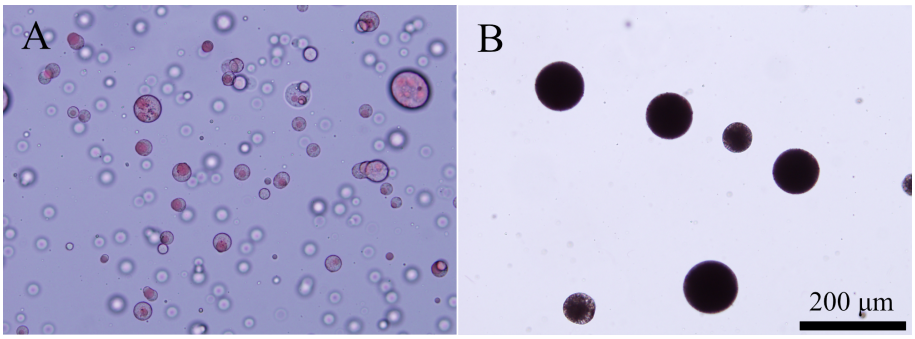

Figure 6.2: Core-shell microcapsules formed by zein simple coacervates in different regions of a binary solvent: (A) coacervation region or (B) precipitation region. The oil phase was dyed with Oil Red O, and the scale bar applies to both panels.

coalescence can be mediated by adjusting the pH or salt concentrations in the solution, thus leading to an optimal pH around 8 at low salt concentrations for capsule formation.

The unique solubility of zein in binary solvents also provides a simple way to solidify the polymer shell after the capsules are formed. This is done via adding more anti-solvent (water), moving from the coacervation region to the precipitation region. By adding more water, the solvent condition becomes less favorable for zein. Thus the shell of the microcapsules will be solidified. As shown in Figure 6.2, the polymer shell of the capsules does not transmit light after solidification. The solid particles are also re-dispersible in water.

This binary solvent method provides a facile and scalable approach for using zein to produce simple coacervates. We believe that the processing method applied to zein can also be extended to other prolamins. Depending on specific applications and desired properties, different solvent combinations can be chosen, pH and salt concentration can be used to adjust the interactions among the proteins. Other than core-shell microcapsules, simple coacervates from prolamins can also be used to design films and adhesives.[14, 15, 16]

In chapter 4, we explored a different protein source, proteins from legume seeds, for formulating complex coacervates with oppositely charged polysaccharides. Complex coacervates of proteins and polysaccharides are usually formed by cationic proteins and anionic polysaccharides due to the lack of positively

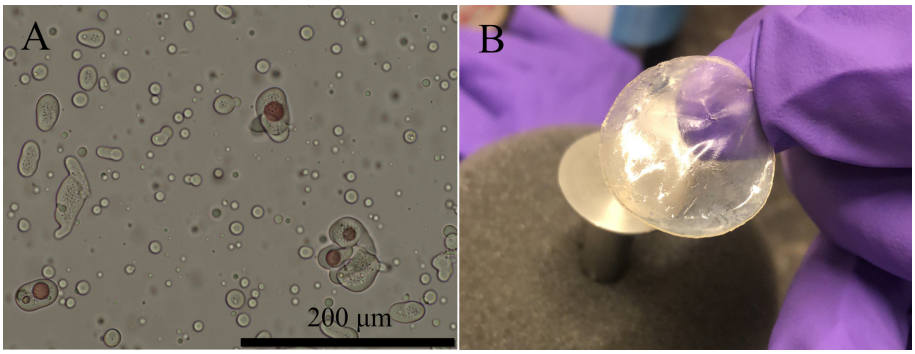

Figure 6.3: (A) Micrograph of core-shell capsules formed by complex coacervates consisting of Gum arabic and the soy protein extracted in acids around pH 3. The oil core was dyed with Oil Red O. (B) An example of the crosslinked coacervate by heating on a rheometer equipped with a 25 mm cone plate geometry.

charged polysaccharides, except for chitosan.[17] Here, the challenge is to obtain soluble cationic proteins (at pH lower than their isoelectric points) for the complex coacervate formation because protein isolates or concentrates from legume seeds are usually highly denatured and aggregated. Previous studies show that irreversible aggregates of proteins are formed at their isoelectric points. The isoelectric point precipitation has been widely used to collect proteins from solutions in the extraction process.[7, 8] Therefore, we used soy and pea as two examples and started the protein extraction from their flours at low pH. The resulting protein extracts were mixed with anionic polysaccharide solutions to obtain the complex coacervates (Figure 6.3A). In this way, we can avoid adjusting pH to go through the isoelectric points of proteins, which causes the formation of precipitates.

Many food proteins show a thermal gelation behavior,[18, 19] and legume proteins are no exception. After the core-shell capsules are formed, the continuous coacervate layer around oil droplets can be further crosslinked by heating, which turns the viscous liquid into an elastic gel (Figure 6.3B). The crosslinked coacervates exhibit enhanced mechanical strength and chemical resistance.

This study found a simple route to formulate complex coacervates by using proteins directly from legume flours. We show that extensive purification of proteins is not always necessary to create well-defined microstructures. It is also

possible to start from raw ingredients. This method provides a sustainable way of using raw ingredients for designing advanced functional materials. Moreover, the use of heating as a crosslinking method is likewise more sustainable than crosslinking using synthetic chemicals. We believe this work should stimulate more research on designing functional materials by using raw ingredients, thus promoting their use in the industry.

In this thesis, we focused on two different plant proteins and found distinctive solutions for processing them into coacervates. However, there are still some open questions waiting to be addressed before applying them in real-life applications. The first approach obtains simple coacervates from prolamins in binary solvents. Here the potential problem is the use of co-solvents that may interfere with payload encapsulation or which may not be allowed in food grade processes. The second approach uses acid-extracted legume proteins to form complex coacervates with anionic polysaccharides. Can we increase the protein extraction efficiency to use more of the raw materials by applying sonication or slightly increasing the temperature in the extraction step? Furthermore, can we apply the same approach to more plant protein sources, such as nuts and leaves? In the future, more attention should also be placed on finding sustainable polymer sources to replace those from petrochemical and animal sources for a broader range of applications.

Last but not least, it was observed in several studies that coacervate droplets show age-dependent properties.[20, 21] As shown in Figure 6.4, the late coacervate droplets show slower recovery of the fluorescence intensity after photobleaching, indicating a liquid-to-solid transition of the coacervate droplets over time. We have also observed similar behaviors for the coacervate systems explored in this thesis. The simple coacervate made of zein can change from a viscous liquid state to a solid state within a few days after preparation. The complex coacervates composed of legume proteins and Gum arabic show the same transition but require less time (after about one day). Therefore, the coacervates used to form core-shell microcapsules were always freshly prepared in this thesis. So far, it is not clear why the liquid-to-solid transition occurs in the coacervate systems investigated in this thesis. Further research on understanding the aging properties would help optimize the industrial production process, such as improving the

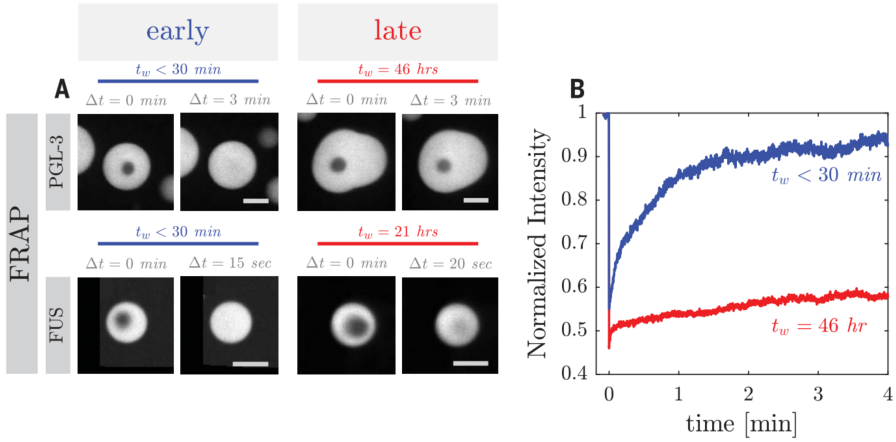

Figure 6.4: (A) Fluorescence Recovery After Photobleaching (FRAP) of complex coacervate droplets consisting of PGL-3–GFP and FUS-GFP, respectively. Images are showing early (freshly prepared) and late (some time after preparation) droplets immediately after photobleaching (Δt=0 min) and after different waiting time after photobleaching (Δt). (B)Recovery of the fluorescence intensity of the photobleached area for the PGL-3–GFP droplets shown in (A) for both early (blue) and late (red) droplets. Reprinted from[20] with permission from American Association for the Advancement of Science.

storage time of coacervates.

6.2 (Micro-)Rheology

With our work on microrheology, we aimed at revealing the underlying physics governing the core-shell microcapsule formation. This is a complex three-phase transportation phenomenon where the mechanical properties of coacervates play a vital role.[22] Thus, understanding these mechanical properties is essential for designing suitable delivery systems for specific payloads and optimize the processing conditions. Coacervates exhibit diverse mechanical properties at different lengths and time scales.[23] They are predominantly viscous fluids showing elasticity only at short time scales.[24] Coacervates usually have ultra-low interfacial tensions with their coexisting polymer-dilute phases (typically in the order of 100 μN/m).[25] Therefore, the flow behaviors of coacervates

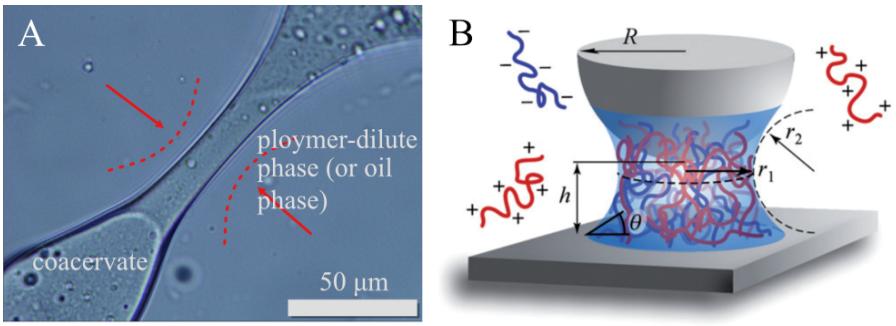

Figure 6.5: (A) Illustration of the capillary thinning method. A coacervate filament is suspended in its polymer-dilute phase or oil phase. The neck width is monitored to measure the thinning dynamics. Reproduced from[26] with permission from The American Chemical Society. (B) Illustration of the CP-AFM method. The capillary bridge consisting of coacervates is formed between the probe and substrate. Reprinted from[25] with permission from The Royal Society of Chemistry.

in bulk are dominated by the viscoelasticity, and the influence of interfacial tensions can be neglected at macroscopic length scales, above the capillary length (usually on the order of 100 μm or smaller). Nevertheless, for encapsulation and many other applications of coacervates, one deals with length scales below the capillary length where interfacial tension plays a key role.

In chapter 3, we have determined the interfacial tensions of the zein simple coacervate with its polymer-dilute phase or the oil phase by using a capillary thinning method, as shown in Figure 6.5A. This method combines the thinning dynamics of the coacervate filament within either the polymer-dilute phase or the oil phase, which is a process driven by interfacial tensions, and the viscosity of coacervates is opposing the thinning process. This is an appropriate way to estimate the interfacial tensions of coacervates because the combination of the ultra-low interfacial tension and high viscosity usually makes the thinning process very slow, such that it can easily be followed and analyzed.

Although the capillary thinning method provides a quick way of estimating the interfacial tensions, the accuracy is still limited by the coarse design of the experimental setup, which poorly controls the stability and geometry of the coacervate filament in a second liquid. Moreover, if the thinning process does not follow the behavior of Newtonian fluids, it will require more parameters to es-

timate the interfacial tensions. Therefore, a better designed micro-extensional rheometry would be highly interesting and helpful to improve this technique in the future.

For applications of coacervates, length scales are often at the micron or submicron scale. The behavior of coacervates is governed by the interplay of microscale rheology and interfacial tension. A method that precisely probes this interplay at the relevant length scales would be ideal.

Therefore, in chapter 4, we applied a CP-AFM based technique (Figure 6.5B) to measure the interfacial tension between the coacervate phase and polymer-dilute phase more accurately. The CP-AFM method measures the pull-off force upon retracting the capillary bridge consisting of coacervates formed via capillary condensation between the probe and substrate. The pull-off force is usually solely attributed to the interfacial tension.[25, 27] However, we found that the pull-off force also depends on the retraction rate, which indicates that the viscoelasticity of the coacervate also contributes to the pull-off force. Hence we have shown that for a proper analysis we need to take into account the microscale rheology of the coacervate and its interfacial tension simultaneously.

As we have mentioned at the beginning of this section, coacervates show different mechanical properties at different time scales. Both the capillary thinning method and CP-AFM retraction method described above only characterize the mechanical properties of coacervates at a single time scale. In chapter 5, we have further advanced the CP-AFM based technique by performing sinusoidal modulation on the capillary bridge between the probe and substrate at different frequencies. The dynamic response of the capillary bridge consisting of coacervates is studied at different time scales. Moreover, we have built a mechanical model that describes the capillary bridge's stress response under sinusoidal modulation. Our results show that the interfacial tension dominates the stress response at low frequencies. The viscosity causes more phase lag at medium frequencies, whereas the elasticity takes over the stress response at high frequencies. This microrheological technique provides a powerful way to study the interfacial tension and viscoelasticity of coacervates and their interplay over a wide range of time scales. The results that we have obtained from the microrheology measurements deepen our understanding of the coacervate-based

core-shell microcapsule formation.

Currently, there is still a significant error in the measurements done with the new method. We found that the stability of the cantilever limits the accuracy of this technique at low frequencies. Using a stiffer cantilever might be able to overcome such an issue but could also compromise the sensitivity of the measurement. Moreover, we have simplified the mechanical model by assuming that the coacervate elasticity and viscosity factors are independent of frequency in this study. In the future, new theoretical models that can even more accurately describe the stress response will be very helpful to understand the microrheology data.

Our new technique is generally valid for all kinds of coacervates. In addition to understanding the core-shell microcapsule formation, it could be highly relevant for studying coacervates in other research fields, such as model membraneless organelles.[29, 30, 28] More recently, coacervates have received increasing attention in biology due to their link to the membraneless organelles (MLOs) in intracellular structures, including nucleoli,[31] P granules,[32] and stress granules,[33] which are liquid compartments composed of nucleic acids and various proteins. Because of the similar composition and physical properties between MLOs and coacervates, many coacervate systems have been designed as model MLOs to investigate the underlying biophysical principles of cells.[24] As shown in Figure 6.6, some possible functionalities of MLOs composed of protein condensates in cells are summarized by Alberti et al.[28] Many of these assumptions are still waiting to be proven. An increasing number of studies are proposing that the mechanical properties of MLOs could be highly relevant to their functionalities. For example, when they act as the biochemical reactor, MLOs can localize the molecules of interest and physically separate them from thousands of (macro-)molecules in cell space to facilitate the reaction. The fluidity enables protein condensates to carry on rapid transportation and exchange of their contents within the compartment or with the surrounding environment. Therefore, the microrheological technique that we have developed in chapter 5 could be a useful tool to investigate the mechanics of MLOs, deepening our understanding of biological processes based on physical principles.

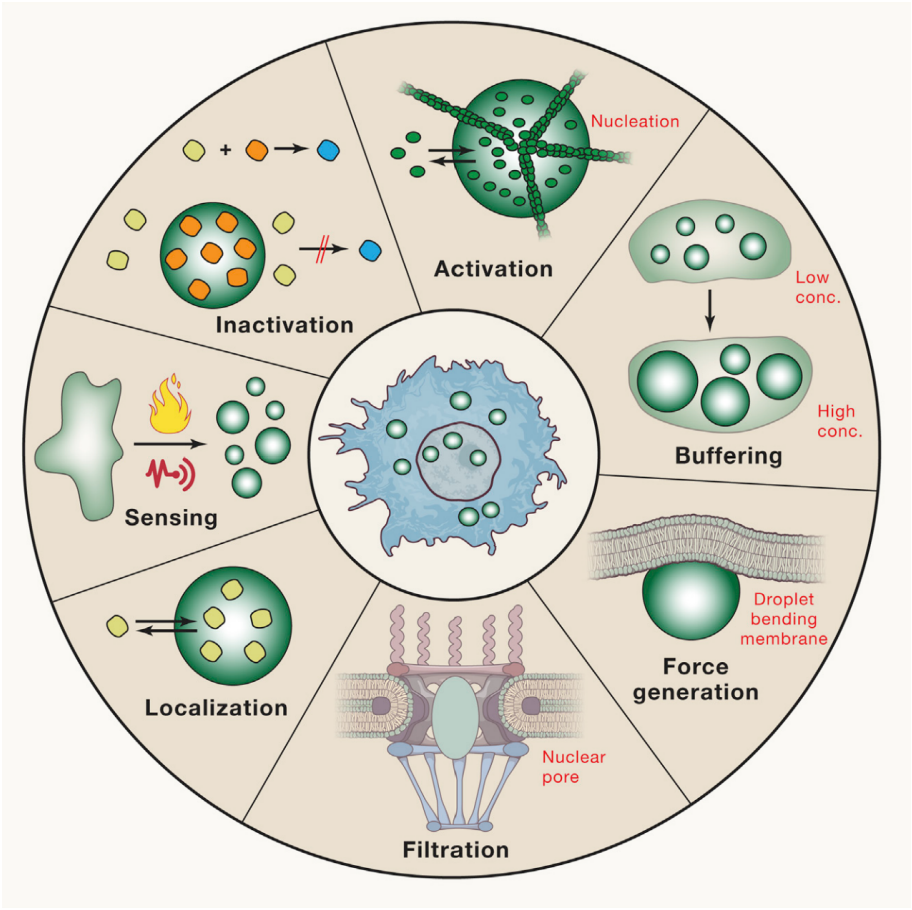

Figure 6.6: Examples of possible functionalities of protein condensates in cells. Reprinted from[28] with permission from Cell Press.

6.3 Summary and Outlook

In this chapter, we have highlighted the key findings of this thesis on the use of plant proteins for coacervate-based core-shell microcapsules and place them in a broader context. The primary challenge of using plant proteins in coacervate formulations at an industrial scale is to find suitable processing methods, either keeping the proteins in their native states or finding ways to resolubilize them. This thesis presents different ways of processing two types of plant proteins with distinctive properties. For further research and applications, more

polymer sources from plants should be explored. The new method for studying the interplay between the rheology and interfacial tension of coacervates at the microscale will be invaluable not only for exploring plant proteins for encapsulation applications but also for studying other important examples of coacervation, such as in membraneless organelles.

References

[1] Jasper Van der Gucht, Evan Spruijt, Marc Lemmers, and Martien A Cohen Stuart. Polyelectrolyte complexes: Bulk phases and colloidal systems. *Journal of colloid and interface science*, 361(2):407–422, 2011.

[2] Dimitrios Priftis and Matthew Tirrell. Phase behaviour and complex coacervation of aqueous polypeptide solutions. *Soft Matter*, 8(36):9396–9405, 2012.

[3] F Weinbreck, RH Tromp, and CG De Kruif. Composition and structure of whey protein/gum arabic coacervates. *Biomacromolecules*, 5(4):1437–1445, 2004.

[4] Masoomeh Raei, Ali Rafe, and Fakhri Shahidi. Rheological and structural characteristics of whey protein-pectin complex coacervates. *Journal of Food Engineering*, 228:25–31, 2018.

[5] Yi Lv, Fan Yang, Xueying Li, Xiaoming Zhang, and Shabbar Abbas. Formation of heat-resistant nanocapsules of jasmine essential oil via gelatin/gum arabic based complex coacervation. *Food Hydrocolloids*, 35:305–314, 2014.

[6] Gregory Dardelle, Marlène Jacquemond, and Philipp Erni. Delivery systems for low molecular weight payloads: core/shell capsules with composite coacervate/polyurea membranes. *Advanced Materials*, 29(23):1606099, 2017.

[7] Caren Tanger, Julia Engel, and Ulrich Kulozik. Influence of extraction conditions on the conformational alteration of pea protein extracted from pea flour. *Food Hydrocolloids*, 107:105949, 2020.

[8] Wim H Van Megen. Solubility behavior of soybean globulins as a function of ph and ionic strength. *Journal of agricultural and food chemistry*, 22(1):126–129, 1974.

[9] V Ducel, J Richard, P Saulnier, Yves Popineau, and F Boury. Evidence and characterization of complex coacervates containing plant proteins: application to the microencapsulation of oil droplets. *Colloids and Surfaces A: Physicochemical and Engineering Aspects*, 232(2-3):239–247, 2004.

[10] Sumudu N Warnakulasuriya and Michael T Nickerson. Review on plant protein–polysaccharide complex coacervation, and the functionality and applicability of formed complexes. *Journal of the Science of Food and Agriculture*, 98(15):5559–5571, 2018.

[11] Peter R Shewry and Arthur S Tatham. The prolamin storage proteins of cereal seeds: structure and evolution. *Biochemical journal*, 267(1):1, 1990.

[12] Rishi Shukla and Munir Cheryan. Zein: the industrial protein from corn. *Industrial crops and products*, 13(3):171–192, 2001.

[13] Ralph H Manley and Cyril D Evans. Binary solvents for zein. *Industrial & Engineering Chemistry*, 35(6):661–665, 1943.

[14] Hyun Jin Park, MS Chinnan, and RL Shewfelt. Edible corn-zein film coatings to extend storage life of tomatoes. *Journal of food processing and preservation*, 18(4):317–331, 1994.

[15] Gudrun Schmidt, Bruce R Hamaker, and Jonathan J Wilker. High strength adhesives from catechol cross-linking of zein protein and plant phenolics. *Advanced sustainable systems*, 2(3):1700159, 2018.

[16] Yanxia Wei, Jinrong Yao, Zhengzhong Shao, and Xin Chen. Water-resistant zein-based adhesives. *ACS Sustainable Chemistry & Engineering*, 8(20):7668–7679, 2020.

[17] Cornelus G De Kruif, Fanny Weinbreck, and Renko de Vries. Complex coacervation of proteins and anionic polysaccharides. *Current opinion in colloid & interface science*, 9(5):340–349, 2004.

[18] Cheng Hsin Wang and Srinivasan Damodaran. Thermal gelation of globular proteins: influence of protein conformation on gel strength. *Journal of Agricultural and Food Chemistry*, 39(3):433–438, 1991.

[19] Sinead M Fitzsimons, Daniel M Mulvihill, and Edwin R Morris. Denaturation and aggregation processes in thermal gelation of whey proteins resolved by differential scanning calorimetry. *Food hydrocolloids*, 21(4):638–644, 2007.

[20] Louise Jawerth, Elisabeth Fischer-Friedrich, Suropriya Saha, Jie Wang, Titus Franzmann, Xiaojie Zhang, Jenny Sachweh, Martine Ruer, Mahdiye Ijavi, Shambaditya Saha, et al. Protein condensates as aging maxwell fluids. *Science*, 370(6522):1317–1323, 2020.

[21] Simon Alberti and Anthony A Hyman. Biomolecular condensates at the nexus of cellular stress, protein aggregation disease and ageing. *Nature Reviews Molecular Cell Biology*, 22(3):196–213, 2021.

[22] Gregory Dardelle and Philipp Erni. Three-phase interactions and interfacial transport phenomena in coacervate/oil/water systems. *Advances in colloid and interface science*, 206:79–91, 2014.

[23] Louise M Jawerth, Mahdiye Ijavi, Martine Ruer, Shambaditya Saha, Marcus Jahnel, Anthony A Hyman, Frank Jülicher, and Elisabeth Fischer-Friedrich. Salt-dependent rheology and surface tension of protein condensates using optical traps. *Physical review letters*, 121(25):258101, 2018.

[24] N Amy Yewdall, Alain AM André, Tiemei Lu, and Evan Spruijt. Coacervates as models of membraneless organelles. *Current Opinion in Colloid & Interface Science*, page 101416, 2020.

[25] Evan Spruijt, Joris Sprakel, Martien A Cohen Stuart, and Jasper van der Gucht. Interfacial tension between a complex coacervate phase and its coexisting aqueous phase. *Soft Matter*, 6(1):172–178, 2010.

[26] Xiufeng Li, Philipp Erni, Jasper Van Der Gucht, and Renko De Vries. Encapsulation using plant proteins: Thermodynamics and kinetics of wetting for simple zein coacervates. *ACS applied materials & interfaces*, 12(13):15802–15809, 2020.

[27] J Sprakel, NAM Besseling, FAM Leermakers, and MA Cohen Stuart. Equilibrium capillary forces with atomic force microscopy. *Physical review letters*, 99(10):104504, 2007.

[28] Simon Alberti, Amy Gladfelter, and Tanja Mittag. Considerations and challenges in studying liquid-liquid phase separation and biomolecular condensates. *Cell*, 176(3):419–434, 2019.

[29] Carsten Donau, Fabian Späth, Marilyne Sosson, Brigitte AK Kriebisch, Fabian Schnitter, Marta Tena-Solsona, Hyun-Seo Kang, Elia Salibi, Michael Sattler, Hannes Mutschler, et al. Active coacervate droplets as a model for membraneless organelles and protocells. *Nature communications*, 11(1):1–10, 2020.

[30] Tiemei Lu and Evan Spruijt. Multiphase complex coacervate droplets. *Journal of the American Chemical Society*, 142(6):2905–2914, 2020.

[31] Denis LJ Lafontaine, Joshua A Riback, Rümeyza Bascetin, and Clifford P Brangwynne. The nucleolus as a multiphase liquid condensate. *Nature Reviews Molecular Cell Biology*, 22(3):165–182, 2021.

[32] Geraldine Seydoux. The p granules of c. elegans: a genetic model for the study of rna–protein condensates. *Journal of molecular biology*, 430(23):4702–4710, 2018.

[33] Chih-Yung Lee and Geraldine Seydoux. Dynamics of mrna entry into stress granules. *Nature cell biology*, 21(2):116–117, 2019.

Summary

High-performance delivery systems are of great interest in many fields, including food, personal care, and pharmaceutical industry. Replacing the traditionally used petrochemical or animal polymers with plant based polymers in such systems plays a vital role in the transition to a sustainable society. Rational design of delivery systems by using these polymers is appealing yet challenging due to their high complexity and lack of understanding of the material properties as basic building blocks. In this thesis, we focus on a specific delivery system: coacervate based core-shell microcapsules. By selecting suitable polymers from plant sources and choosing appropriate processing methods, we fabricate the microcapsules and study the underlying physics governing the capsule formation by using microrheology techniques.

In **Chapter 2**, we start by reviewing recent advances in using the complexes of plant proteins and polysaccharides for interfacial stabilization, thus searching for suitable technological routes for designing delivery systems. We find that, compared with proteins from animal sources, plant proteins are generally less soluble in aqueous solvents and sensitive to processing conditions. This causes a challenge for solution processing of the dissolved plant proteins yet also offers an opportunity to create delivery systems with better barrier properties. Pickering emulsions, the emulsions stabilized by solid particles, are the most widely studied technique for using plant proteins to stabilize interfaces. The amphiphilicity of the plant protein particles can be enhanced by combining more hydrophilic polysaccharides. However, using plant proteins to formulate coacervates is much less studied largely due to the difficulty of dissolving them, which is crucial for coacervation. Therefore, we decide to explore the opportunities of

using plant proteins to formulate coacervates by selecting suitable materials and processing conditions, and study the more general rules of the core-shell microcapsule formation based on coacervates.

In **Chapter 3**, we study simple coacervates instead of the traditionally used complex coacervates for coatings around oil droplets containing lipophilic payloads. We use a prolamin, zein, as an example to investigate its phase behavior in a binary solvent, from which three domains are defined: precipitation, coacervation, and solution. The interfacial tensions of the coacervate phase with its polymer dilute phase or the oil phase are measured by a capillary thinning method, which combines bulk rheology and thinning dynamics of the coacervate filaments in either phase. The wetting of the coacervate droplets at the interface is proved to be thermodynamically favorable due to the extremely low interfacial tensions of the coacervate in its polymer-dilute phase and oil phase. However, the significant net charge carried by the simple coacervate droplets leads to unique kinetics of the coacervate deposition and coalescence at the interface that are opposed by the net charge. The net charge can be tuned by adjusting pH, an optimal condition for capsule formation is found around pH 8 at low salt concentrations.

In **Chapter 4**, we demonstrate a simple method for fabricating core-shell microcapsules by directly extracting proteins from legume flours in acids, such as soy and pea, followed by forming complex coacervates with oppositely charged polysaccharides, for example, Gum Arabic. By extracting proteins in an acidic condition, we can avoid adjusting pH to go through the isoelectric points, which will cause irreversible protein aggregates, eventually leading to the formation of precipitates instead of coacervates. We show that crosslinking the coacervate shell into a gel is achieved by simple heating, resulting in core-shell microcapsules with enhanced mechanical and chemical resistance. Moreover, we measure the interfacial tension between the coacervate phase and the coexisting polymer-dilute phase by using CP-AFM. Our results show that the stress response upon retracting the probe is sensitive to the retraction velocity. A low reaction velocity is preferred to minimize the effect of coacervate viscosity, thus avoiding over-prediction of the interfacial tension.

In **Chapter 5**, we develop a microrheology technique to study the interfacial

and viscoelastic properties of coacervates and their interplay at different time scales. This technique is based on CP-AFM, which we use to measure the stress response of the capillary bridge consisting of coacervates between the probe and substrate under sinusoidal modulation. We look at the amplitude ratio and phase lag between the resulting stress response and driving force. A mechanical model is built to describe the stress response by treating the coacervate as a Maxwell fluid and the interfacial tension as an elastic element. The model is simplified by assuming the viscoelastic elements of the coacervate are independent of the modulation frequency. The model shows well agreement with the experimental data even after such simplification. Our results show that the interfacial tension dominates the stress response at low frequencies, the viscosity causes most of the phase lag at medium frequencies, and the coacervate exhibits more dominant elasticity at high frequencies.

Finally, in **Chapter 6**, we place our findings in a broader scientific context, elaborate on the scientific gaps we fill, and provide an outlook for future research on the design of functional materials by using biopolymers from nature.

List of Publications

THIS DISSERTATION:

- Li, X., & De Vries, R. (2018). **Interfacial stabilization using complexes of plant proteins and polysaccharides.** *Current Opinion in Food Science*, 21, 51-56. (Chapter 2)
- Li, X., Erni, P., Van Der Gucht, J., & De Vries, R. (2020). **Encapsulation using plant proteins: Thermodynamics and kinetics of wetting for simple zein coacervates.** *ACS Applied Materials & Interfaces*, 12(13), 15802-15809. (Chapter 3)
- Li, X., Van Der Gucht, J., Erni, P., & De Vries, R. (2021). **Core-shell microcapsules from unpurified legume flours.** *ACS Applied Materials & Interfaces*, 13(31), 37598-37608. (Chapter 4)
- Li, X., Van Der Gucht, J., Erni, P., & De Vries, R. **Active microrheology of protein condensates using colloidal probe-AFM.** *In preparation* (Chapter 5)

OTHER WORK:

- Li, X., Rombouts, W., Van Der Gucht, J., De Vries, R., & Dijksman, J. A. (2019). **Mechanics of composite hydrogels approaching phase separation.** *PLoS One*, 14(1), e0211059.
- Erni, P., Dardelle, G., Ouali, L., Thiebaut, N., Van Der Gucht, J., De Vries, R., Li, X. (2020). **Coacervate core-shell microscapsules.** *EU Patent filed.*

Acknowledgments

As a student from the other side of the continent, exploring science and experiencing different ways of living in the Netherlands made this journey even more special. I am thrilled and thankful to share this moment with many people. Without your guidance, support, and company, this thesis would not be here today, and I would certainly not have had such an incredible journey.

Renko, thanks for offering me this interesting PhD position and providing excellent guidance throughout the project. Your patience and positive attitude motivated me to go through the challenges I have encountered in the past four years. I have learned loads from you, from building up a research project to the lessons you have learned from your own career path. I could not ask more from a supervisor. I enjoyed our (bi-)weekly meetings talking about science and our trips to Switzerland and China. **Jasper**, it was enjoyable and inspiring to work with you. You have a natural way of approaching people and mathematical philosophy of understanding soft matter. Your critical thinking and deep insights brought my research to a higher level. **Philipp**, I enjoyed working with you and your team in Firmenich, and thanks for your hospitality during my visits to Geneva. Your input is invaluable for my thesis, especially those about rheology and your perspectives from the industry side. Thanks for sharing your experience as a scientist working in the industry, and of course, the travel information in Switzerland.

Colleagues at **De Freeze group** & **PCC**, it has been a pleasant journey working with you, thanks for organizing all the wonderful group activities, which really made me feel at home. I hope for a very successful future for every one of you.

爸爸，妈妈，谢谢你们的付出与支持，让我一路走来可以遵循内心的选择。我并不是一个人完成了博士学位，这里也有一部分属于你们。在荷兰生活的六年让我倍感相聚的不易，愿我们未来有更多可以期待和一起经历的生活。

泽峰，我想今年对于我们两人都是意义非凡的一年。看到你也进入人生新的阶段，我从心里替你高兴。愿你今后依然能够胸怀理想，脚踏实地，走出自己精彩的人生轨迹。

明伯父，沈阿姨，谢谢你们对我的理解与信任，以及对我和樱子的支持与帮助。你们带我发掘了我在武汉四年也未曾见过的这个城市的一面，愿未来我们也可以一起探索更多的风景与故事。

樱子，你的出现是我在荷兰六年最美好的收获。有太多的感谢想对你讲，你的倾听与支持激励着我不断的成长。未来我们有更长的道路要一起走，更多美好的生活要一起经历。

Xiufeng

About the Author

Xiufeng Li was born on 11 October 1992 in Weifang, China. From kindergarten to high school, he lived in the same city where he was born. After high school, he started his undergraduate studies in Chemistry at South-Central University for Nationalities in Wuhan, from which he graduated in 2015. Later that year, he went on to study Molecular Life Sciences for MSc at Wageningen University, the Netherlands. As an integral part of the MSc program, he went to the University of Amsterdam for an internship. After finishing MSc in 2017, Xiufeng continued his study as a PhD candidate at the Laboratory of Physical Chemistry and Soft Matter of Wageningen University, under the supervision of Dr. Renko de Vries, Dr. Philipp Erni, and Prof. Jasper van der Gucht. This thesis, entitled "Plant Proteins as Physical Barriers: Coacervate-Based Core-Shell Microcapsules", is the result of that PhD project.

Overview of Completed Training Activities

Discipline specific activities

- Dutch Soft Matter Meeting, The Netherlands (University of Twente, 2017)
- Physics@Veldhoven, The Netherlands (NWO, 2018; 2020)
- Han-sur-Lesse Winterschool, Belgium (Wageningen University & Research, 2018)
- Food Colloids Conference, United Kingdom (University of Leeds, 2018)*
- Rheology Course: The do's and don'ts, The Netherlands (VLAG, 2018)
- International Symposium on Polyelectrolytes, The Netherlands (Wageningen University & Research, 2018); China (East China University of Science and Technology, 2021)
- CHAINS, The Netherlands (NWO, 2018)
- Dutch Society of Rheology Meeting, The Netherlands (Wageningen University & Research, 2019)
- International Symposium on Food Rheology and Structure, Switherland (ETH Zürich, 2019)**

- International Graduate Summer School on Soft Matter and Nonequilibrium Physics, China (Xiamen University, 2019)
- Plant Protein Functionality Conference, The Netherlands (NIZO, 2020)

*Poster
**Oral presentation

General courses

- SoildWorks, The Netherlands (Wageningen University & Research, 2017)
- Electron Microscopy-the Basics: from A to W, The Netherlands (Wageningen University & Research, 2018)
- PhD Week, The Netherlands (VLAG, 2018)
- Reviewing a Scientific Manuscript, The Netherlands (Wageningen University & Research, 2019)
- COMSOL Introduction, The Netherlands (Wageningen University & Research, 2019)
- Microscopy and Spectroscopy in Food and Plant Sciences, The Netherlands (Wageningen University & Research, 2019)
- Scientific Artwork, The Netherlands (Wageningen University & Research, 2020)
- Scientific Writing, The Netherlands (Wageningen University & Research, 2020)

Optionals

- Preparation of Research Proposal, The Netherlands (VLAG, 2017)
- Weekly PCC Group Meeting, The Netherlands (PCC, 2017-2021)

- Weekly Biopolymer Group Meeting, The Netherlands (sub-group in PCC, 2017-2021)
- Journal Club, The Netherlands (PCC, 2017-2021)

The research described in this thesis was financially supported by Firmenich SA (grant no: OVK 16/001/20170605).
Financial support from Wageningen University for printing this thesis is gratefully acknowledged.

Cover design by Xiufeng Li & Yingzi Ming

Printed by Digiforce-Proefschriftmaken.nl